NUREG/CR-6915
LA-UR-05-4881

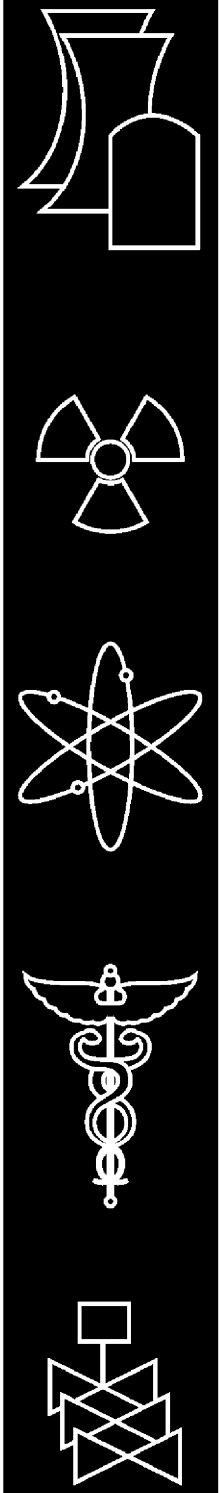

Aluminum Chemistry in a Prototypical Post-Loss-of-Coolant-Accident, Pressurized-Water-Reactor Containment Environment

Los Alamos National Laboratory

U.S. Nuclear Regulatory Commission
Office of Nuclear Regulatory Research
Washington, DC 20555-0001

This page intentionally left blank.

NUREG/CR-6915
LA-UR-05-4881

Aluminum Chemistry in a Prototypical Post-Loss-of-Coolant-Accident, Pressurized-Water-Reactor Containment Environment

Manuscript Completed: August 2006
Date Published: December 2006

Principal Investigator: M. Klasky

Prepared by
M. Klasky, J. Zhang, M. Ding, and B. Letellier (Los Alamos National Laboratory)
D. Chen and K. Howe (University of New Mexico)

Los Alamos National Laboratory
Los Alamos, NM 87545

University of New Mexico
Department of Civil Engineering
Albuquerque, NM 87110

T.Y. Chang, NRC Project Manager

Prepared for
Division of Fuel, Engineering and Radiological Research
Office of Nuclear Regulatory Research
U.S. Nuclear Regulatory Commission
Washington, DC 20555-0001
NRC Job Code N6285

NUREG/CR-6915 has been reproduced from the best available copy.

Aluminum Chemistry in a Prototypical Post-Loss-of-Coolant-Accident, Pressurized-Water-Reactor Containment Environment

ABSTRACT

An analysis of the integrated chemical effects tests (ICET) experiments has been performed by a comprehensive examination of both the test solutions and precipitates. In addition, a comprehensive review of the literature has been performed to assist in explaining the behavior of aluminum in alkaline solutions. The objective of this analysis was to elucidate the behavior of precipitate that formed when the ICET Tests 1 and 5 solutions were allowed to cool so that the behavior of other solutions with different conditions, i.e., pH, temperature, etc., could be predicted throughout the pressurized-water reactor following a loss-of-coolant accident (LOCA). This examination included supplemental analytical measurements using x-ray diffraction, ^{27}Al and ^{11}B nuclear magnetic resonance for both liquid and solid states, and quasi-elastic light-scattering measurements. Surrogate solutions were developed and compared with the analytical measurements of the ICET Tests 1 and 5 solutions. Finally, the characterization of the particle sizes and corrosion properties, including the corrosion mechanism and the corrosion rate of aluminum under LOCA conditions, has been elucidated. The current study should allow for the development of a head-loss correlation using the existing cake filtration theory, which could be used in conjunction with a corrosion model to predict system performance following a LOCA.

This page intentionally left blank.

FOREWORD

The U.S. Nuclear Regulatory Commission (NRC) established Generic Safety Issue (GSI)-191, "Assessment of Debris Accumulation on PWR Sump Performance," to assess the issue of potential blockage of pressurized-water reactor (PWR) sump screens during a loss-of-coolant accident (LOCA), and to determine the need for further regulatory actions. In this context, the definition of "debris" includes material (such as insulation and paint coatings) damaged by direct jet impingement from a LOCA, as well as latent dust and dirt that may be present in the containment buildings. During a review of GSI-191 in 2003, the NRC's Advisory Committee on Reactor Safeguards (ACRS) raised a concern about "chemical effects." Specifically, certain resultant products attributable to chemical interactions between emergency core cooling system (ECCS)/containment spray water and exposed materials (such as metal surfaces, paint chips, and insulation debris) could form another source of debris that has the potential to impede the performance of ECCS recirculation following a LOCA at a PWR plant.

To address this concern, the NRC and the nuclear energy industry jointly sponsored an integrated chemical effects test (ICET) program, and the NRC is publishing the results of that program in the six-volume NUREG/CR-6914. As noted in that report, ICET Tests #1 and #5 raised questions regarding the behavior of aluminum in sump pool solutions, and especially the behavior of aluminum-related chemical products that formed when ICET Tests #1 and #5 solutions were allowed to cool. In order to answer these questions, the NRC sponsored a follow-on study, performed at Los Alamos National Laboratory, which included an analysis of both the test solutions and aluminum-related chemical products of ICET Tests #1 and #5, as well as a comprehensive review of the literature to improve our understanding of the behavior of aluminum in sump pool solutions. That follow-on study is the subject of this report.

In particular, this report provides information about the characterization of particle sizes and corrosion properties of aluminum under LOCA conditions. It also provides information that will allow extrapolation of ICET behavior to predict the behavior of aluminum under the various pH and temperature conditions that might exist in PWR plants following a LOCA. This information will be useful to the nuclear utility industry and the NRC staff in assessing aluminum chemical effects on sump performance in a post-LOCA PWR containment environment.

The findings and conclusions documented in this report were presented and discussed at several external Chemical Effects Peer-Review Group meetings and ACRS Committee meetings. As such, they have been tested for consistency with the professional experience of multiple individuals and compared to recent data generated at other national laboratories.

Brian W. Sheron, Director
Office of Nuclear Regulatory Research
U.S. Nuclear Regulatory Commission

This page intentionally left blank.

CONTENTS

FIGURES

Page

TABLES

Page

This page intentionally left blank.

EXECUTIVE SUMMARY

The Integrated Chemical Effects Test (ICET) program was conceived as a limited-scope exercise to simulate representative chemical conditions in pressurized-water-reactor (PWR) containment buildings following a postulated loss-of-coolant accident (LOCA). Principal objectives of the series included (1) monitoring long-term tests for the formation of chemical products that could adversely affect emergency-core-cooling-system sump performance, (2) identifying the composition of adverse products, and (3) explaining the formation processes of adverse products. The enclosed stainless-steel test apparatus was designed to accommodate both submerged and suspended material samples that were introduced in proportion to representative inventories found in containment. Various debris sources included fiberglass and calcium-silicate insulation, crushed concrete, and common dirt. Heated 60°C solution was sprayed over suspended coupons for 4 hours, and the tank was circulated and monitored continuously for 30 days.

While data were collected during Test 1, an extensive literature search was conducted to help explain the trends that were observed and additional bench-scale experiments were performed post-test to confirm the conclusions that were drawn regarding the formation of observed products. Test 5 shared many of the same attributes, including aluminum corrosion in a high-pH environment and complex interactions between sodium, aluminum, silicon, and boron. This report summarizes the findings of the literature search and benchscale experiments and synthesizes plausible explanations for the aluminum chemistry trends and chemical products that were observed in ICET Tests 1 and 5.

A comprehensive examination of both the test solutions and precipitates from ICET Tests 1 and 5 has been performed. In addition, a comprehensive review of literature and additional benchmark experiments of surrogates has been performed to assist in explaining the behavior of the aluminum present in the chemical solutions. The objective of this analysis was to elucidate of the behavior of precipitate that formed when ICET Tests 1 and 5 solutions were allowed to cool. This examination included supplemental analytical measurements using x-ray diffraction (XRD), ^{27}Al and ^{11}B nuclear magnetic resonance (NMR) (both liquid and solid state), and quasi-elastic light-scattering measurements. The results of this investigation permit extrapolation of the behavior of the ICET tests to predict the behavior of aluminum under different pH and temperature conditions that might exist throughout the PWR following a LOCA. Finally, characterization of the particle sizes and corrosion properties of aluminum under LOCA conditions have also been studied. These findings would facilitate development of a head-loss correlation using existing cake filtration theory, which could be used in conjunction with a surface corrosion model to predict system performance following a LOCA.

Based on both inductively coupled plasma (ICP) analysis and examination of the ICET Tests 1 and 5 aluminum coupons, it was concluded that the aluminum weight loss from the metal coupons in these tests was consistent with the measured aluminum coupons. Furthermore, by examining the plateau of viscosity (at 23^{o}C), hydrogen production, and aluminum concentration, it was hypothesized that the plateau in the aluminum

concentration was a result of passivation of the aluminum metal surface. The measured concentrations of aluminum in ICET Tests 1 and 5 solutions did not approach predicted solubility limits, and calculations confirmed that cooling of ICET Tests 1 and 5 solutions to ambient temperature would produce precipitation, as observed in practice.

Examinations of the precipitates of ICET Tests 1 and 5 revealed that the precipitates, after being washed to ensure that sodium borates were not allowed to develop during the drying process, were largely composed of amorphous aluminum hydroxide, with a substantial quantity of boron adsorbed onto the surface. A survey of the literature suggested that the presence of the amorphous form of aluminum is expected because of the solution's high concentration of anions, which have been shown to retard crystallization at temperatures below 60°C. Thus, if amorphous-phase aluminum does form during cooling of the ICET Test 1 solution, as both XRD and TEM analyses would indicate, then it is not surprising that a significant amount of boron would also be found as a result of the adsorption of boron from solution. ICP results indicate that up to 35% of the boron from the initial solution may have been adsorbed onto the amorphous aluminum hydroxide precipitate. This degree of adsorption is certainly feasible. In fact, data from Su (1995) at a pH of ~9.5 predict a boron adsorption of ~35%. A review of the literature and NMR measurements, which revealed complexation between aluminum and boron, corroborate the hypothesis that complexation was responsible for impeding the crystallization of aluminum compounds. Furthermore, the measured weight percentage of boron on the aluminum precipitate was consistent with previous predictions based on adsorption models.

Aluminate ions ($Al(OH)_4^-$) are the only stable form of aluminum in an alkaline solution. The solubility is a function of solid hydroxide phases and increases with pH. It is noted that the presence of some organics and inorganics can increase the aluminum solubility. The solubility can also be affected by the particle size presented in the solution. Nanometer-sized particles are found in the ICET Tests 1 and 5 solutions, and the particle size distribution is affected by the hydroxide phases and the addition of organic compounds. To determine if colloids exist in ICET Tests 1 and 5 solutions, dynamic light scattering was used. Results of these measurements revealed that colloids did exist at ambient temperature with a mean radius of 65 nm.

Aluminum corrosion in alkaline solutions is an electrochemical process. In a static solution, the corrosion rate decreases with exposure time. In a dynamic solution, the corrosion rates increase with increasing flow velocity in mass-transfer-controlled regimes and do not depend on flow velocity in actively controlled regimes. The corrosion rate is influenced by adding organic and inorganic inhibitors to the alkaline solution and by the addition of some metal elements into the aluminum alloy. Sodium silicates have been found to be an effective inhibitor, with inhibition efficiency almost 100%. Thus, in ICET Test 4, the corrosion of aluminum was inhibited by the dissolution of calcium silicate.

ACKNOWLEDGMENTS

The authors would like to thank several individuals for their insightful comments and generous assistance in the preparation of this report. John Apps from Berkeley Laboratory and Paul Klein from the NRC staff reviewed early drafts for technical accuracy. Their comments helped greatly to improve the practical content and applicability of the document. Steve Chipera from Los Alamos National Laboratory (LANL) graciously donated his time and x-ray diffraction equipment to help identify the chemical compounds present in ICET Test #1 precipitates. His assistance provided key evidence supporting the phenomenological explanation of trends observed in the ICET chemical systems. Debra Wrobleski from LANL also provided no-cost access to in situ, constant-temperature, particle-size diagnostics that helped confirm the presence of colloidal structures in the chemical solutions. The entire ICET investigation team provided a continual sounding board to exchange hypotheses and insights. LANL editor Lisa Rothrock again provided professional, cheerful assistance to transform our rambling collection of notes into a publication-quality document. Without her effort, we would not have obtained the permissions necessary to release this report. Finally, gratitude is offered to NRC project manager Rob Tregoning for recognizing the value of this analysis effort and providing the opportunity to share our work.

This page intentionally left blank.

ABBREVIATIONS

ATR-FTIR	Attenuated Total Reflectance—Fourier Transform Infrared Spectroscopy
BA	Benzoin Acid
CMP	Chemical Mechanical Planarization
DFB	Desferriferrioxamine B
DLS	Dynamic Light Scattering
EDS	Energy Dispersive Spectroscopy
EDTA	Ethylenediaminetetraacetic
FA	Fulvic Acid
ICET	Integrated Chemical Effects Tests
ICP-AES	Inductively Coupled Plasma—Atomic Emission Spectroscopy
IR	Infrared
LANL	Los Alamos National Laboratory
LOCA	Loss-of-Coolant Accident
NMR	Nuclear Magnetic Resonance
NPSH	Net Positive Suction Head
NTU	Nephelometric Turbidity Unit
NUREG	Nuclear Regulatory Commission Report
PZC	Point of Zero Charge
PWR	Pressurized Water Reactor
RH	Relative Humidity
SAXS	Small-Angle X-Ray Scattering
SDAHC	Spray-Dried Aluminum Hydroxycarbonate
SEM	Scanning Electron Microscopy
TEM	Transmission Electron Microscopy
TGA	Thermogravimetric Analysis
TOA	Takeoff Angle
TSP	Trisodium Phosphate
TSS	Total Suspended Solids
XPS	X-Ray Photoelectron Spectroscopy
XRD	X-Ray Diffraction
XRF	X-Ray Fluorescence

This page intentionally left blank.

1. INTRODUCTION

During a loss-of-coolant accident (LOCA), the chemical environment generated by the injection of chemical agents into the emergency-core-cooling-system water, which is used to sequester the iodine, may create a chemical environment that facilitates the corrosion of metals and/or generation of precipitate. This corrosion may exacerbate the sump-screen head loss in a pressurized-water-reactor (PWR) containment sump pool. The integrated chemical effects tests (ICET) demonstrated that the interaction of sodium hydroxide with exposed aluminum surfaces that may be present in PWR containment may release substantial quantities of aluminum into solution via corrosion.[1] Consequently, in this report we analyze the behavior of aluminum following a LOCA. Furthermore, previous small-scale testing, in which aluminum was artificially generated in solution by introducing aluminum nitrate, indicated that these chemical products may exacerbate sump-screen clogging and consequently lead to an unacceptable net-positive-suction-head (NPSH) margin.[2] Although ICET demonstrated the feasibility of generating substantial quantities of aluminum in solution, which on cooling could lead to the formation of gelatinous material, a detailed understanding of this material, including the conditions necessary for its production, was not provided in the ICET reports. Furthermore, additional analyses are needed to extrapolate these results to conditions outside the five ICET tests and for the ultimate development of filtration models that are needed to predict head loss.

The objective of this report is to present the results of an extensive literature review and supplemental bench-scale testing of aluminum/sodium hydroxide solutions for a more detailed understanding of the generation of aluminum compounds (corrosion), their solubility properties, chemical speciation of these products, and particle size distributions in representative sodium hydroxide systems that are characteristic of those that may be encountered following a LOCA. Such an analysis may be used to allow for a determination of both the total quantity of chemical product formed under varying temperature and pH conditions.

This page intentionally left blank.

2. SUMMARY OF THE BEHAVIOR OF ALUMINUM OBSERVED DURING ICET TESTING

ICET testing was performed to investigate the possibility of chemical products being formed under conditions that might exist following a LOCA, which may compromise the filter screen and consequently prevent recirculation of cooling water to the reactor. Five tests were performed to address differences in both the chemical solutions and fiber insulation present throughout the PWR industry. Table 1 presents a summary of the five tests that were performed for the ICET project. Additional detail on the tests may be found in United States Nuclear Regulatory Commission report NUREG/CR-6914.[1]

Table 1. Experimental Conditions in the ICET Tests[a,b]

Test #	Boron[c] Added (mg/L)	NaOH Added (mg/L)	TSP[d] Added (mg/L)	Test pH Range	pH Buffering Agent[e]	Insulation Debris Volume[f]	
						Fiberglass	Calcium Silicate
1	2800	7677	-	9.3–9.5	Borate	100%	-
2	2800	-	4000	7.1–7.4	Phosphate	100%	-
3	2800	-	4000	7.3–8.1	Phosphate	20%	80%
4	2800	9600	-	9.5–9.9	Borate	20%	80%
5	2400	-	-	8.2–8.5	Borate	100%	-

a Temperature was maintained at 60°C (±3°C) in all tests.

b The following chemicals were also added to the solution: LiOH = 0.7 mg/L and HCl = 100 mg/L in Tests 1 through 4. LiOH = 0.3 mg/L and HCl = 42.8 mg/L in Test 5. Also, 63.7 g of latent debris and 21.21 g of concrete dust were added to the mixture prior to each test initiation.

c The required boron concentration of 2800 mg/L was added as 16,000 mg/L H_3BO_3 in Tests 1 through 4. To attain the required boron concentration of 2400 mg/L for Test 5, 18,500 mg/L of $Na_2B_4O_7{\cdot}10H_2O$ (sodium tetraborate) in 143 gal. of water was added to 16,000 mg/L of H_3BO_3 in 107 gal. of water.

d Trisodium phosphate (TSP) = $Na_3PO_4{\cdot}12H_2O$.

e Although other additives establish system pH on a wide scale, the buffering agent keeps pH relatively stable by resisting minor fluctuations from its pK_a.

f All tests consisted of 0.137 ft^3 of insulation represented per cubic foot of water. For each test, the insulation was present as fiberglass and/or calcium silicate material with the proportion of volume shown in the table.

2.1. Analysis on Aluminum Concentration of ICET Tests 1 and 5

Throughout the ICET test series, measurements were taken of elemental solution concentrations, pH, hydrogen production, precipitate formation, turbidity, and total suspended solids. The results of the ICET tests have revealed that aluminum-based chemical products can be generated via the corrosion mechanism in solutions in which sodium hydroxide is added. During the first 25 days of the test, both filtered (pore size 0.7 μm) and unfiltered samples were taken for analysis. Because of nondistinct differences between the filtered and unfiltered samples, only unfiltered samples were taken to be analyzed after Day 25 and for the duration of the test. From previous

experimental work, it should be noted that filters of this size are incapable of removing the very small nanoparticles that are known to exist within aluminum solutions.[3] Figure 1 presents the aluminum concentration found in the solutions for ICET Tests 1 and 5. From this figure we observe that the results from inductively coupled plasma—atomic emission spectroscopy (ICP-AES) analyses indicated that in Test 1, the aluminum concentration increased from nearly undetectable levels to ~350 mg/L after ~10 days, at which point the concentration reached a plateau. Likewise, we may observe that in Test 5, the aluminum concentration increased from nearly undetectable levels to ~50 mg/L after 20 days, at which point the concentration reached a plateau. Aluminum concentrations in Tests 2, 3, and 4 were below the levels of detection. Therefore, it may be concluded that aluminum was not present in solution to any appreciable degree in systems in which TSP was present. The pH is a major factor in determining the corrosion rate of aluminum, which will be discussed in Section 4. The changes of pH during ICET tests are shown in Figure 2. The figure indicates that the pH remains almost constant during the tests.

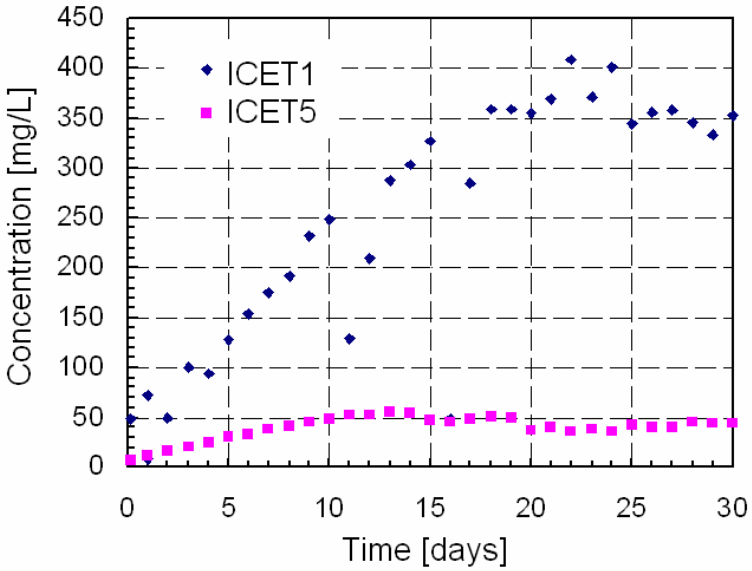

Figure 1. Aluminum concentration versus time.

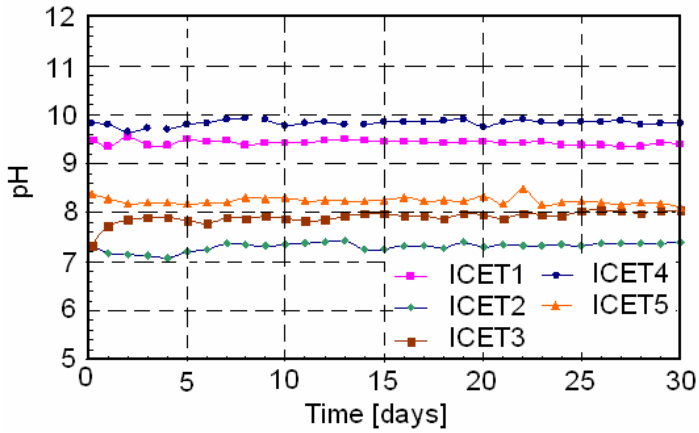

Figure 2. ICET Benchtop pH comparison.

2.2. Corrosion of ICET Metal Coupons

To determine if the measured concentrations of aluminum in Tests 1 and 5 were consistent with the observed weight loss of the aluminum coupons, the metal coupons were weighed after drying (no cleaning was performed before weighing). Weight loss/gain measurements, presented in Table 2, indicate that the submerged aluminum coupons experienced a significant weight change, which is consistent with the reduction and oxidation (redox) potentials of the metal coupons. The aluminum specimens in Test 1 lost ~25% of their pre-test mass, whereas the carbon steel sample lost ~2% of its pre-test mass and the concrete sample gained <3% additional mass. The concrete weight gain may have resulted from retained water. Other samples either gained or lost much less than 1% of their pre-test mass. Likewise, the Test 5 coupons were weighed, and it was determined that only the submerged aluminum coupons experienced signification weight change: 3% of their weight.

Table 2. Mean Weight Gain/Loss Data for Submerged Coupons (g)

		Weight Changes (g)				
Coupon Type	**Initial Weight (g)**	**#1**	**#2**	**#3**	**#4**	**#5**
Copper	1317.3	0.1	<0.1	0.3	0.2	-0.2
Inorganic Zinc	1625.2	3.1	3.8	1.8	2.3	1.6
Galvanized Steel	1054.83	0.0	28.6	15.0	0.3	0.1
Aluminum	392.0	-98.6	-0.9	0.6	0.0	-11.2
Uncoated Steel	1025.2	-23.3	1.4	-1.1	0.2	0.0
Concrete	8586	233.0	240.7	180.5	239.6	225.9

Based on the number of coupons and volume of water in the tank, the corrosion of the aluminum coupons would contribute 313 mg/L of aluminum to the tank solution in Test 1 and 36 mg/L to the tank solution in Test 5. It should be noted that because of a buildup of corrosion products on the coupon surface, the weight loss of an aluminum coupon may underestimate the aluminum concentration in the solution. As a result, these values are fairly consistent with the measured aluminum concentrations, as shown in Figure 1. Therefore, it is unlikely that significant bulk precipitation occurred. Additional support for this conclusion is provided by supporting measurements, i.e., hydrogen generation, room temperature turbidity, and kinematic viscosity measurements presented later in this section. In addition, analysis of the passivation of aluminum surfaces, Section 4, and solubility of aluminum, Section 5, provide further substantiation of this hypothesis.

As previously mentioned, the lack of aluminum present in solution in Test 4 (see Table 2) was initially surprising because the test conditions, with respect to pH, were similar to the initial test conditions of Test 1. That is, it was anticipated that the pH conditions in Test 4 would facilitate corrosion of the aluminum, just as in Test 1, and that aluminum concentrations comparable to that of Test 1 would be observed. However, a primary

difference between the two tests was the insulation material; the Test 1 insulation was 100% fiberglass, and the Test 4 insulation was 20% fiberglass and 80% calcium silicate.

To gain a preliminary qualitative understanding of the passivation of the aluminum surface, scanning electron microscopy (SEM) was performed on the Tests 1 and 4 aluminum coupons. An SEM image of an aluminum coupon after 30 days of submersion in Test 4 is shown in Figure 3, and a corresponding energy dispersive spectroscopy (EDS) analysis associated with this coupon is shown in Figure 4. The EDS image indicates that the major components are aluminum, oxygen, silicon, sodium, and calcium, with small amounts of carbon and magnesium. Corresponding SEM and EDS spectrums of the Test 1 corrosion surface are provided in Figure 5 and Figure 6, respectively. A comparison of Figure 4 and Figure 6 indicates that silica is present to a much larger degree in Test 4 than in Test 1. An additional analysis of the effect of silica on passivating the aluminum surface is presented in Section 8.3.

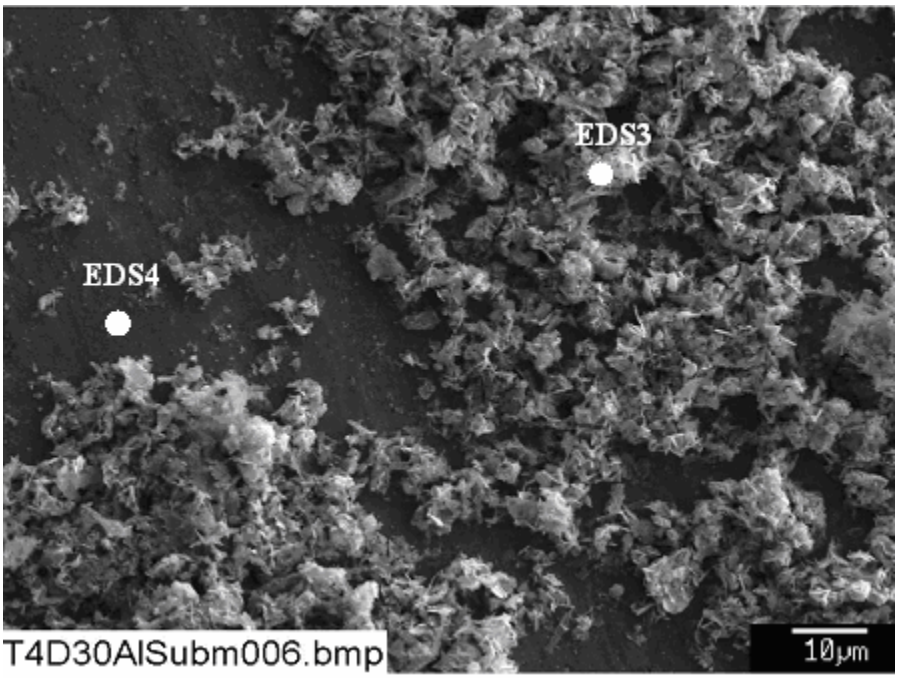

Figure 3. Annotated SEM image magnified 1000 times for a Test 4, Day-30, submerged aluminum coupon sample.

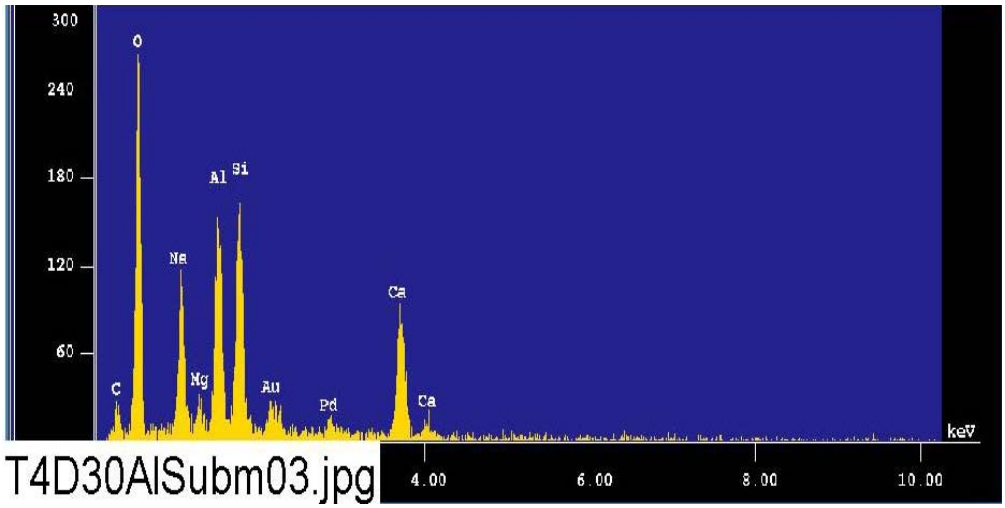

Figure 4. **EDS counting spectrum for the deposits (EDS3) on the coupon surface shown in Figure 3.**

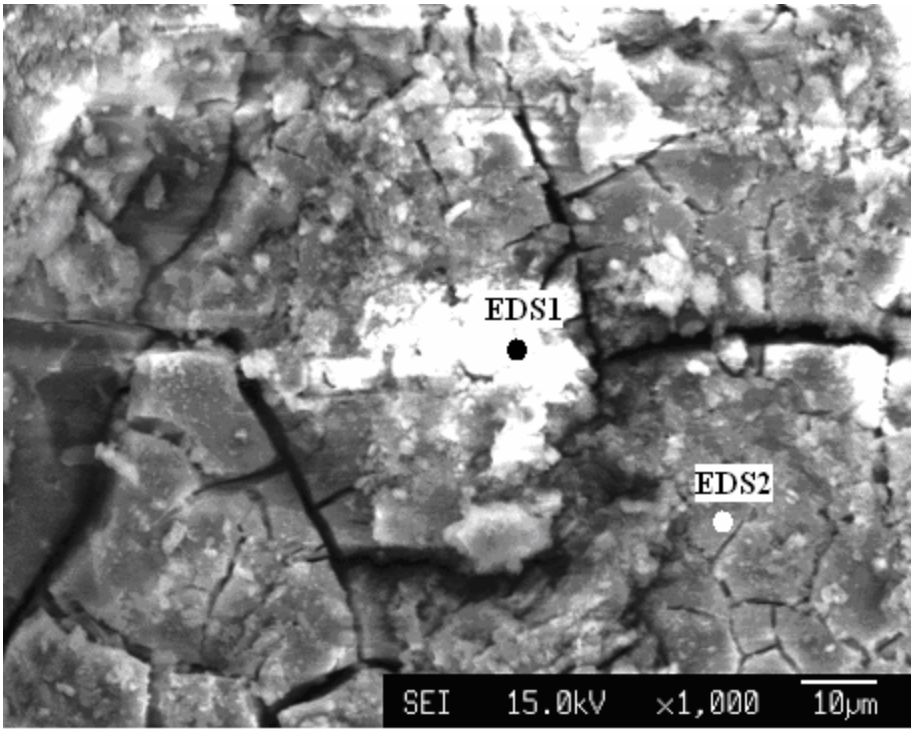

Figure 5. **SEM image magnified 1000 times for a Test 1, Day-30, submerged aluminum coupon sample.**

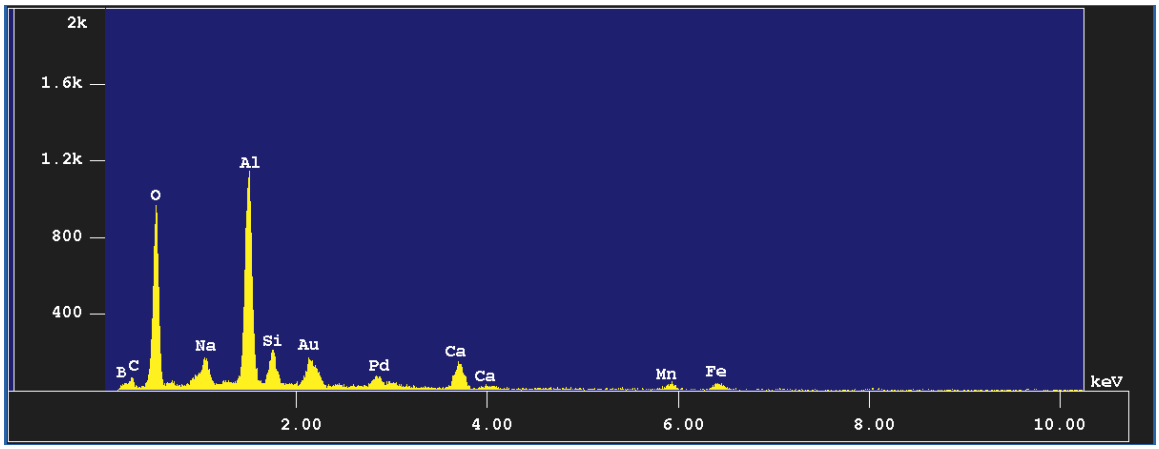

Figure 6. **EDS counting spectrum for the light spot (EDS1) on the coupon surface shown in Figure 5.**

2.3. ICET Turbidity and Total Suspended Solids (TSS) Measurements

To assess whether precipitate was being formed under test conditions, both turbidity measurements and total suspended solids were measured daily at test conditions. Results of these measurements are presented in Figure 7 and Figure 8, respectively. From these figures we observe that after an initial decline, presumably due to the settling of the debris, the values are fairly constant, after accounting for measurement uncertainty. Consequently, it would not appear that bulk aluminum precipitation occurred at test temperature. In fact, visual examination of the ICET solutions at 60°C did not reveal any precipitate. (This observation does not address the possibility that colloids could be generated that would not be detectable via a turbidity measurement, nor would the TSS sample that contained solids via filtration through a 0.7-µm-sized filter identify colloids. Additional discussion on colloids is provided in Section 6.)

Turbidity measurements were also performed at ambient temperature [23 (±2.0)°C], as presented in Figure 9. During the first day of Test 1, turbidity at ambient temperature was identical to turbidity at the test temperature. However, on Day 2 it was noted that turbidity at ambient temperature was higher than at the test temperature. It was also noted on Days 2 and 3 that the ambient-temperature turbidity was time dependent and increased as the holding time increased. Therefore, a procedure was implemented on Day 4 that required the ambient-temperature turbidity to be recorded after a cooling time of 10 minutes. (The determination of turbidity at room temperature was extremely sensitive to the time at which the turbidity was measured and may also have been strongly affected by the rate at which the cooling takes place. In fact, the observance of visible precipitate from Test 5 was not seen for several days.)

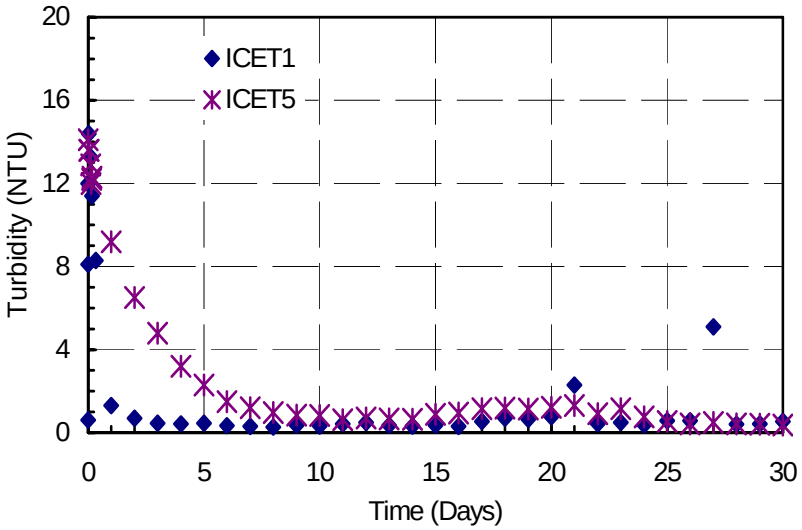

Figure 7. Turbidity versus time at 60°C.

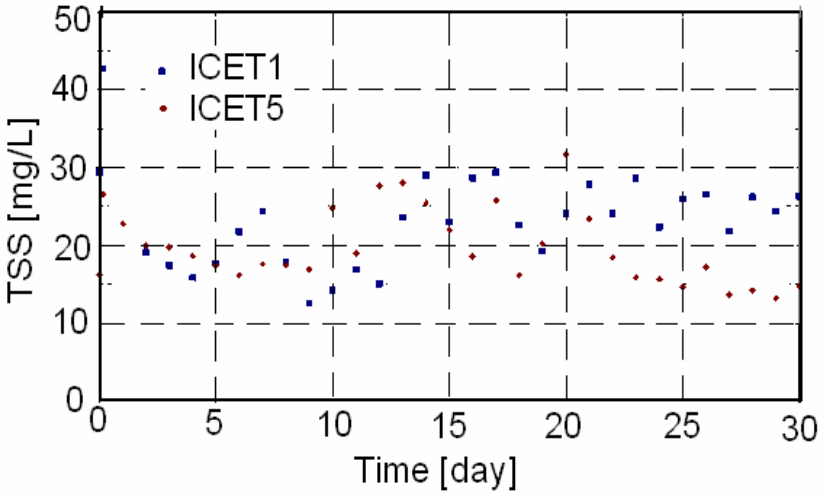

Figure 8. Total suspended solids versus time.

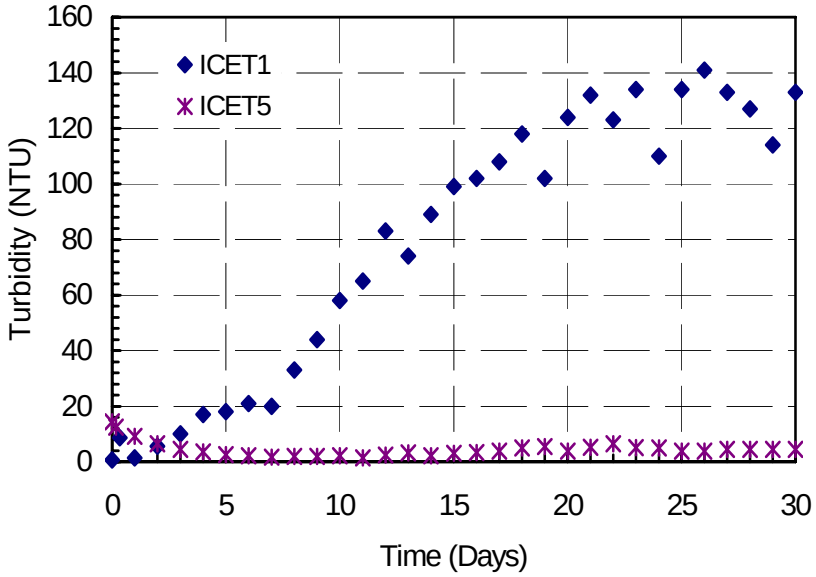

Figure 9. Turbidity versus time at 23°C.

From Figure 9, it may be observed that on cooling, the turbidity in Test 1 appeared to be rising relatively uniformly until approximately Day 18, when the turbidity appeared to reach an asymptotic limit of 133 nephelometric turbidity units (NTU). (From Day 18 on, the predominant behavior seemed to be determined primarily by variations due to measurement.) An explanation for a rapid rise in turbidity during cooling may be the appearance of a white, finely divided precipitate that gradually settled to the bottom of the sample storage bottles. The amount of visible room-temperature precipitation increased with time, and the precipitate formed more quickly at room temperature as testing progressed. A comparison of Figure 1 and Figure 9 suggests that the increasing turbidity as a function of time, at ambient temperature, may be related to the aluminum concentration. Furthermore, the plateau in the aluminum concentration and the turbidity appear to coincide, again suggesting a strong correlation. It should also be noted that the turbidity at room temperature for Test 5 increased from ~2 NTU after Day 2 to ~5 NTU after Day 17. Additional discussion on the nature of the white precipitate, the solubility of the aluminum, and the kinetics of aluminum precipitation is provided in Section 2.8, Section 5, and Section 6, respectively.

2.4. ICET Hydrogen Concentration Measurements

The hydrogen concentration was measured in the test tank atmosphere, although it should be noted that the tank was vented during the course of the experiment. The results of these measurements are presented in Figure 10. Although substantial variability can be found in the daily measurements, two points may be made: (1) measurable hydrogen, which is produced via the dissolution of aluminum, was observed in both Tests 1 and 5; and (2) the hydrogen concentrations for both Tests 1 and 5 appear to decline after approximately Days 20 and 18, respectively. The termination of hydrogen production, as

noted by the absence of any hydrogen concentration in the tank headspace, is consistent with the plateaus in the aluminum concentration and the turbidity measurement at room temperature for Test 1. This observation again substantiates the hypothesis that the plateau in the aluminum concentration was a result of passivation of the submerged aluminum surfaces and not a consequence of reaching a solubility limit.

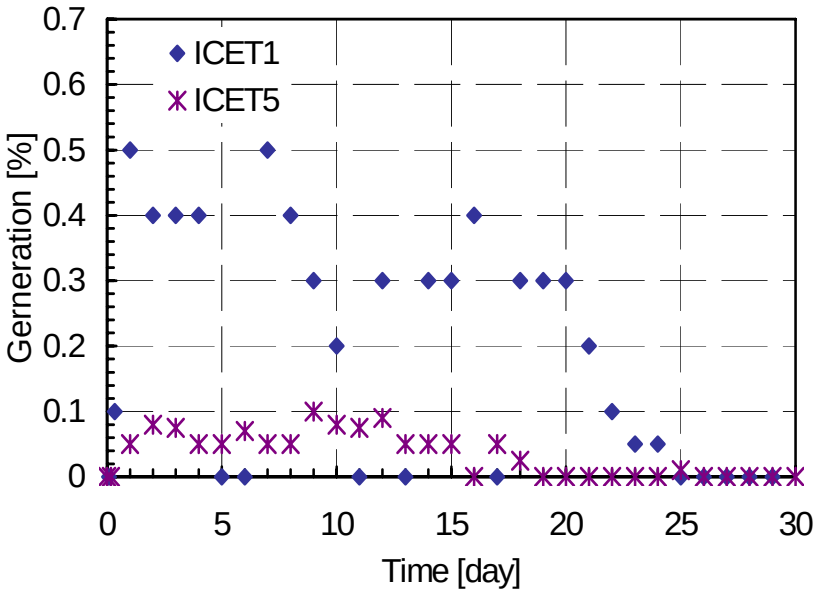

Figure 10. Hydrogen concentration above tank versus time.

2.5. ICET Viscosity Measurements

Kinematic viscosity measurements were also made to characterize the liquid phase at both 60°C and 23°C. Figure 11 and Figure 12 present the results of kinematic viscosity at 6°C and 23°C, respectively. Measurements of Test 1 at 60°C indicate that the viscosity was 0.51 mm^2/s, as compared with a nominal value for water of 0.475 mm^2/s (Ref. 4). Furthermore, from Figure 11 we observe that the kinematic viscosity for both Tests 1 and 5 was relatively constant throughout the test. The lack of quantification of the uncertainty in the measurement precludes further analysis regarding the slightly elevated values observed during the first 20 days of the test. Uncertainty in the viscosity measurements was attributed variability in first few days of Test 1 because of technique.

At room temperature we observed that the kinematic viscosity of Test 1 was substantially elevated relative to the starting value. However, substantial variability in the data was noted and is a consequence of the sensitivity of the measurement procedure because of potentially substantial variations resulting from small variations of temperature over time. Finally, the time behavior of the viscosity at 25°C for Test 1 appears to exhibit a strong positive correlation with the measured aluminum concentration. That is, the aluminum concentration and viscosity measured at 25°C both appear to be constant at approximately the same time.

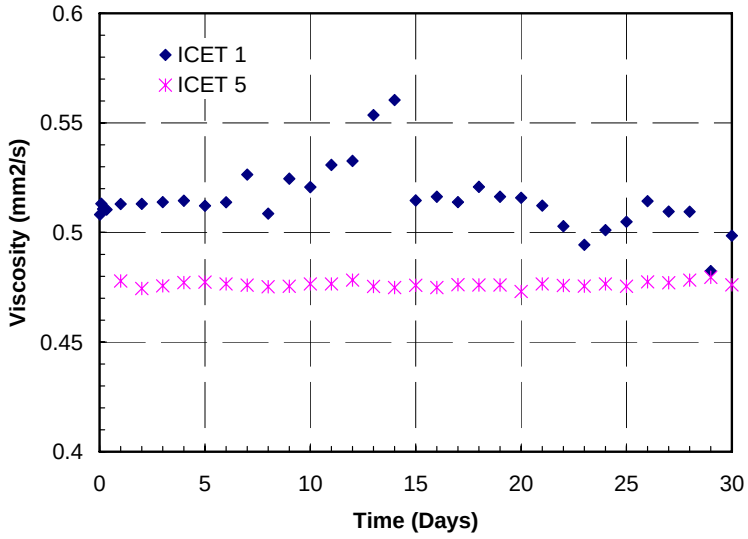

Figure 11. ICET kinematic viscosity versus time at 60°C.

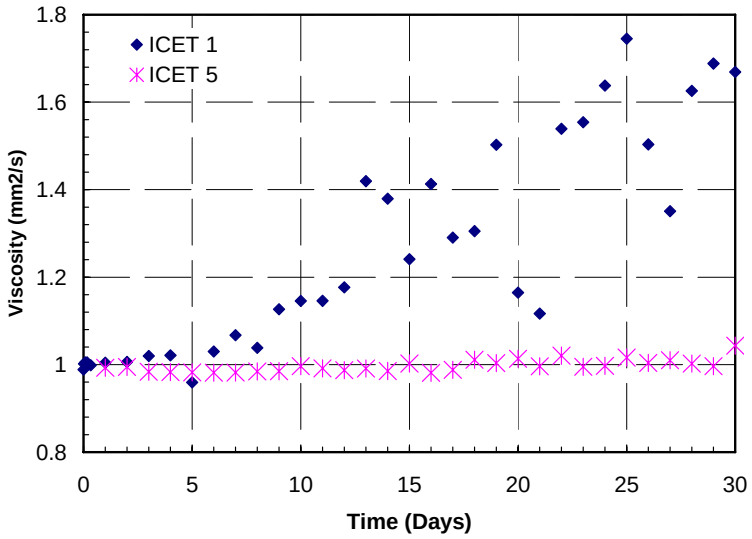

Figure 12. ICET kinematic viscosity at 25°C.

2.6. ICET Calcium and Silica Concentrations

Throughout the ICET test series, daily water samples were taken for ICP-AES analysis to determine the elemental constituents of the test solution. The concentrations of calcium and silicon are plotted in Figure 13 and Figure 14. In Figure 13 and Figure 14, we also have included the results of Test 4. It should be noted that 80% of the Test 4 insulation was calcium silicate. (In Section 4, we will examine the role of these species on the aluminum corrosion.) We note from Figure 14 that the silica concentrations of Tests 1 and 5 are ~8 mg/L. This concentration of silica is significantly less than predicted by previous investigators.[5] In fact, as may be seen in SEM images of the fiberglass (which is

presumably a source for silica and is presented later in the report), the surfaces of the fibers appear to be uniform and not to have disintegrated. A possible explanation for the apparently low silica concentrations is the fact that it has been reported that the presence of aluminum reduces the solubility of silicon, thereby reducing the driving force for the dissolution of the silica.

Analysis of the ICP-AES results indicated negligible quantities of copper, magnesium, and zinc in the Tests 1, 4, and 5 solutions.

As previously mentioned, precipitate was observed both in Tests 1 and 5 on cooling the solution to room temperature. To characterize the precipitates formed from the test solution, ICP spectroscopy, x-ray diffraction (XRD), and x-ray fluorescence (XRF) analyses were performed.

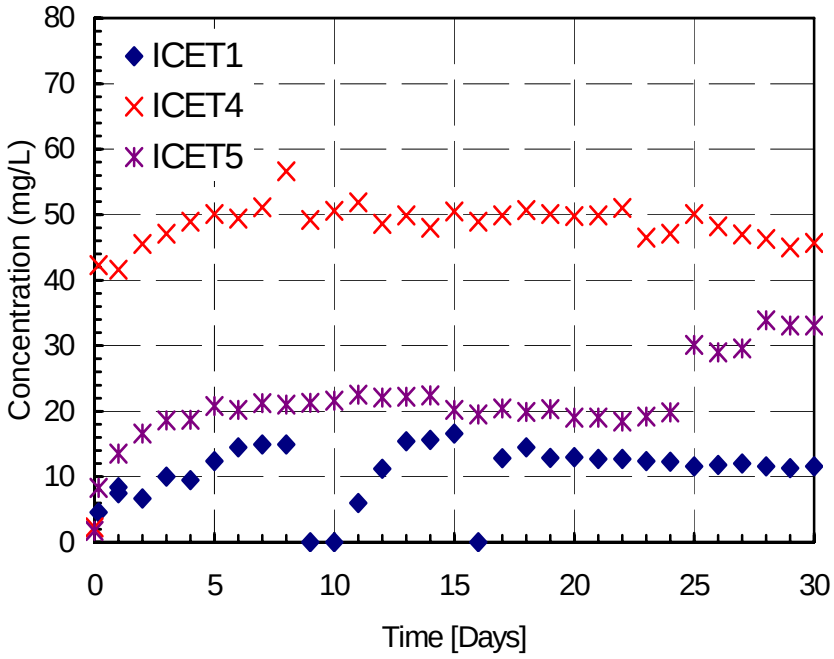

Figure 13. Calcium concentration versus time.

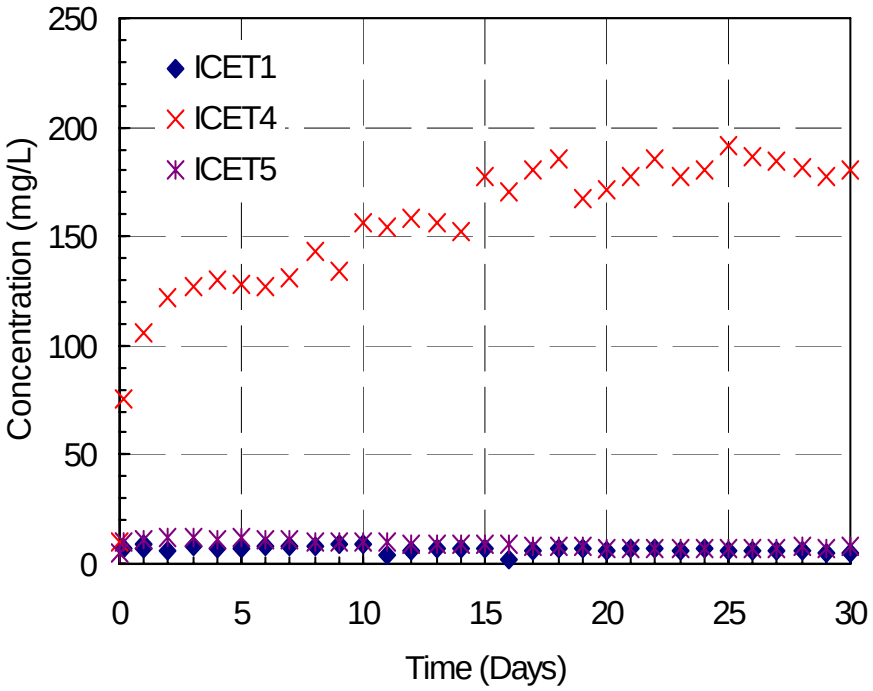

Figure 14. Silica concentration versus time.

2.7. Analysis of Tests 1 and 5 Precipitates

The precipitate examined from Test 1 was obtained from a high-volume water sample that was passed through filter paper (with a pore size of 0.7 μm) on Days 15 and 30. During this process, which naturally allowed for cooling of the solution, a white precipitate was observed to form on the filter paper. This material was the most physically homogeneous material extracted from the ICET experiment. Though consistent in appearance with a chemical-physical precipitate formed via precipitation, the white material may also have been formed by the aggregation of smaller particles that were not visible at the test temperature or by nucleation on small particles of other compounds that resided in solution at the test temperature. The precipitate was visually examined using both SEM and transmission electron microscopy (TEM). In addition, elemental analysis was obtained via EDS, ICP, XRD, and XRF. It should be noted that the precipitate was analyzed without washing. Figure 15 shows a typical EDS spectrum for a Day-30, high-volume filtered sample. It should be noted that gold (Au) and palladium (Pd) are present in almost all EDS spectra because of the sputtering technique used to prepare the SEM samples. The highly conductive sample surface provided by metallic sputtering prevented a charge from building up under the electron beam and destroying the image quality. Peak counting intensities were proportional to the elemental concentration but had to be compensated for by the energy-dependent detector response function and normalized to an assumed set of elemental constituents before proportional compositions could be inferred. Substantial variability in measured elemental

concentrations was observed between samples analyzed with the same method and between diagnostic methods applied to the same sample. A survey of these measurements was performed to recommend suitably averaged mass proportions for the dominant constituents that were observed (see Table 3).

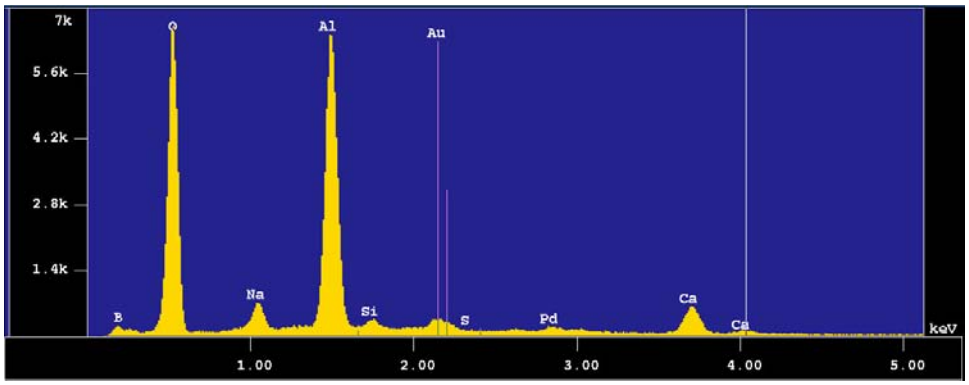

Figure 15. Day-30, high-volume sample counting spectrum (T1D30-EDS1) on the filtrate.

Table 3. Elemental Composition (wt %) of Test 1, Day-30, High-Volume Filter Sample

Method	O (%)	Al (%)	Ca (%)	Na (%)	B	CO_3^{2-}	H_2O + CO_2
EDS	48	11	2	16	21	--	--
ICP-AES	--	11	0.4	43	18	28	--
XRF	45	7	0.8	24	--	--	34

In addition to the precipitate, a thin film was noted on the filter paper after passing the test solution through the filter paper. A representative EDS spectrum for the film is provided in Figure 16. Films also appeared to exist between fiber strands that were also examined at various stages during Test 1. Web-like structures between the fiber strands revealed an elemental composition that was very similar to that of the films observed on the filter paper. The elemental composition of the film-like material found on the fiber, as given by EDS, is provided in Table 4. It was found that the elements sodium, boron, and oxygen made up 97% of the measured composition. A comparison of the elemental composition of the compound found between the fiber strands/films with known sodium borate compounds has been performed. This comparison suggests that the compound likely is a sodium borate compound. If we consider that borax and tincalconite are both 23% sodium, 21% boron, and 56% oxygen, it is reasonable to believe that the compounds are probably one of these or both.

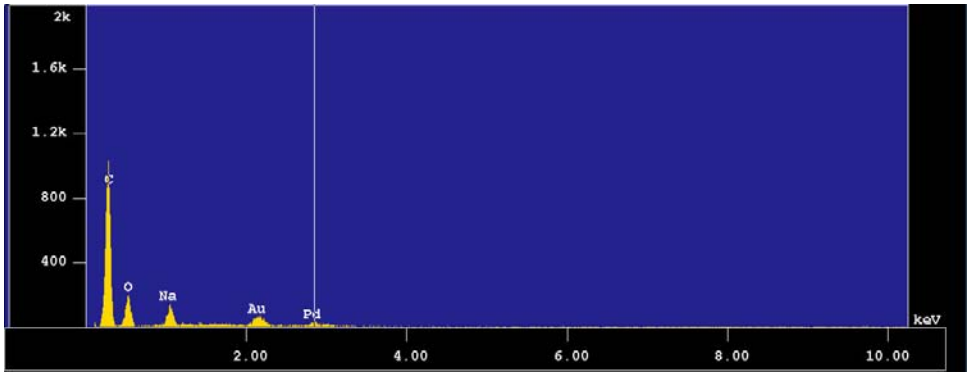

Figure 16. Day-15, Test 1 counting spectrum (EDS 1-2) for the surface on the film overlying the filter.

Table 4. Elemental Composition of Test 1 Film Material

Element	Mass %
O	56
Na	25
Al	0.6
B	16
Ca	0.17
Cl	1

When the information from Table 3 and Table 4 is examined, it can be seen that the elemental compositions of the precipitate and the thin film on the filter paper are different. That is, the precipitate appears to have a large concentration of aluminum, whereas the thin film does not have a significant aluminum concentration.

After Test 1 was completed, the solution was drained from the tank. The resulting solution was then distributed into 5-gallon plastic buckets and plastic bottles, where a white precipitate formed as the solution cooled. The precipitate was somewhat denser than the bulk solution because it settled largely to the bottom of the bottle. Furthermore, it appeared to be gelatinous in nature. This material was examined through SEM, EDS, and ICP and appeared to be of an elemental composition similar to the material captured on the filter paper.

To understand further the nature of the Test 1 precipitate formed on cooling, the precipitate captured following the completion of Test 1 was examined using XRD. The samples were obtained from the Test 1 precipitate, which formed on cooling the Test 1 solution and was captured following the draining of the tank. XRD measurements are presented in Figure 17 and Figure 18. In Figure 17, the lower red pattern is the paste, still wet in the sample mount, whereas the top blue pattern is the precipitate after it was dried and powdered. Both of these samples denote a largely amorphous material. An additional sample was obtained for XRD examination (see Figure 18). In this case, the sample was dried on a 50°C hot plate and then powdered for the x-ray mount. Results indicate a

significant amorphous component, along with tincalconite and borax at a ratio of ~90:10 wt % of tincalconite to borax. In Figure 18, the red pattern is the T1 sample, the blue pattern is tincalconite, and the green pattern is borax.

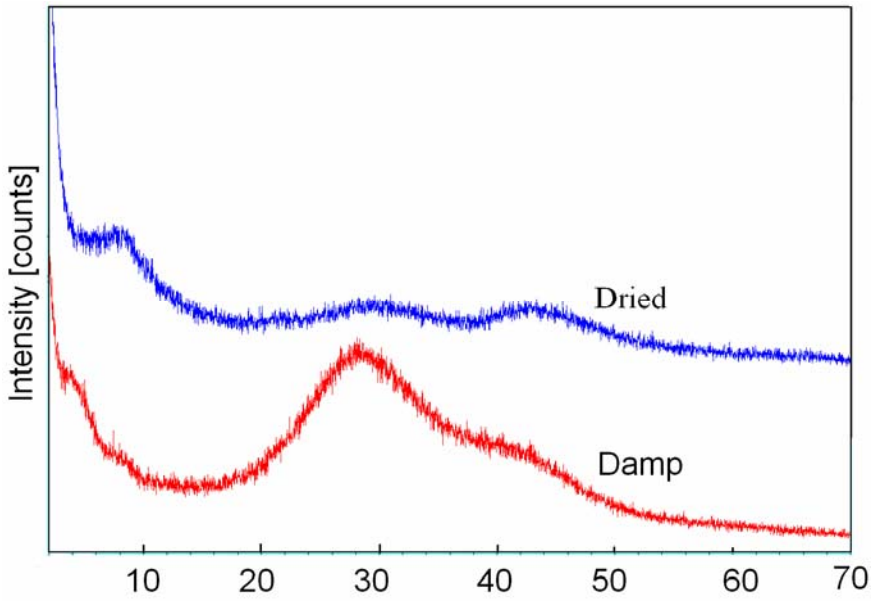

Figure 17. XRD of precipitate (damp, red; dried, blue).

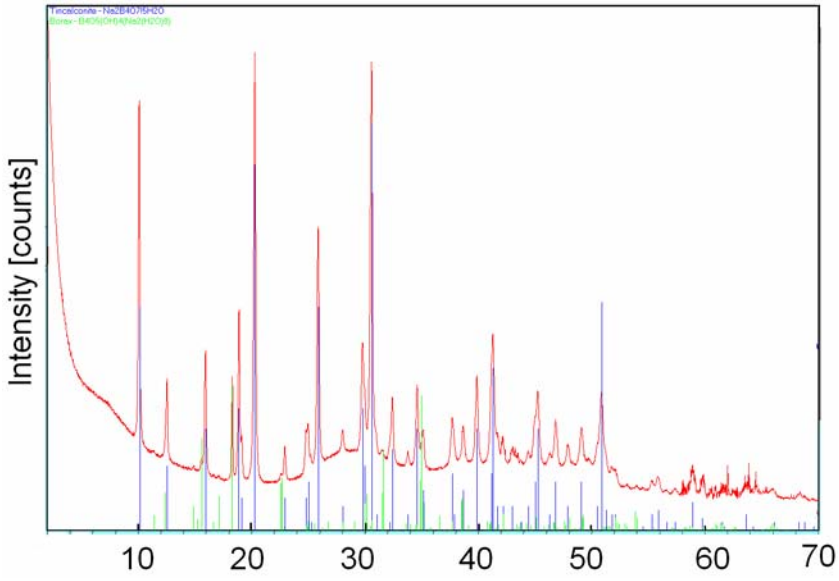

Figure 18. XRD of precipitate sample (collected on 2/24/05, 1745 dried at 50°C).

From these figures we observe that the impact of drying appears to affect the materials formed. To understand the affect of the drying process further and also to gain a more quantitative understanding of the precipitate, a supplemental XRD analysis of the samples was performed.

After the initial bulk analyses, the Test 1 post-test showed that the precipitate seen in Figure 18 contained both tincalconite and amorphous material. A closer examination of this material revealed that the sample was composed of two distinct materials, as may be observed from Figure 19. One material is a green-amber, translucent, harder material; the other is a white, softer, powdery material. XRD analyses conducted on the two separate splits revealed that the white material was relatively pure tincalconite and that the green-amber material was amorphous.

A Rietveld refinement of the XRD analysis revealed that the material had crystal cell dimensions of a = 2.84440, b = 12.25996, and c = 3.68212 (Å) and a crystallite size of

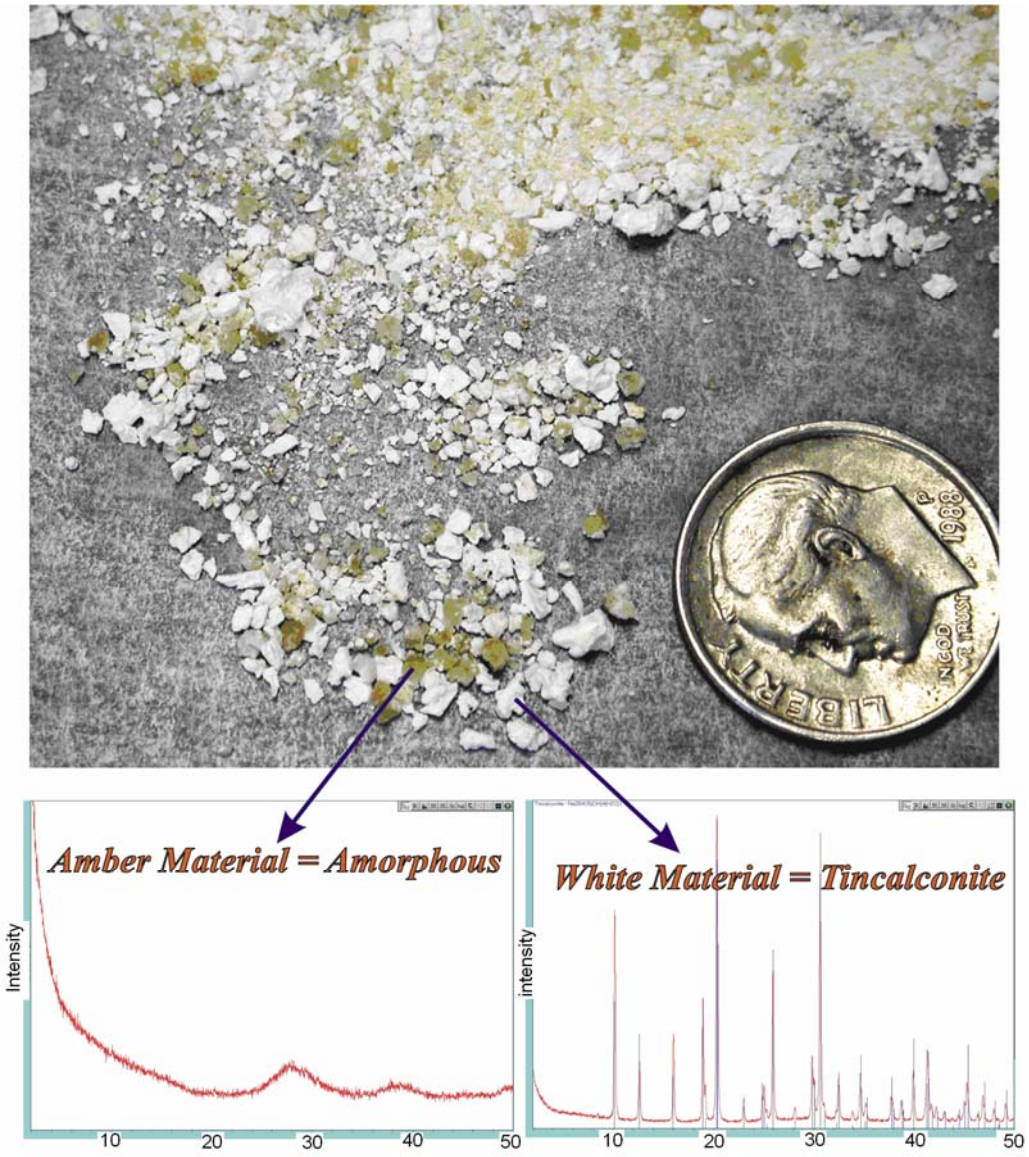

Figure 19. Test 1 separated precipitate collected on 2/24/05, 1745 bcl, dried at 50°C.

20 (±1) Å. This material appears to be consistent with poorly crystalline boehmite,[6] which is an aluminum hydroxide phase having a composition of AlOOH.

If we consider that it has been found that the sodium borate is likely a manifestation of the drying process, then a reanalysis of the elemental composition is needed. Consequently, samples of the precipitate from Tests 1 and 5 were washed to eliminate the sodium borates and were analyzed with ICP to determine the elemental composition. Table 5 presents the results of this analysis.

Table 5. Distribution of Main Elemental Components of Precipitates from Tests 1 and 5

Precipitate Sample	Al (wt %)	B (wt %)	Ca (wt %)	Na (wt %)	Other
Test 1					
11/28 (Day 7)	62	24	7	7	0
12/20 (Day 29)	41	46	2	10	1
Average	51	35	5	8	0.5
Test 5					
08/02 (Day 7)	43	36	13	8	0
08/24 (Day 29)	39	40	13	7	0
Average	41	38	13	8	0

Comparing the information in Table 3 and Table 5 reveals that the washing of the precipitate removed most of the sodium, which presumably was a constituent of the initial sodium borate additive.

To gain an understanding of the amount of hydration of the pseudo boehmite, a drying investigation was conducted. Figure 20 presents the results of this investigation. From this figure we note that the precipitate is composed largely of water.

2.8. TEM of Aluminum Precipitate

To gain a further understanding of the details of the precipitate, TEM was used to examine the precipitate from both Tests 1 and 5. In Test 1, the precipitates formed early in the test, within a few minutes of cooling, and the quantity increased over the course of the test. However, in Test 5, the precipitates took longer to form (several days), and the quantities were much smaller. TEM images for both the Day-15 and Day-30, high-flow Test 1 samples are provided in Figure 21 and Figure 22. From these figures it may be seen that the precipitate appears to be composed of nanoparticles and that the size of the particles increases with time.

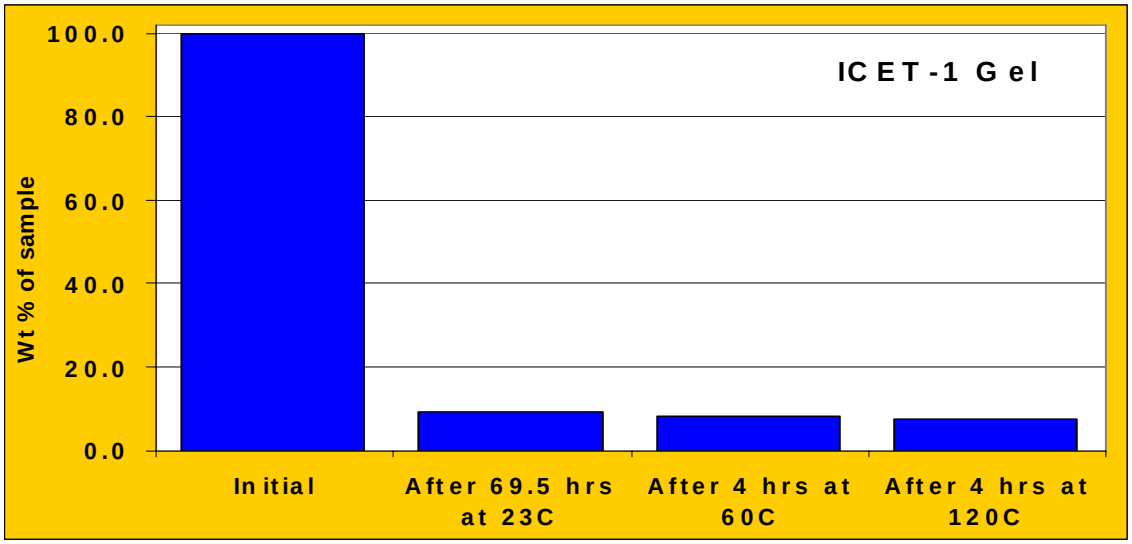

Figure 20. **Weight loss due to drying of ICET-separated precipitate (boehmite).**

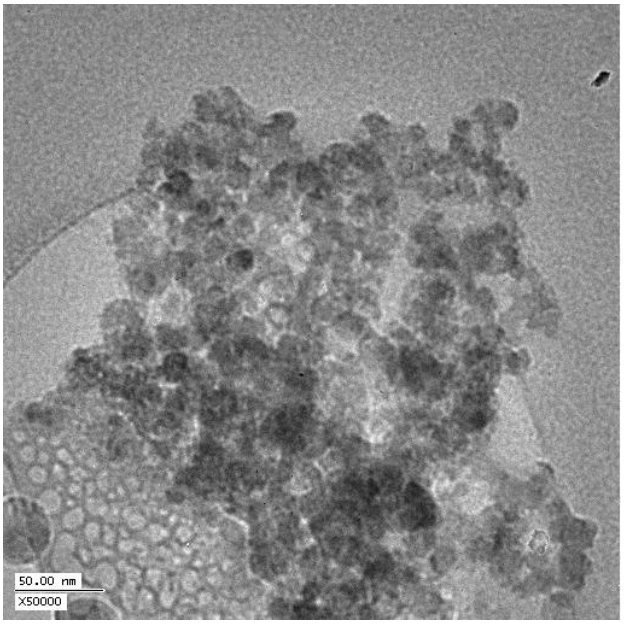

Figure 21. **Electron micrograph of the Day-15 filtered test sample magnified 50,000 times.**

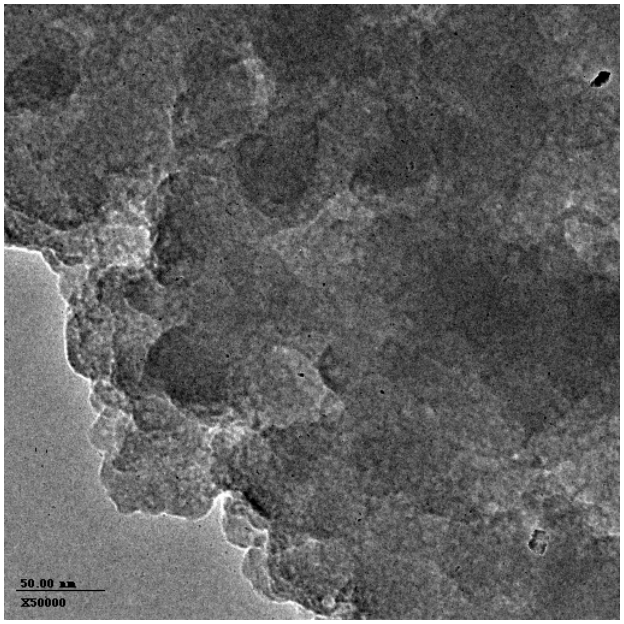

Figure 22. Electron micrograph of the Day-30 filtered test sample magnified 50,000 times.

Precipitate from Test 5 was also observed after several days at the bottom of the plastic bottles used to capture the Test 5 solution. Figure 23 and Figure 24 also present the results of Day-15 and Day-30 precipitates.

From these TEM images, we again see that the basic building blocks of the precipitate appear to be nanosized particles and that the aggregates appear more fully developed after 30 days as compared with 15 days for both Tests 1 and 5. In addition, an examination of the precipitate with TEM did not reveal prevalent crystalline behavior.

2.9. Particle Size Measurements of Test 1 Solutions

Although precipitate was not observed during Tests 1 and 5 at 60°C, we cannot rule out the possibility that colloids may exist in solution. The determination of whether the aluminum species is truly soluble or colloidal may have a significant impact on the pressure drop across a filter during the course of a LOCA. The reason for this is that if colloids indeed are present in the solution, they may attach to the filter debris on the sump screen as they transverse the system. Thus, as a function of time, gel-like material may gradually build up as the colloids traverse the coolant circuit and lead to an increased pressure drop across the screen relative to the debris itself. To examine the possibility that colloids are present in the Test 1 solution, a particle size analysis was performed using dynamic light scattering (DLS). DLS provides information regarding particle sizes and size distributions in colloidal suspensions via the fluctuations in the intensity of light as a result of the Brownian motion of the particles. The rate of these fluctuations is a function of the density difference between the particle and the solvent. The diffusion coefficient and the particle size can both be estimated from these

fluctuations. Figure 25 presents the particle size distribution of the Test 1 precipitate solution at ambient temperature. It should be noted that the range of sensitivity of the instrument was 50–1000 nm. Larger particles were removed by first filtering the solution. It should also be noted that all solutions were significantly diluted.

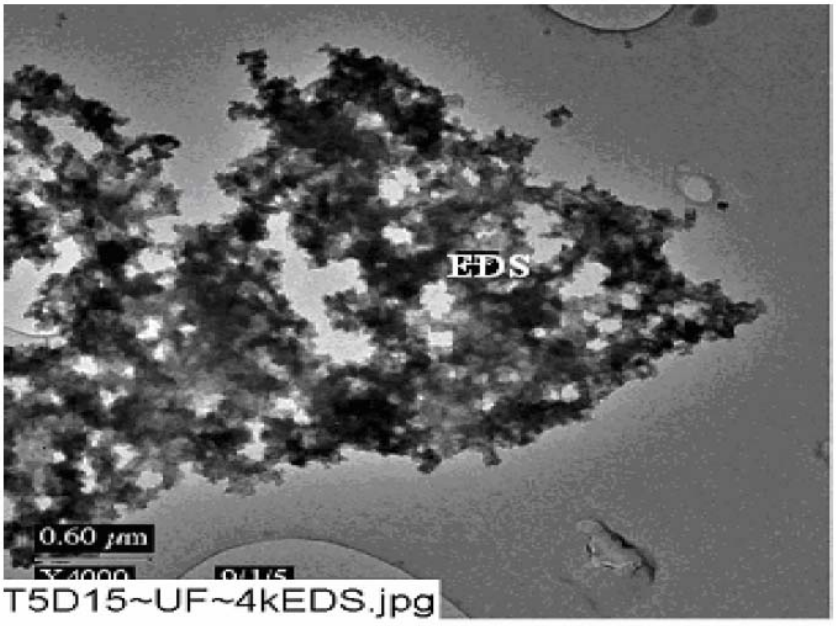

Figure 23. TEM of the Day-15, Test 5 precipitate, magnified 4000 times.

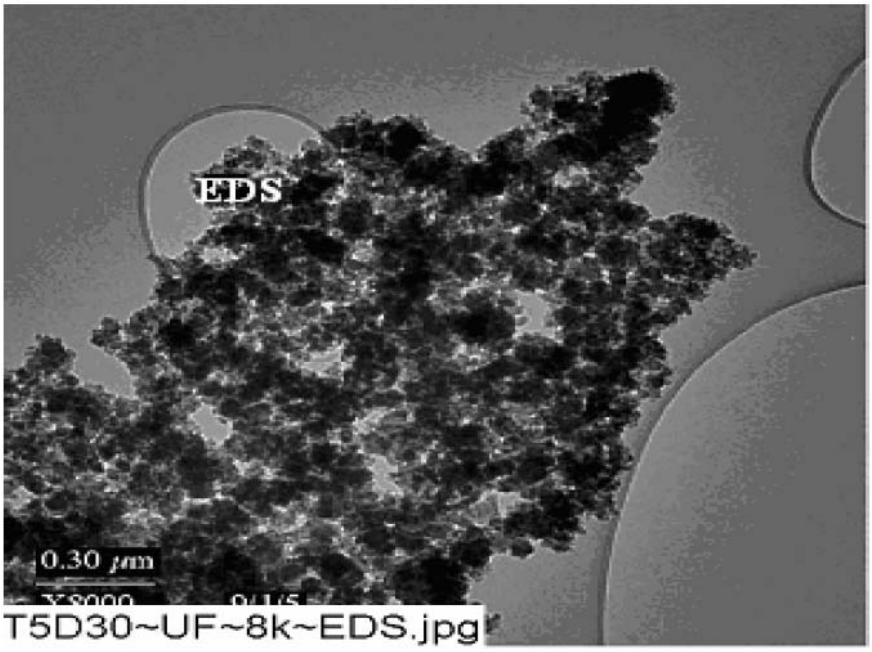

Figure 24. TEM of the Day-30, Test 5 precipitate, magnified 8000 times.

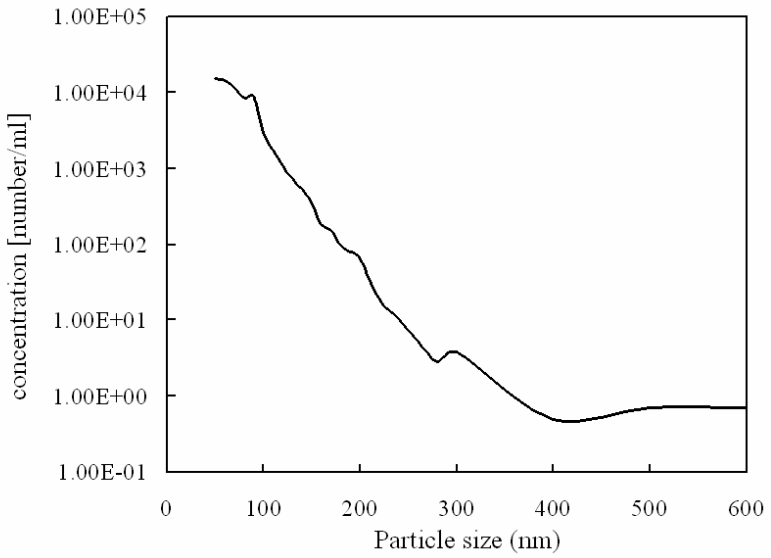

Figure 25. Particle size (nanometer) distribution for the Test 1 "precipitate supernatant" solution at room temperature (aged 4 months).

This measurement was made of the precipitate solution after approximately 4 months. From the measurement, it is seen that the particle distribution appears to be broad, in the 50–90 nm region. Unfortunately, measurements at lower particle sizes are not possible with the laboratory equipment used. Furthermore, the measurements were conducted at room temperature in lieu of test conditions because of the limitations of the equipment. However, examination of the particle size distribution reveals that nanoparticles existed in the solution at room temperature.

In conclusion, particle size measurements have been performed on room-temperature, Test 1 solutions using DLS. Results of these measurements indicate that colloids are indeed present. Additional investigations of the system at 60°C are not possible because all of the solutions were allowed to cool. However, surrogate solutions have been produced to address this issue (Section 9.4).

This page intentionally left blank.

3. OVERVIEW OF OUTSTANDING ISSUES

Although a significant understanding of ICET tests has been presented, significant issues still need to be resolved. Resolution of these issues is imperative to allow the information from the limited ICET tests to be used to assess the properties of systems with slightly different characteristics i.e., extrapolation/interpolation of the current test results. Furthermore, to ultimately address the issues of the resulting incremental head loss across the sump screen, additional information is needed to characterize the total quantity of chemical product that may be formed, its rate of production, and its physical characteristics for the development of a filtration model. Consequently, in the remainder of this report we present the results of supplemental bench-scale testing and analysis of the ICET tests, along with a comprehensive review of the literature. This supplemental analysis will allow the knowledge basis to be advanced to address these major objectives, along with the following outstanding issues:

What led to plateau of the aluminum concentration in Tests 1 and 5? Did an oxide layer develop on the aluminum surface that ultimately inhibited corrosion? What was the reason for the abrupt passivation of the aluminum surface in Test 4?

1. Was the aluminum fully soluble in the test solution at 60°C, or were nanoparticles present?
2. Was the solution supersaturated with aluminum? Did nucleation take place on the nucleation sites on the fiberglass?
3. How is the boron incorporated into the aluminum hydroxide gel that apparently forms when the solution cools? Is boron adsorbed onto the aluminum surface? What role does boron have in the phase behavior of aluminum and solubility?
4. What is the role of the organic material within the ICET test? Was this material responsible for the increased solubility of aluminum during the test conditions?
5. Can we predict the aluminum phase behavior and consequently the observed solubility behavior with respect to pH, temperature, and aging? What precluded the formation of crystalline aluminum hydroxide?
6. At what temperature did the agglomeration occur that led to the formation of the gelatinous material when the solution was cooled? To what extent is the gelatinous material redissolved?
7. What are the settling characteristics of the gel if it is formed, and what will the impact be on the aluminum corrosion if localized precipitation, away from the aluminum surfaces, does occur, i.e., the impact of nonisothermal conditions that are likely to be present in the actual containment?
8. Can the formation of the gelatinous material and the deposition on the fiberglass be precluded through the modification of the solution chemistry?
9. Can a surrogate solution/precipitate be developed for filtration testing of the aluminum systems?

This page intentionally left blank.

4. ALUMINUM-PHASE BEHAVIOR

It has been noted that all ICET tests were performed in alkaline environments, as indicated in Table 1. In this section, we examine the formation of the phase-controlling species in alkaline solutions and address some of the factors that determine the nature of the phase formed, including the kinetics of phase transitions (aging) and the experimental conditions.

4.1. Hydroxide Phases

In an aluminum-alkaline solution system, a determination of the dissociation of the aluminum solid phase is needed to determine the solubility of aluminum in the solution. That is, the equilibrium of the following dissolving reaction must be considered:

$$Al(OH)_3(s) = Al^{3+} + 3OH^- , \quad (1)$$

with an equilibrium constant:

$$K_1 = [Al^{3+}][OH^-]^3/[Al(OH)_3] , \quad (2)$$

where [] is the species activity in the solution. If we consider that the aluminum hydroxide in Eq. (1) is solid, its activity is set to be unity.

It has been noted that the equilibrium constant in Eq. (2) is a function of the aluminum hydroxide phase. The phase may exist in an amorphous form or as one of three crystalline forms: gibbsite, bayerite, or nordstrandite. The crystalline polymorphs differ only in the packing arrangement of the layers.[7] That is, the Al-O-Al layer framework is identical.[8] Each aluminum atom has three neighboring Al atoms coordinated with pairs of hydroxyl groups. The coordination around aluminum is thus octahedral. The layers are held together by a network of hydrogen bounds. The ordering of these layers forms the essential difference between these structures. In gibbsite, the hydroxyl groups of one layer are stacked directly on top of the hydroxyl groups of the next layer, creating a crystal of hexagonal morphology, and its relationships are clearly of type AB-BA-AB, as shown in Figure 26. The hydroxyl groups of bayerite reside in the depressions of the layers below and above, creating a conically shaped crystal. The bayerite has an AB-AB-type lattice. Nordstrandite also has an AB-AB-type lattice and is composed of alternating layers of gibbsite and bayerite.[8] It is reported that the solubilities of gibbsite and bayerite have at times been shown to overlap, but some information suggests that gibbsite is slightly more insoluble than bayerite.[9]

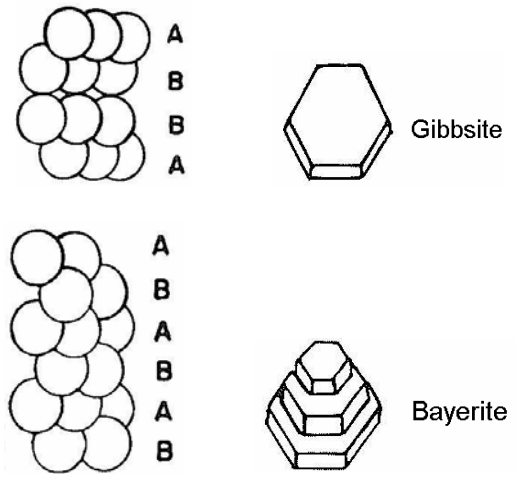

Figure 26. Gibbsite and bayerite layer stacking patterns.[7] [Used with permission of the publisher.[*]]

XRD has been used to characterize the phase of aluminum hydroxide solids. Gibbsite (α) is identified by the presence of three principal diffraction lines at 4.85, 4.37, and 4.32 Å, which correspond to scattering angles of sin 2θ of 7.17, 7.98, and 8.05, respectively. Bayerite(β) is distinguished by strong diffraction lines at 4.72 and 4.36 Å, whereas nordstrandite (γ) is detected by the presence of three major diffraction lines at 4.79, 4.33, and 4.22 Å.

Another common crystal in aluminum-alkaline solution is boehmite, with a composition of AlOOH. Pseudoboehmite is built up out of the same fundamental unit as boehmite, a double sheet of octahedral crystals with aluminum ions at their center; however, the amount of water varies between double octahedral layers, which are identified by broad diffraction peaks at 6.6, 3.2 and 2.3 Å. The major distinction between pseudoboehmite and boehmite is that the former has broad diffraction peaks and that the spacing of the first peak is larger than the first peak of 6.11 Å for boehmite. The amorphous precipitate produces a diffraction pattern that is only a halo around the region of 3-4 Å.[10]

4.2. Phase Transitions

Numerous experiments have been conducted in alkaline systems to examine the nature of the aluminum species, solubility, and solid phase(s) present; this work has been summarized in Sposito.[11] Precipitation studies in a basic medium have the distinct advantage that the hydrolysis is less complicated as compared with acid systems. In weakly aluminum solutions, the aluminate ion is the dominant species. Furthermore, experiments have revealed that solubility is very sensitive to the solid phase in

[*] Reprinted from *The Environmental Chemistry of Aluminum*, S. Goldberg et al., "Chapter 7: The Surface Chemistry of Aluminum Oxides and Hydroxides," 2nd Ed., CRC Press, Copyright 1996, with permission from Copyright Clearance Center, Inc.

equilibrium with the solution and that the solid phase formed is a complex function of the experimental conditions and the nature of the materials used, i.e., particle size and surface area.[11]

To address the sensitivity of the results to experimental conditions, an elaborate device was designed in which acidified aluminum nitrate solutions were titrated with alkali (NaOH or KOH).[12] Considerable effort was devoted to ensuring vigorous mixing of the reactants so as to avoid developing local hydroxyl ion concentrations appreciably larger than the overall concentration because this would result in the formation of a precipitate that is most reluctant to redissolving, even though it is unstable.

Results from this investigation[12] indicate that visible precipitate in a system with an initial aluminum nitrate concentration of 0.072 M first occurred at a pH of ~6.1 at 25°C. Decreases in temperature led to a lowering of the onset pH of precipitation. It should be noted that this determination was also made with light scattering. The structure of the precipitate was determined after filtering, washing, and drying at 120°C using XRD. Table 6 provides the results of this investigation.

Table 6. Structure of Precipitates, as Revealed by XRD [Used with permission of the publisher.*]

pH	Temperature (°C)				
	24	**28**	**40**	**60**	**90**
6	A[a]				A
7	Microbay[b]		A	A	A
8	Microbay		A	A	
9	Microbay		A	A	Gellbo[c]
10	Microbay ↓ Bayerite	Bayerite	A ↓ Bayerite	Microbay ↓ Bayerite ↓ Gibbsite	Gelbo (Gibbsite) (Bayerite)

[a] Amorphous.
[b] Amorphous with few diffuse lines of bayerite.
[c] Gelatinous boehmite.

In these studies neither precipitate nor colloids were found at OH/Al ratios of <2.5, even after aging for 2 months. (The value of OH/Al = 2.5 is very close to the vector percolation threshold of 2.4, which represents the minimum number of cross links required for a three-dimensional structure to attain rigidity.[8]) However, in more common

* Reprinted from *Journal of Colloid and Interface Science*, A. C. Vermeulen et al., "Hydrolysis-Precipitation Studies of Aluminum (III)," **51**:3, pp. 449–458, Copyright 1975, with permission from Elsevier.

investigations where the hydroxyl ion concentration is nonuniformly added, a different behavior is observed. Depending on the rate of alkali addition, the solid phase can be formed at OH/Al ratios of <2.5. In addition, the nonuniform addition of the alkali yields a more-crystalline product than the amorphous product that is found in a more uniform setting.[9,13]

In another investigation of the phase behavior of aluminum hydroxide systems, Hayden found that the phase behavior was also dependent on the aging.[14] Table 7 presents the results of this investigation.

Table 7. Effect of Age on the pH and Crystalline Structure of Aluminum Hydroxide Prepared from 0.0378-M Aluminum Nitrate Solutions (Solution also 0.30 in Sodium Nitrate) [Used with permission of LANL legal counsel]

OH/Al Ratio	2.90	2.95	2.95^{+}	3.02	3.25
Initial pH	5.00	5.50	5.50	8.00	9.50
1 Day (pH)	4.85 Amorphous	5.48 Amorphous	5.54 Amorphous	7.85 Weak Pseudoboehmite	10.64 Mixed Pseudoboehmite/ Bayerite
1 Week (pH)	4.82 Amorphous	5.18 Amorphous	5.41 Amorphous	7.60 Mixed Pseudoboehmite/ Bayerite	10.74 Mixed Pseudoboehmite/ Bayerite/Gibbsite
1 Month (pH)	4.29 Amorphous	4.35 Amorphous	5.04 Amorphous	7.50 Mixed Pseudoboehmite/Bay-erite	10.79 Mixture Bayerite Gibbsite
Heated (pH at 65°C)	4.05 Gibbsite	4.10 Gibbsite	4.42 Amorphous	7.25 Pseudoboehmite	9.47 Gibbsite

From these results it is clear that increasing the hydroxyl concentration and aging lead to the appearance of a more crystalline product. In addition, as may be seen at a low pH (i.e., <9.5), aging decreases the pH, whereas at pH = 9.5, aging increases the pH. Furthermore, an increase in temperature in all cases decreases the pH. The observed changes in pH illustrate that two distinct processes are occurring. The first process is the result of precipitation, as given by

$$Al(OH)_3\,(s) + Al(OH)_4^- = 2\ Al(OH)_3\,(s) + OH^-, \qquad (3)$$

whereas the decrease in the pH is the result of the formation of double hydroxide bridges. The second process occurs by the sequential deprotonation and dehydration reactions shown in Eqs. (4) and (5) as

$$Al(OH2)_6^{3+} = Al(OH)(OH_2)_5^{+2} + H^+ \quad (4)$$

and

$$2Al(OH)(OH_2)_5^{+2} = Al_2(OH)_2(OH_2)_8^{+4} + 2H_2O. \quad (5)$$

Results are also reported in the literature in terms of the OH/Al ratio. Because it is generally accepted that under slight alkaline conditions the rate-limiting step in the precipitation of aluminum hydroxide is the formation of Al-OH-Al bridges, the ratio OH/Al is of paramount importance.[15] That is, below an OH/Al ratio of ~2.5, the pH at 25°C shows a gradual increase from a pH of 1.2, at very low OH/Al ratios, to ~2.4 at an OH/Al ratio of 2.5.

This pH behavior reveals two fundamentally different processes. On the first plateau, polynuclear hydroxo complexes are being formed. Based on acid kinetic and light-scattering studies, it has been concluded that these complexes are largely planar in structure, with OH bridges connecting the Al(III) cations. These units therefore resemble basal planes of the bayerite or gibbsite lattices. On the second plateau, separated from the first plateau by the rise in pH, the primary building blocks formed earlier are being linked into three-dimensional structures largely by the hydrogen bonding of additional OH^- ions and Van der Waals interactions. This second stage in the precipitation process represents the actual nucleation and initial growth step. It should be noted that formation of the polynuclear species is not a necessity for precipitation because experiments have also been performed in which aluminum nitrate is titrated into a solution of base, as described previously.[9] In fact, ICET is such a configuration in that the aluminum is introduced into a very large excess of OH^-; therefore, polynuclear species probably will not be generated in such a configuration.

In this investigation, the phase transition was found to proceed according to $X = pH + pA_T$, where

$$pH = -\log[H^+] \quad (6)$$

and

$$pA_T = -\log[\text{total aluminum concentration}]. \quad (7)$$

In cases where $X < 12$, the transition of phases is amorphous-pseudoboehmite-bayerite, whereas if $12 < X < 12.55$, the phase transition will be pseudoboehmite-bayerite, and if $X > 12.55$, bayerite will be immediately formed.[9] Thus, in the ICET configuration, the value of X is 11.3 and will result in the initial formation of amorphous aluminum hydroxide.

Additional investigations have been performed on the transformation of aluminum hydroxycarbonate in aqueous solutions to address the mechanism of formation of crystalline aluminum species.[16] Aluminum hydroxycarbonate is actually amorphous aluminum hydroxide in which some carbonate anions substitute for surface hydroxyl

anions.[17] The findings of this investigation[16] indicate that when a suspension of aluminum hydroxide in water is aged at a pH of 7 or higher, it undergoes a two-step aging process: amorphous aluminum hydroxide transforms into poorly ordered boehmite (pseuoboehmite),[18] which in turn transforms into bayerite, the stable polymorph. It has also been shown that supersaturated aluminate solutions form the most-soluble phase first, become saturated with that phase, and subsequently form the next soluble phase.[9] This process precisely follows the Ostwald rule of stages. For example, a solution supersaturated with respect to amorphous $Al(OH)_3$, pseudoboehmite, and bayerite (phases in order of decreasing solubility) will first form the amorphous $Al(OH)_3$, then pseudoboehmite, and finally bayerite. Upon aging of the precipitate, amorphous $Al(OH)_3$ will convert first to pseudoboehmite, which will subsequently convert to bayerite.

The amorphous solid is initially high in both water and hydroxyl anion concentration. The rate of transformation to the more crystalline form is controlled by the rate at which hydroxyl anions replace water in amorphous solid.[15] Boehmite is formed by solid-state interparticle and intraparticle condensation/aggregation.[16] This reaction occurs as water is removed.[19] It has been proposed that a hydroxyl anion reacts topochemically with another hydroxyl anion in the amorphous solid. This reaction forms a water molecule and under neutral or alkaline conditions produces the aluminum oxyhydroxide known as boehmite.[9] It has also been shown that the solubility of poorly ordered boehmite determines the rate of nucleation and growth of the crystalline aluminum polymorphs.[20] Additional support for rapid precipitation and crystallization in neutral and alkaline media to produce bayerite has been provided.[21] Finally, the solubility of the system also decreases through the transition process.

Figure 27 and Figure 28 present the results of the investigation using commercial spray-dried aluminum hydroxycarbonate (SDAHC) in water.[16] The surface pH of the SDAHC was initially approximately 5. When the SDAHC was saturated with water, the surface pH was determined to be 10. This high surface pH is thought to cause SDAHC to age in the same fashion as aluminum hydroxide suspensions precipitated at a high pH or adjusted to a high pH.[10] These figures clearly illustrate the role of aging in the transformation of the initially amorphous material into crystalline material. A comparison of Figure 27 and Figure 28 also illustrates the importance of temperature in the kinetics of the transformation. As may be seen from Figure 28, the phase transformation at 50°C proceeds quickly, and the stable form is crystalline boehmite.

The transformation into bayerite is believed to occur at a pH of 10 because of the tight packing of the particles. The point of zero charge (PZC) of aluminum hydroxide is 9.6.[16] Thus, the net surface charge of SDAHC disappears as the surface pH reaches 10. The absence of a substantial surface charge allows the particles to form bayerite, the most tightly packed polymorph of aluminum hydroxide.

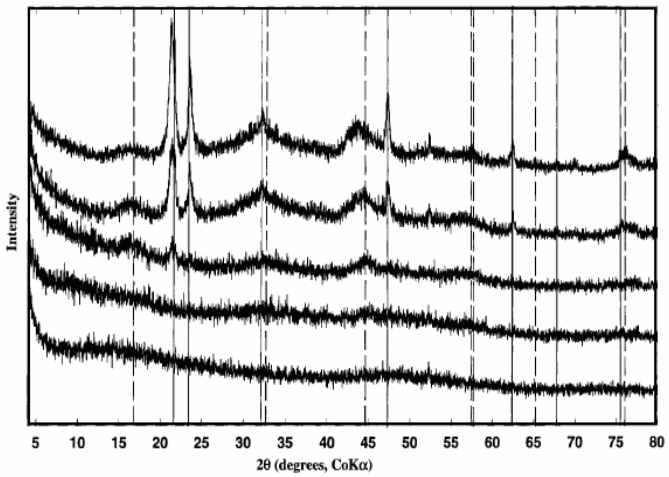

Figure 27. **X-ray diffractograms of SDAHC after it has aged at 100% relative humidity (RH) and 25°C for 0 days (bottom), 62 days (second from bottom), 118 days (middle), 215 days (second from top), and 384 days (top). Diffraction bands associated with boehmite or bayerite are represented by dashed or solid lines, respectively. [Used with permission of the publisher.*]**

.

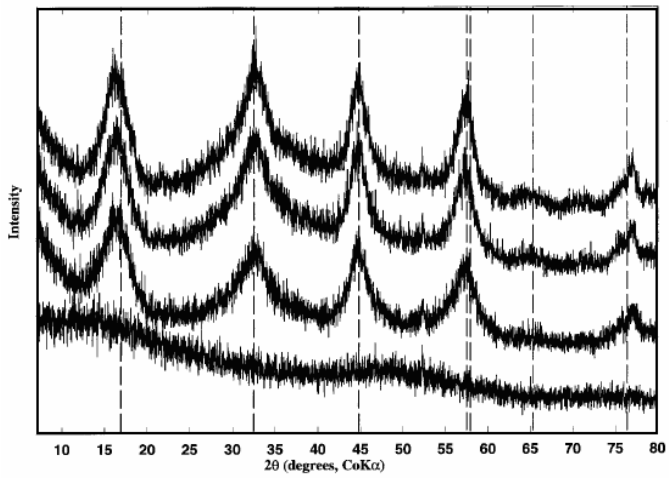

Figure 28. **X-ray diffractograms of SDAHC after it has aged at 100% RH and 50°C for 0 days (bottom), 6 days (lower center), 36 days (upper center), and 78 days (top). Diffraction bands associated with boehmite are indicated by dashed lines. [Used with permission of the publisher.*]**

Additional evidence of the phase transformation of amorphous aluminum hydroxide as a result of aging is provided by the infrared (IR) and XRD examination of amorphous aluminum hydroxide.[22] In this investigation, both IR and XRD measurements, Figure 29

* Reprinted from *Journal of Colloid and Interface Science*,, K. E. Hancock et al., "The Effect of Humidity on the Physical and Chemical Stability of Spray-Dried Aluminum Hydroxycarbonate," **183**:2, pp. 431–440, Copyright 1996, with permission from Elsevier.

and Figure 30, on aluminum hydroxide gel, produced by titrating ammonium into aluminum chloride solution to a pH of 7, were performed. In this pH regime, the experimentally observed phase is expected to be gibbsite. (By comparing the IR spectra results in Figure 29 to the O-H stretching and bending frequencies of crystalline aluminum phases in Table 8, transformation to the crystalline structure may be seen.) Further evidence of this transformation is also seen in the XRD diffraction lines in Figure 30.

Table 8. Characteristic Stretching and Bending Frequencies for Crystalline Aluminum Phases

Phase	Frequency cm^{-1}	
	OH Stretching Region	**O-H Bending Region**
Gibbsite	3612	1030
	3520	970
	3440	
	3395	
Bayerite	3650	1010
	3540	970
	3460	
Boehmite	3300	1150
	3095	1070

An examination of aluminum precipitation from supersaturated solutions showed that the rate of nucleation was determined largely by two parameters: the degree of supersaturation, Π, and the interfacial tension, σ.[9] Adsorption of lattice or foreign ions may (drastically) change the magnitude of the interfacial tension and thereby alter the rate of nucleation. Adsorption of surface-active species is also known to influence the rate and mechanism of crystal growth. The crystallization process may be retarded, or the crystal habit of the precipitate may change significantly[23] and the polydispersity of the product may be controlled by adding surface-active species to the supersaturated solution. Consequently, in the next two subsections, we examine the role of the anion/cation and organics in the phase behavior of aluminum.

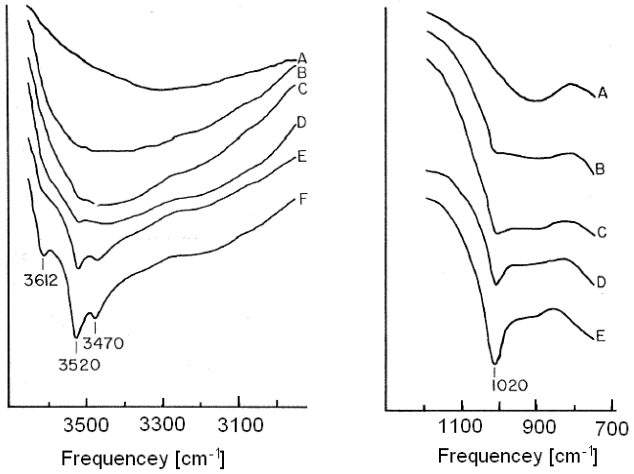

Figure 29. Change in the O-H stretching frequency region of the IR spectrum of aluminum hydroxide gel during aging at 25°C for (A) 5 days, (B) 42 days, (C) 54 days, (D) 61 days, (E) 69 days, and (F) 124 days. [Used with permission of the publisher.*]

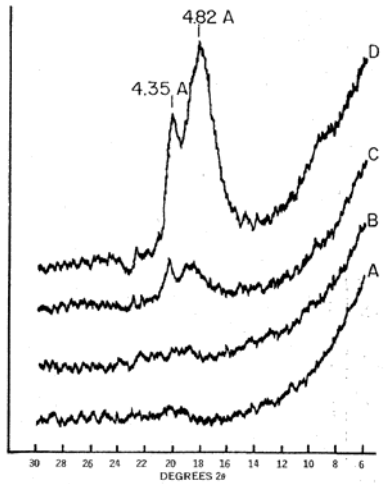

Figure 30. Change in XRD pattern of aluminum hydroxide gel during aging at 25°C for (A) 57 days, (B) 65 days, (C) 71 days, and (D) 124 days. [Used with permission of the publisher.*]

4.3. General Cation/Anion Effects on the Aluminum Phase

In the previous section we examined the phase transformation behavior of aluminum in aqueous solutions due to aging. From this section we observed that the aging of the precipitate generally led to the formation of more crystalline material. However, the measured aluminum concentrations of the Tests 1 and 5 solutions, accompanied by the

* Reprinted from *Journal of Pharmaceutical Sciences,* Nail, S. L., et al., "Comparison of IR Spectroscopic Analysis and X-Ray Diffraction of Aluminum Hydroxide Gel," **64**:7, pp. 1166-1169, Copyright 1975.

XRD analysis of the wet precipitate obtained after draining the Test 1 tank solution while allowing it to cool, reveal a mostly amorphous form with a detectable crystalline structure of only sodium pentaborate (a sodium/boron compound). Consequently, in this section we seek to explain the persistence of the aluminum amorphous phase.

When an aluminum hydroxide solid is prepared by precipitation from an aluminum salt solution, a highly random structure is formed. Anions present during precipitation are absorbed by the aluminum hydroxide gel and are believed to be important in stabilizing the colloidal system. Studies have shown that the crystallization of gibbsite from amorphous aluminum hydroxide can be greatly inhibited by the presence of sulfate,[24] silic acid,[25] and citric acid.[26] Nitrate has a rather weak effect, and perchlorate has no effect at all.[27] Figure 31 illustrates the mechanism of anion interference to crystallization.[28]

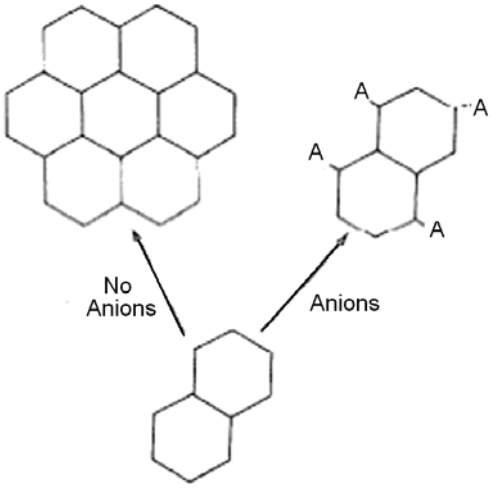

Figure 31. Possible pathways for polymerization of $Al(OH)_3$. [Used with permission of the publisher.*]

Based on the adsorption capacity of aluminum hydroxide for several anions at different pH conditions, three types of anion adsorption have been proposed.[29] (A relatively high degree of adsorption of anions occurs when aluminum hydroxide gel is precipitated at pH conditions <9.2, its PZC.) Nonspecific adsorption was suggested for anions such as nitrate, chlorate, and chloride, which are loosely held in the diffuse layer and therefore are adsorbed only by positively charged surfaces. Specific adsorption of anions of completely dissociated acids, such as sulfate and fluoride, is based on chemical adsorption and involves ligand exchange with surface water. A third type of adsorption is the specific adsorption of incompletely dissociated acids such as phosphate and silicate.[29]

* Reprinted from *Soil Sci Soc Am J*, Beyrouty, C. A., et al., "Evidence Supporting Specific Adsorption of Boron on Synthetic Aluminum Hydroxides," **48**:2, 284–287, Copyright 1984, with permission from ASA-CSSA-SSSA.

IR spectroscopy has proven useful in determining if the ligands are within the coordination sphere.[30] IR spectroscopy studies have been performed using aluminum hydroxide gels prepared by stirring 1.9 M NaOH into the respective aluminum salt solution (0.25 M) until a pH of 6.5 was obtained. The influence of carbonate and bicarbonate also has been studied.[31] The freshly precipitated aluminum hydroxide gels were air dried and examined by XRD and found to be amorphous.

Gels produced with the nitrate anion show a nitrate band split in the aluminum hydroxide gel appearing at 1395 and 1350 cm^{-1}, as compared with the undisturbed 1358 cm^{-1} IR band.[28] The splitting of the nitrate band indicates that some perturbation occurs when the nitrate anion is incorporated into the aluminum hydroxide gel. It has been observed that the ν^3 vibration splits into two new frequencies when the nitrate anion has a lowered symmetry due to the perturbation.[32] The magnitude of the split appears to increase as the dissymmetry occurs. Based on previous observations, the relatively small degree of splitting observed for the nitrate anion in the aluminum gel, 45 cm^{-1}, indicates an electrostatic interaction in which the nitrate anion is outside the coordination sphere of the aluminum cation.[32] This observation is in good agreement with the nonspecific adsorption attributed to this anion.[29]

The affinity of the carbonate anion for the aluminum cation is evidenced by the presence of carbonate in reactive aluminum gel.[33] The IR spectra of the carbonate-containing aluminum hydroxide gel indicate that the carbonate anion is in a state of lower symmetry.[31] The adsorption at 1090 cm^{-1} in the carbonate-containing aluminum hydroxide gel is active only in the Raman when the carbonate anion has full symmetry. In addition, the ν^3 vibration splits into two new adsorption bands at 1500 and 1435 cm^{-1}.[31] The nature of the carbonate-to-aluminum bond in aluminum hydroxide gel can be inferred by comparison with carbonate complexes and carbonate surface oxides.[34] The magnitude of the splitting, 115 cm^{-1}, indicates that the carbonate anion is directly coordinated to the aluminum cation; therefore, specific adsorption is indicated.[28]

Figure 32[35] is an electron micrograph illustrating the role of the anion PO_3-in retarding the formation of crystalline growth. It appears that the primary particles aggregate to form larger secondary particles. This micrograph appears similar to the Test 1 micrographs depicted in Figure 21 through Figure 24. Thus, it may be concluded that many anions interfere with $Al(OH)_3$ crystallization. The interference is influenced by many factors, including the anion-aluminum stability constant, the anion ionic size and structure, and the anion concentration.[21]

Studies also have been conducted to investigate the role of organics in the crystallization of aluminum. Experiments conducted to examine the effect of small concentrations of citric acid showed that the effect was to reduce the amount of precipitate at ambient temperature. Analysis of the precipitate revealed an amorphous material.[27] It has been found that citric acid retards the crystallization of aluminum.[27] The noncrystalline nature of the precipitate apparently was due to the occupation of coordination sites of aluminum ions by citric acid on dissociation of the proton, resulting in a distortion in the arrangement of the hexagonal ring units normally found in crystalline aluminum

hydroxides. Crystalline behavior became apparent only with sufficient OH^- and with aging.

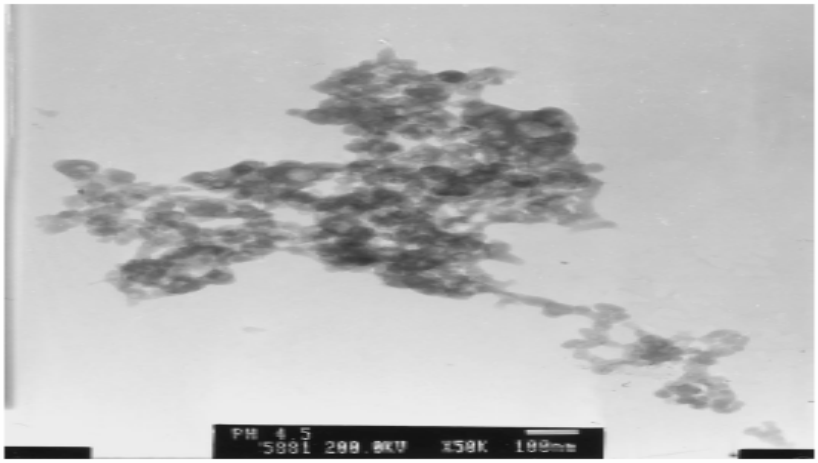

Figure 32. Electron transmission micrograph of aluminum adjuvant precipitated at pH = 4.5 in the presence of phosphate. [Used with permission of the publisher.*]

It has been suggested that the retardation of crystalline behavior was the result of activity at the solid/solution interface.[36] Adsorption of the citrate also can lead to changes of the surface charge and interfacial tension and can influence the kinetics of numerous elementary steps involving the incorporation of the growth unit from the solution into the growing solid phase.[31] However, the principal effect was suggested to be the occupation of certain surface sites, which caused the growth unit to be blocked.[29]

Additional experiments have been conducted in which small quantities (0–50 mg) of fulvic acid (FA) were added to aluminum chloride solutions, 450 ml of a 10^{-3} M solution.[10] (FA resembles citric acid in that it contains CO_2H and aliphatic OH groups; it resembles quercetin in that it also contains phenolic hydroxyl and ketonic C=O groups. It is through these functional groups that FA can form stable complexes with aluminum.) The solutions were then titrated with 0.1 M NaOH to raise the pH to 6, 8, and 10. It was found that FA inhibited the formation of gibbsite at a pH of 6, leading to the formation of pseudoboehmite. In systems with a pH of 10, the addition of as little as 0.0125 mg/L of FA was sufficient to prevent the formation of any precipitate.[10] A simple explanation may be that at a pH of 10, the surface of the aluminum and FA are both negative such that electrostatic repulsion between the two components appears responsible for the lack of precipitation.

* Reprinted from *Vaccine*, L. Burrel, "Aluminum Phosphate Adjuvants Prepared by Precipitation at Constant pH: Part 2, Physicochemical Properties," **19**:2-3, p. 282, Copyright 2001, with permission from Elsevier.

In summary, we have seen that the presence of certain organic and inorganic agents, even in small quantities, is sufficient to modify the solubility of aluminum and also preclude crystallization. In the next section we investigate the effect of boron.

This page intentionally left blank.

5. ALUMINUM-BORON COMPLEX

Boron is present within the Test 1 solution at concentrations approaching 2800 mg/L. We have previously noted that the precipitate that formed on cooling the ICET solution had a high weight percentage of boron. Consequently, an examination of the interaction of boron in solutions containing aluminum in conjunction with sodium hydroxide is warranted. To this end, research has been conducted on the role that boron may play in the formation of complexes, the determination of the solubility of aluminum, and the adsorption of boron onto aluminum surfaces.

5.1. Boron Behavior in the Solution

Boric acid is a Lewis acid and hydroxyl acceptor that through hydrolysis produces a change in coordination from planar to tetrahedral.[37] The dissociation constant, pKa, for boric acid is 9.24, and therefore boric acid exists predominantly as undissociated boric acid [$B(OH)_3$] in dilute aqueous solution below a pH of 7. Above a pH of 10, the metaborate anion $B(OH)_4$ becomes the main species in solution. Between a pH of 6 and 11 and at high concentration (>0.025 mol/L), highly water-soluble polyborate ions such as $B_3O3(OH)_4^-$, $B_4O_5(OH)_4^{2-}$, and $B_5O_6(OH)_4^-$ may be formed.[37]

Calculation of the aqueous solution chemistry of boron is generally confined to hydrolysis because of the lack of thermodynamic data for aqueous cation complexes containing boron. Only one paper reports thermodynamic data for the aluminum boron complex.[38] These data have drawn critical comments from several sources.[39] Furthermore, the kinetic data have been unsuccessful in explaining the appearance of a white amorphous precipitate that appeared in testing an Al = 0.005 M and B = 0.04 M solution titrated with sodium hydroxide.[40] This experimental finding is consistent with the white precipitate that was observed in the benchtop test performed. In addition, ^{27}Al and ^{11}B NMR measurements previously were unable to detect chemical complexes at either pH = 2 or pH = 12.[37] However, ^{27}Al and ^{11}B solid-state NMR measurements performed at Los Alamos National Laboratory (LANL) on the Test 1 precipitate revealed the presence of increased coordination between aluminum and boron (as shown in Figure 33) as the temperature of the solution was reduced from 60°C to room temperature.

A previous investigation also revealed that aluminum borate complexes are present at 25°C.[41] The ^{27}Al spectra performed at pH = 9 in Al-B solutions with B = 0.02 M show the presence of two peaks at 80.5 and 74.5 ppm, which correspond to $Al(OH)_4^-$ and a single substituted dimmer, $Al(OH)_3OB(OH)_2$. In 0.08- and 0.2-M borate solutions, a third peak appeared at 68.5 ppm, which could be assigned to the trimmer, $Al(OH)_2O_2(B(OH)_2)_2^-$. Solubility studies were also performed that allowed for the determination of the equilibrium constant for the dimmer reaction

$$Al(OH)_4- + B(OH)_{3\ aq}^{o} = Al(OH)_3OB(OH)_2^- + H_2O\ . \qquad (8)$$

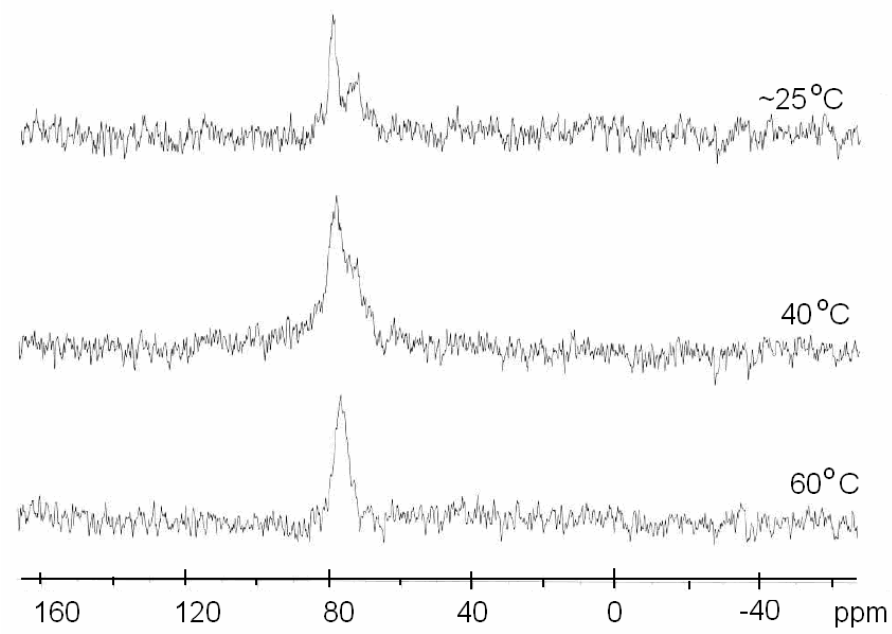

Figure 33. **The ^{27}Al nuclear magnetic resonance (NMR) of benchtop aluminum nitrate/boron/sodium hydroxide solution at pH = 9.5 at 60°C, 40°C, and 25°C after 4 weeks of aging.**

Furthermore, the temperature dependence for the equilibrium constant has been found to be

$$\log K = 241.94\ (+-130.7)/T(K) + .81(+-.36)\ .$$

At 25°C, Log K was found to be 1.62.

The impact of the aluminum borate complex on the equilibrium has been shown to lead to significant solubility in aluminum (up to factors of 6) for both gibbsite and boehmite.[38] Future equilibrium calculations for the ICET configuration must include the borate complex to determine the important effects of the presence of borate in the solution on the aluminum solubility.

Aluminum borates were synthesized by a precipitation process in which dilute solutions of aluminum nitrate nonahydrate $Al(NO_3)_3{:}9H_20$ and boric acid were precipitated into a basic solution of ammonium carbonate; the resulting mixture was evaporated to dryness. It was found that until excessive heating was applied, the material was largely amorphous in nature.[42,43,44] The amorphous nature of the precipitate from the Test 1 solution has also been confirmed via XRD at LANL. As previously discussed, the temperature of the precipitation may affect the quantity of boron absorbed.

5.2. Boron Adsorption

In a study of the adsorption of boron onto aluminum hydroxide surfaces, a solution was synthesized by the dropwise addition (~2 ml min^{-1}) of 0.5 M NaOH (the base typically contained 0.75 M H_3BO_3) into 100 ml of 0.5 $AlCl_3$ until the pH was 7.0. The solution was then analyzed using IR analysis,[24] and the boron content, with respect to the $Al(OH)_3$, was then determined. It was found that the boron present in the gel was held predominantly on the hydroxide surface as a specifically absorbed ion. This mechanism of anion exchange with hydroxyl ions led to specific surface adsorption.[45] Specific adsorption of anions produced a shift in the ZPC of the mineral to a more-acid value. Furthermore, aging studies were conducted, and it was found that the adsorption of boron onto the aluminum surface precluded crystallization.

Figure 34 presents the IR results obtained as a result of aging the aluminum hydroxide gels.[28] As may be seen, the commercially prepared hydroxide shows three well-resolved peaks in the OH stretching region at 3605 cm^{-1}, 3510 cm^{-1}, and 3450 $cm^{-1}$and a doublet at 3380 $cm^{-1}$and 3360 cm^{-1}. These bands are characteristic of gibbsite, as may be seen from a comparison with Table 8. The 13-day-aged solution without boron also shows evidence of a high degree of structural order. These peaks indicate a gibbsite and bayerite mixture, as seen from Table 8. In contrast, the aged boron containing hydroxide exhibited a very broad adsorption band in the OH stretching region, centering at 3420 cm^{-1}. The absence of any sharp peak confirms the hypothesis that boron was held directly on the hydroxide surface, thereby inhibiting the polymerization process.

Identification of the boron absorbed onto the amorphous aluminum hydroxide was obtained by examining the IR spectra in the 800- to 1500-cm^{-1} region. Although the 1020-$cm^{-1}$and 965-cm^{-1} adsorption bands are not present in the gel with boron, two broader peaks appear at 1060 cm^{-1} and 900 cm^{-1}. In addition, two new bands have also appeared at ~1415 $cm^{-1}$and 1300 cm^{-1}.[28]

Another means by which to evaluate the adsorption of an ion is the change in the PZC. The PZC is defined as the pH at which the net surface charge is zero or cation exchange capability minus anion exchange capacity equals zero. Specific adsorption of an anion makes the surface to which it is adsorbing more negatively charged. This specific adsorption produces a shift in the PZC to a more acidic value. Specific-adsorbed ions are ions held in inner-sphere surface complexes that contain no water between the adsorbed ion and the surface functional group. Kinetic experiments using pressure-jump-relaxation have also been used to confirm that boron adsorbs as an inner-sphere complex on aluminum oxide via a ligand exchange of borate with surface hydroxyl groups.[46] The PZC for the $Al(OH)_3$ free of any specifically adsorbed anions is 9.72, whereas for the boron-containing gel, the PZC was found to be 7.57–8.14.[28]

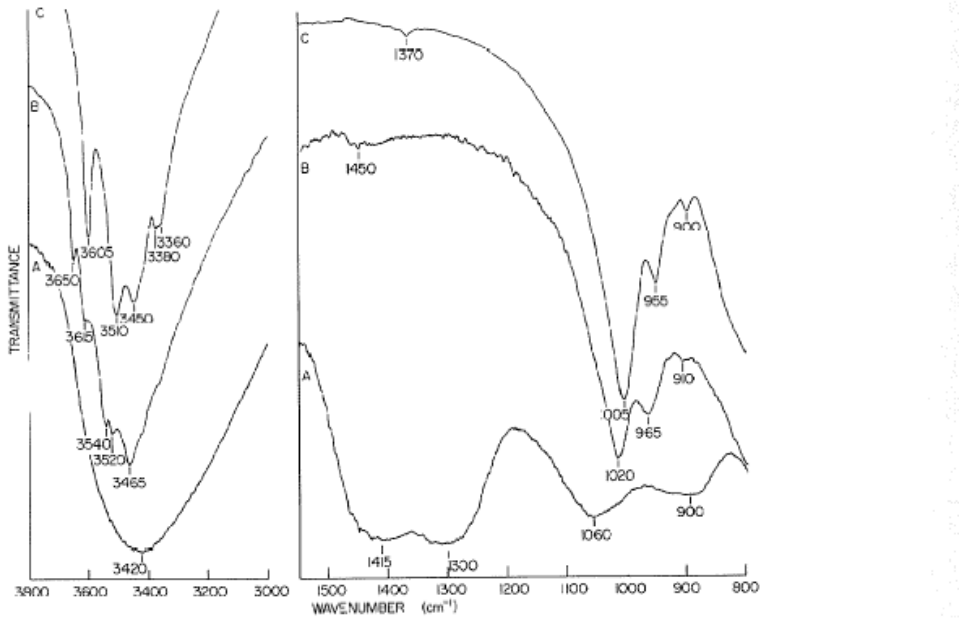

-Spectra of (A) $Al(OH)_3$ with B (89 d old); (B) $Al(OH)_3$ prepared without B (13 d old); and (C) commercially prepared $Al(OH)_3$.

Figure 34. Spectra of (A) $Al(OH)_3$ with boron (89 days old), (B) $Al(OH)_3$ prepared without boron (13 days old), and (C) commercially prepared $Al(OH)_3$. [Used with permission of the publisher.[*]]

In another study on the adsorption of boron onto amorphous aluminum hydroxide, attenuated total reflectance Fourier transform infrared spectroscopy (ATR-FTIR) was used.[47] The study of aqueous solutions of metal ligand systems by conventional IR spectroscopy is limited because water absorbs energy in several areas of the IR spectrum, resulting in very strong, broad bands in the regions of 3650–2930, 1720–1580, and 930–400 cm^{-1}. To minimize this, it is necessary to use solutions of high concentrations in cells with very short optical path lengths, which results in poor band resolution. ATR-FTIR overcomes the conventional IR spectroscopy limitation and allows an IR spectrum of an aqueous solution of a metal ligand to be observed.[48] It was found that trigonal B asymmetric bands shifted to higher frequencies and indicated that both $B(OH)_3$ and $B(OH)_4^-$ were absorbed via a ligand exchange mechanism.[47]

The adsorption of boron onto amorphous aluminum hydroxide surfaces has been previously studied and found to depend on both the pH and temperature.[47] In Ref. 47, 0.25 g of amorphous aluminum hydroxide was added to a 30-ml centrifuge tube and equilibrated with 12.5 ml of 0.1 M NaCl containing ~0.462 mmol/L of boron. The suspension was then pH adjusted with either 1.0 M HCl or NaOH. The addition of HCl or NaOH caused a <8% change in the final volume. The supernatant was separated by

[*] Reprinted from *Soil Sci Soc Am J*, Beyrouty, C. A., et al., "Evidence Supporting Specific Adsorption of Boron on Synthetic Aluminum Hydroxides," **48**:2, 284–287, Copyright 1984, with permission from ASA-CSSA-SSSA.

centrifugation for 30 minutes at 25°C and 5°C, analyzed for pH, and then filtered through a 0.1-mm filter. The boron concentration was determined using a Technicon autoanalyzer and the azomethine H method.[49] The total boron adsorbed was the difference between the total boron added, indicating that the boron remained in solution. Results of this study are depicted in Figure 35.[47] As may be seen in this figure, the decreasing temperature favors adsorption. This decrease occurs mainly because increasing temperature decreases the PZC.[50] A decrease in PZC renders the surface more negative at a given pH and therefore decreases the adsorption of anions. Adsorption is maximized onto high-surface-area materials. The adsorption results at low temperature are also consistent with the ^{27}Al measurements, which indicates that complexation between aluminum and boron is favored at low temperature.

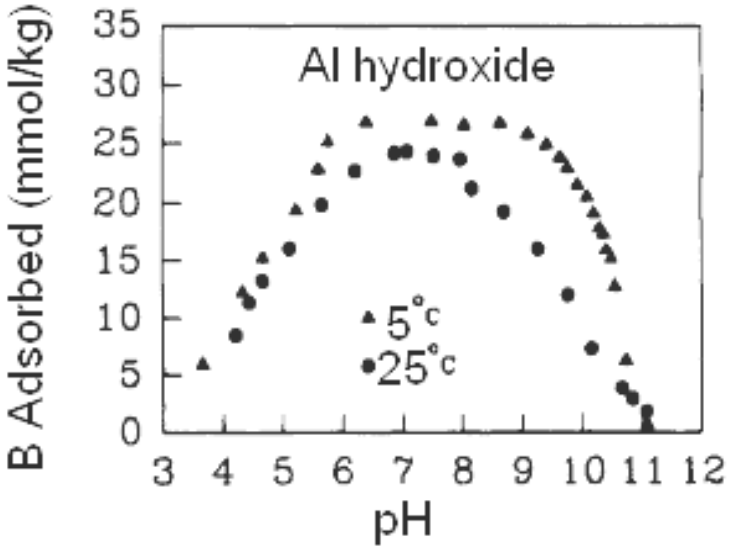

Figure 35. Absorbed boron as a function of pH at 25°C and 5°C. [Used with permission of the publisher.*]

ATR-FTIR spectra for boric acid as a function of pH and total boron concentration are given in Figure 36.[47] The broad bands at 1410 and 1148 cm^{-1} are assigned to the B-O asymmetric stretching of triaganol boron and to B-OH in the plane bending of trigonal boron. These bands are seen to increase in intensity with increasing boron concentration. At a pH of 9, which is near the pKa for the monomeric boron species, roughly half of the total boron is in the form of $B(OH)_3$ and half is in the form of the $B(OH)_4^-$ anion. The band at 955 cm^{-1} is assigned to the asymmetric stretching of tetrahedral boron, and the broad band at 1154 cm^{-1} is a mixture of B-OH bending of both trigonal and tetrahedral boron. Based on the above data, the most useful diagnostic bands are at 1410 cm^{-1} for

* Reprinted from *Environmental Science Technology*, C. Su and D. L. Surez, "Coordination of Adsorbed Boron: A FTIR Spectroscopic Study," **29**, p. 302, Copyright 1995, with permission from The American Chemical Society.

asymmetric stretching of triagonal boron and at 955 cm^{-1} for asymmetric stretching of tetrahedral boron.

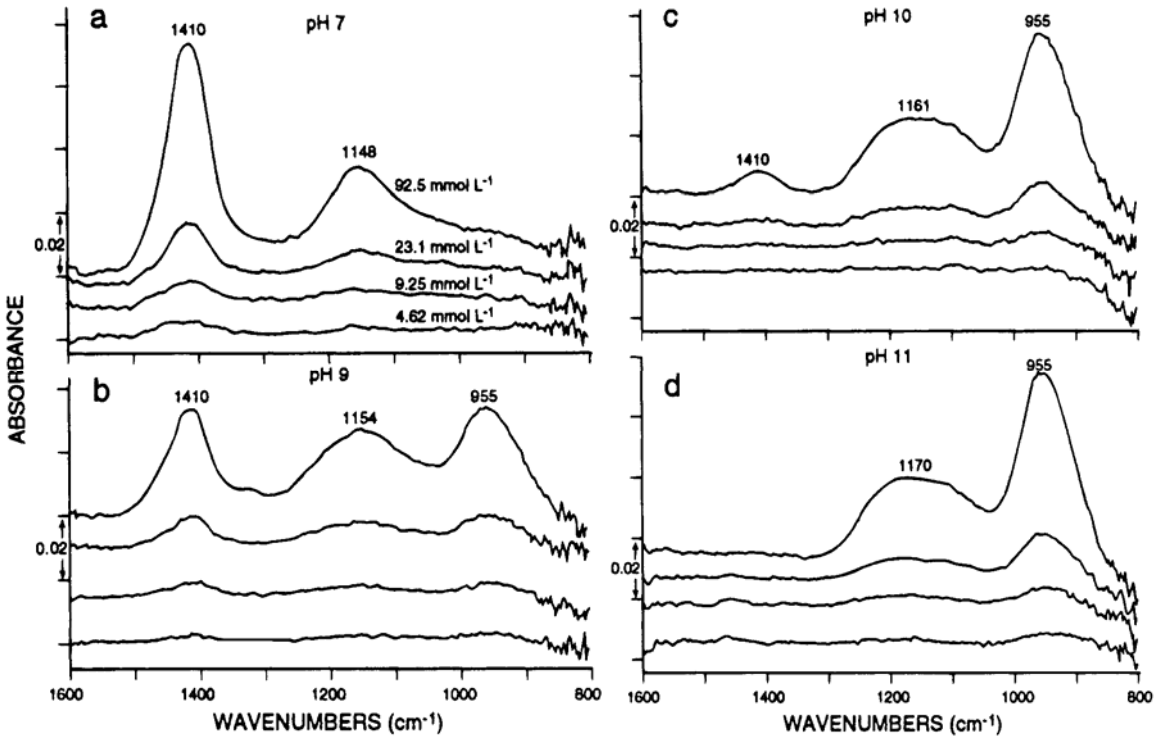

Figure 36. ATR-FTIR spectra of aqueous boric acid as a function of pH and total boron concentration. Each spectrum is the difference between the sample (boric acid in 0.1 M NaCl at each pH) spectrum and the reference (0.1-M NaCl solution) at the same pH. [Used with permission of the publisher.*]

.

Figure 37[47] presents the absorbance spectra for pH = 6.8 and 10.2 aluminum-boron solution for three initial boron concentrations: 4.62, 9.25, and 23.1 mmolL. The concentrations indicated in the figures are given for the equilibrium solution concentrations. Thus, boron is strongly absorbed, ~70% at 5°C. The spectra indicate the presence of triagonal boron, 1420 cm^{-1} and 1280 cm^{-1}. The bands were shifted to higher frequencies than for the pure boric acid (1410 cm^{-1} and 1148 cm^{-1}) at a pH of 7. This shift is probably due to the strengthening of the O-B and B-OH bonds in the surface complex Al-O-$B(OH)_2$ when the boric acid molecule is complexed with surface functional groups such as Al-OH. Thus, at a pH of approximately 7, the trigonal boron is the primary species absorbed.

* Reprinted from *Environmental Science Technology*, C. Su and D. L. Surez, "Coordination of Adsorbed Boron: A FTIR Spectroscopic Study," **29**, p. 302, Copyright 1995, with permission from The American Chemical Society.

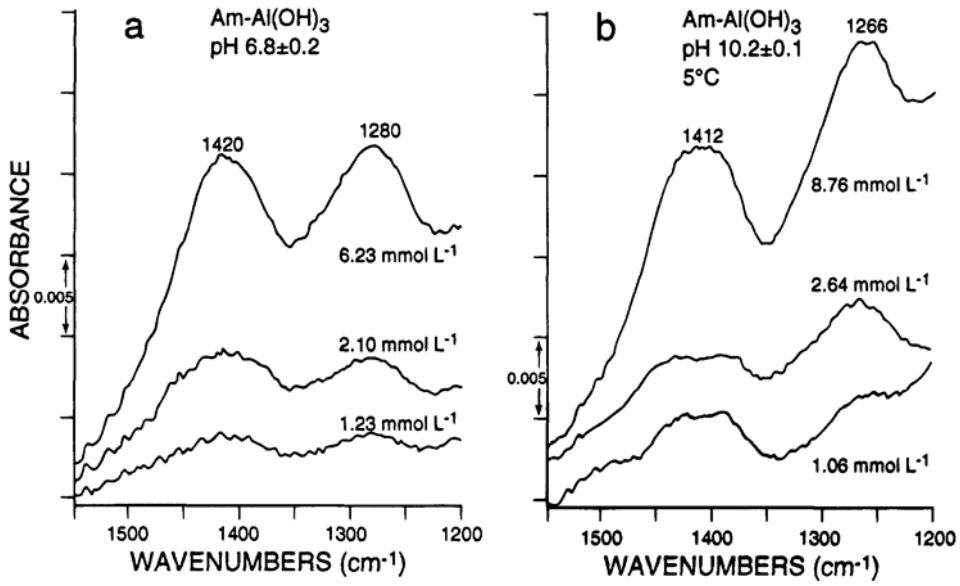

Figure 37. ATR-FTIR spectra of am-Al(OH)$_3$ at (a) 25°C at pH = 6.8 and (b) 5°C at pH = 10.2. [Used with permission of the publisher.[*]]

At a higher pH, the B-O asymmetric stretching of triagonal boron is not significantly shifted compared with 1410 cm^{-1} for pure boric acid. However, the B-OH bending of the triagonal boron band resulted in a narrower width and a higher wave number of 1266 cm^{-1} from 1148 cm^{-1} due to the complexation on the amorphous aluminum hydroxide.[47]

Attempts to characterize the tetrahedral boron failed due to severe band interference in the range of 1000-900 cm^{-1} from the Al-O bond, which has a strong absorbance at 969 cm^{-1}. Although the tetrahedral boron is the dominant species at pH = 10.2 in aqueous solution, it need not be the dominant absorbed species on amorphous aluminum hydroxide due to the negative charge on the solid surface at this pH. The appearance of the triagonal boron on the surface of the amorphous aluminum hydroxide at a pH of 10.2 suggests that the neutral B(OH)$_3$ species could be preferred because its higher affinity for the negatively charged surface of the amorphous aluminum hydroxide is higher than it is for the borate ion, which would experience charge repulsion.[47] (That is, at this pH, the surface charge on the amorphous aluminum hydroxide is negative.)

Several surface complexation models are available to describe the adsorption of boron onto aluminum surfaces. These chemical models provide a molecular description of adsorption using an equilibrium approach with mass action and mass balance equations. In these models, boron adsorption occurs via complex formation with surface hydroxyl groups on aluminum. Surface complexation models define surface species, chemical

[*] Reprinted from *Environmental Science Technology*, C. Su and D. L. Surez, "Coordination of Adsorbed Boron: A FTIR Spectroscopic Study," **29**, p. 302, Copyright 1995, with permission from The American Chemical Society.

reactions, mass balance, and charge balances and calculate thermodynamic properties such as activity coefficients and equilibrium constants. Two models that are particularly well suited for studying boron's adsorption onto amorphous aluminum hydroxide surfaces are the constant capacitance model and the triple-layer model.

The constant capacitance model of the oxide aqueous solution interface has been applied to describe boron adsorption on aluminum.[51] In the constant capacitance model, anion adsorption is assumed to occur via a ligand exchange mechanism with the reactive surface functional group, AlOH; no surface complexes are formed with ions in the background electrolyte. Specifically adsorbed ions reside in the surface plane of adsorption, along with protons and hydroxyl ions. (In some cases, chemically unrealistic values of the protonation-dissociation constants were obtained, potentially reducing the chemical significance of the model application.[52])

The triple-layer model has also been applied to describe boron adsorption on aluminum.[52] In contrast with the constant-capacitance model, the triple-layer model allows anion adsorption to occur specifically via ligand exchange or nonspecifically through the formation of outer-sphere surface complexes with the reactive surface functional group, AlOH. Outer-sphere complexes contain at least one water molecule between the adsorbing ion and the surface functional group. The triple-layer model always includes outer-sphere complexation reactions for ions of the background electrolyte. Surface reactions, equilibrium constants, mass balance, and charge balances for the application of the triple-layer model are provided in Goldberg.[53] However, it has been found that only the inner-sphere adsorption mechanism could successfully describe both equilibrium and pressure jump kinetic data using the triple-layer model.[46]

Desorption of boron may be explained by various mechanisms, including ligand exchange, formation of bidentate surface complexes, and incorporation into lattices. Ligand exchange is reversible with respect to pH changes; however, anion desorption at constant pH exhibits varying degrees of irreversibility.[54]

In conclusion, if amorphous-phase aluminum is indeed present, as both XRD and TEM analyses would indicate in Test 1, then it is not surprising that significant boron would be found in the precipitate as a result of the adsorption of boron from the solution during the cooling process. As indicated from the ICP results, up to 35% of the boron from the initial solution may have been adsorbed onto the amorphous aluminum hydroxide precipitate. This degree of adsorption is certainly feasible. In fact, if we use the data from Su and Surez[47] at a pH of ~9.5, a boron adsorption of ~35% is predicted. It must be emphasized that we have shown that the complexation of aluminum and boron is dependent on the temperature. Consequently, if precipitate were to have formed during the course of Test 1, the appearance of boron would probably not have been found in the precipitate. Thus, it is reasonable to assume that precipitation of aluminum did not occur during Test 1 and was produced only via the cooling process. Finally, the inclusion of boron in the inner sphere of the tetrahedral aluminum has been shown at even very low Al to B ratios (~20) to preclude crystallization of aluminum, even when calcined to 500°C.[44]

6. PARTICLE SIZE DISTRIBUTION

Aluminum behavior, such as solubility in an alkaline solution, is a function of the particle size distribution, which is affected by the aluminum hydroxide phase and the organic elements. In Section 2.9 we observed that colloids were present in aged Test 1 solution that had cooled to room temperature. In this section we briefly review the previous investigations of particle size measurements in alkaline aluminum systems at room temperature.

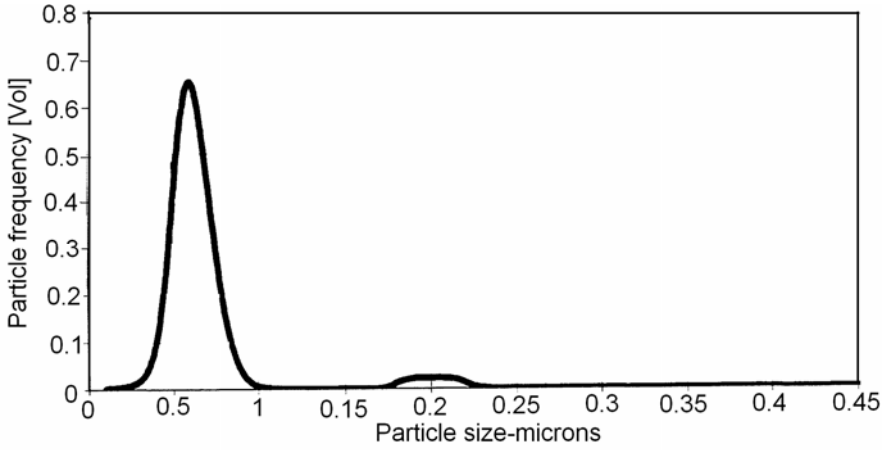

Figure 38. Particle size for aluminum in pH = 4.5 solution. [Used with permission of the publisher.[*]]

Previous investigations into the particle size distribution of aluminum have been made using DLS, small-angle x-ray scattering (SAXS), and acoustic techniques.[8,55,56] A typical particle size distribution, obtained using an acoustic technique for alumina used in chemical mechanical planarization (CMP) at a pH of 4, is given in Figure 38.[55] The mean particle radius was determined to be ~65 nm at ambient temperature, as shown in the figure.

The particle size distribution shown in Figure 38 is representative of particles that are very stable against aggregation because they repel one another. The stability of particle dispersion will depend on the balance of the repulsive and attractive forces that exist between particles as they approach one another. If all particles have a mutual repulsion, the dispersion will remain stable. However, if the particles have little or no repulsive force, some instability mechanism will eventually occur, e.g., flocculation or aggregation.

The degree of particle repulsion can be measured using a zeta potential. The zeta potential of a particle is the overall charge that the particle acquires in a particular medium. The magnitude of the measured zeta potential is an indication of the repulsive

[*] Reprinted from *ACS Symposium Series*, T. Oja et al., "Acoustic Analysis of Concentrated Colloidal Systems," **881**, pp. 231–248, Copyright 2002, with permission from The American Chemical Society.

force that is present and can be used to predict the long-term stability of the product. If all particles in suspension have a large negative or positive zeta potential, they will tend to repel each other, and the particles will have no tendency to come together. However, if the particles have low zeta potential values, no force would prevent them from coming together and flocculating.

At the pH at which the particle size distribution was measured in Figure 38, pH = 4.5, the zeta potential was large and thus the distribution was stable. As the pH was raised by adding base, such as NaOH, the electrical barrier was lowered from a large positive value to zero at around 9.0 and then to a negative potential at a high pH, i.e., >9. At a high pH, the system was again stable against further aggregation. Figure 39 demonstrates the dependence of particle size on the pH.[55]

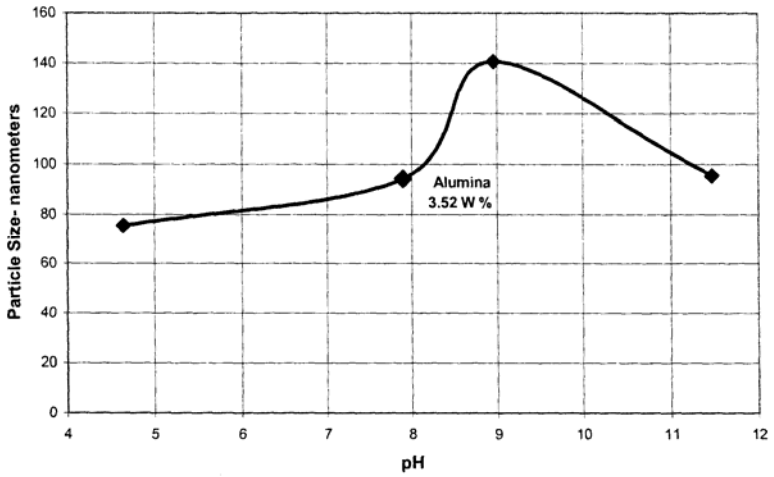

Figure 39. Particle size versus pH for aluminum at ambient temperature. [Used with permission of the publisher.*]

Dynamic studies of the particle size have also been conducted using quasi-elastic light scattering.[57] In these investigations, it was found that in solutions of aluminum chloride, large particles that were quickly formed subsequently shrank until sufficient hydroxide was added, as shown in Figure 40.

* Reprinted from *ACS Symposium Series*, T. Oja et al., "Acoustic Analysis of Concentrated Colloidal Systems," **881**, pp. 231–248, Copyright 2002, with permission from The American Chemical Society.

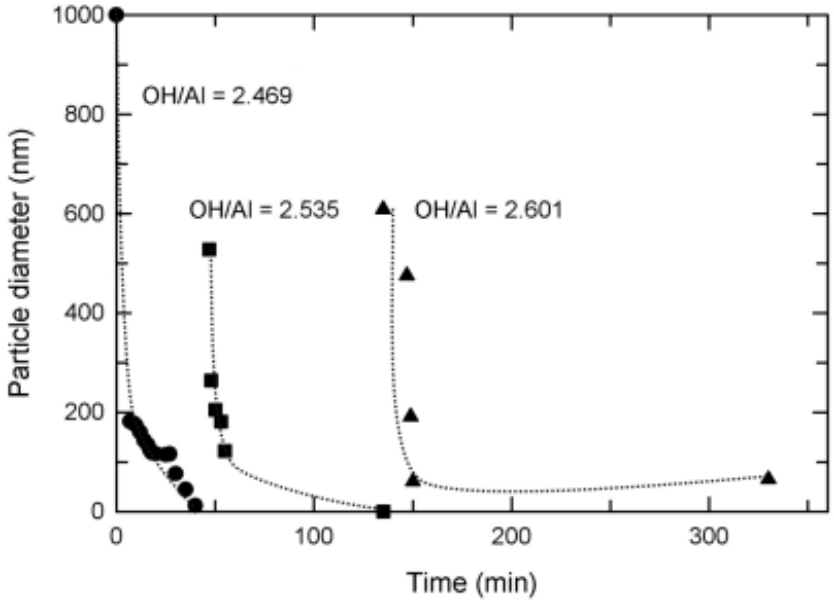

Figure 40. Particle growth dynamics in aluminum chloride solutions as a function of time for various OH/Al ratios at ambient temperature. [Used with permission of the publisher.[*]]

Particle size investigations have also been conducted using SAXS.[58] In nitrate and chloride solutions with concentrations of 0.25 M Al, with a pH of 7–9.8, the average radius and thickness of the particles were determined to be 880 Å and 50 Å, respectively. At reduced concentrations of 0.005 M Al, the radius and thickness of the particles were found to be ~200 Å and 40 Å, respectively. The "platelet" shape that was assumed in the analysis was found to be representative of aged, dried gels; gibbsite, as well as boehmite, has a tendency to form platelets.

[*] Reprinted from *Languir*, D. Dabbs and A. Aksay, "Precipitation and Deposition of Aluminum-Containing Phases in Tank Wastes," **21**, pp. 11690–11695, Copyright 2005, with permission from The American Chemical Society.

This page intentionally left blank.

7. ALUMINUM SOLUBILITY IN ALKALINE SOLUTION

Previously, it was noted that aluminum at concentrations comparable to the Test 1 system formed on cooling but that no precipitates were observed at 60°C during the test. (However, it should be mentioned that a precipitate was observed after several weeks while the solution was being stored in an oven.) To assist in the understanding of this system, we examine the solubility of aluminum in alkaline systems to understand the sensitivity of the aluminum solubility with respect to pH and temperature.

7.1. Predictions of Aluminum Solubility in Alkaline Solutions

The aluminum solubility in alkaline solution is determined by the dissolving reaction of the aluminum hydroxide [Eq. (1)], where the equilibrium is a function of aluminum hydroxide phase. Therefore, the solubility product for Eq. (1) is very dependent on the aluminum hydroxide solid phase. For amorphous aluminum hydroxide, a solubility product of $10^{-31.2}$ at 25°C has been reported, whereas for gibbsite, a solubility product of $10^{-33.9}$ has been reported.[59] Differences in identifying the controlling phase of the precipitate have led to discrepancies in the predicted solubility of aluminum species.

In alkaline or acidic solution, aluminum can exist as the following forms: Al^{3+}, $Al(OH)_4^-$, $AlOH^{2+}$, and $Al(OH)_2^+$. In an equilibrium solution, the following three reactions are in their equilibriums:

$$Al^{3+} + H_2O = AlOH^{2+} + H^+, \quad (9)$$

$$Al^{3+} + 2H_2O = Al(OH)_2^+ + 2H^+, \quad (10)$$

and

$$Al^{3+} + 4\,H_2O = Al(OH)_4^- + 4H^+. \quad (11)$$

The equilibrium data for the above reactions can be found in Ref. 11. The equilibrium solubility of different forms and the corresponding total aluminum concentration in the solution are shown in Figure 41.[59] The figure indicates that the main form is $Al(OH)_4^-$ in alkaline solution, whereas the aluminum ions are not stable. A comparison of Figure 41a and Figure 41b indicates that the amorphous aluminum hydroxide yielded soluble concentrations that were significantly larger than the concentrations for the crystalline gibbsite. The total aluminum concentration approached its smallest value near the neutral point and increased with an increasing pH in alkaline solution and decreased with pH increasing in acidic solution. The figure can be used to predict the aluminum concentration at 25°C, whereas the solubility at other temperatures can be obtained by using a Van't Hoff relationship.

Experimental results have shown that the polynuclear aluminum complexes play no role unless the aluminum concentration is moderately high (>0.1 M).[37] Confirmation that the aluminate ion is the only significant species in alkaline hydroxide solutions containing

<~1.5 M total aluminum up to temperatures of 100°C has been provided via Raman and NMR studies.[11]

At 25°C an estimate of the solubility is 1.5 mg/L for gibbsite and 25 mg/L for amorphous aluminum hydroxide based on Figure 43.[13] By comparison, the concentration of aluminum in Test 1 solution measured after 4 months was determined to be ~49 mg/L at room temperature. When we consider that boron existed in the Test 1 solution, aqueous boron could have been inhibiting precipitation, or the solution had not yet attained thermodynamic equilibrium. Furthermore, the concentration of boron in the solution indicated that a substantial quantity of boron had precipitated along with the aluminum (i.e., the concentration of boron was determined via ICP analysis to be 2000 mg/L, as compared with an initial 2800 mg/L). During the examination of the aged-4-months Test 1 solution, it was observed that the pH had risen from 9.5 to 9.85. The deviation between the measured aluminum concentration and the theoretical prediction may be attributed to any number of factors: (1) the possible presence of complexing agents (organics), (2) the noted variability in the thermodynamic data, or (3) the complexation of aluminum with boron. An indication that the third factor may play a role is the fact that the pH had changed (increased) over the course of the aging process, which would indicate that further precipitation was occurring in the solution.

Aluminum solubility may also be obtained at 60°C using the Van't Hoff relationship. (It can be shown due to the weak dependency of the enthalpy on temperature over the small temperature range of interest, i.e., 25°C–60°C, that the Van't Hoff approximation is appropriate.) For ICET 1 conditions, i.e., a pH of 9.6, an aluminum solubility of 48 mg/L is predicted if gibbsite is the controlling phase, whereas if the amorphous form of aluminum hydroxide is assumed, a solubility of ~1.3 gL is predicted.

Based on the concentrations measured in Test 1, it would appear that the amorphous phase may be the phase controlling aluminum concentration. That is, the concentration of aluminum in Test 1 at 60°C was above the solubility limit of gibbsite and below the predicted solubility limit of the amorphous phase. Thus, the aluminum hydroxide may indeed be soluble under the isothermal Test 1 conditions. Additional support for this hypothesis is that the concentrations of measured aluminum were equivalent for both filtered and unfiltered water samples. Further support for the amorphous phase being the phase controlling species is given by the observation that the wet precipitate, containing ~51 wt % Al, was found to be largely amorphous (Figure 19). Furthermore, the ICP analysis revealed that boron also was present and, as is discussed in Section 5, the presence of boron, even in very small quantities relative to aluminum, precludes crystallization.

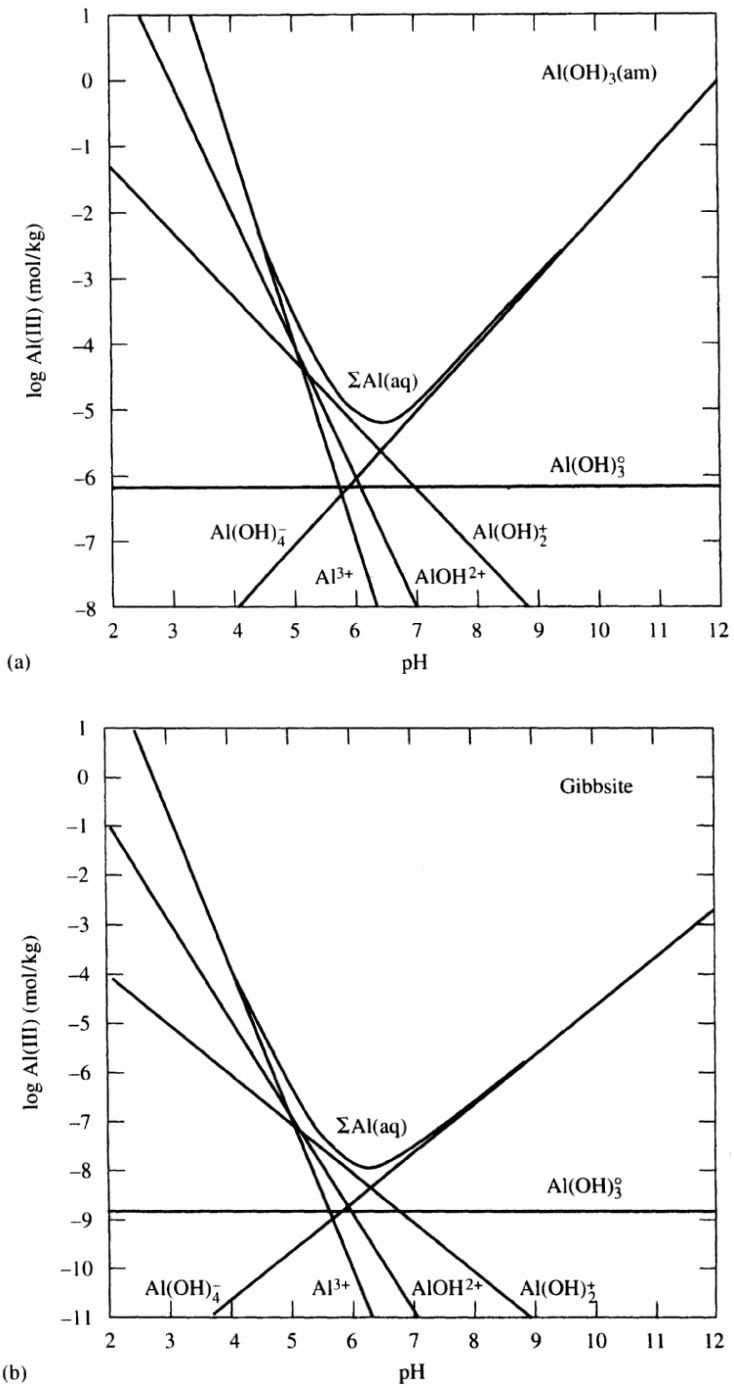

Figure 41. Solubility of (a) amorphous $Al(OH)_3$, and (b) gibbsite [$Al(OH)_3$] as a function of pH at 25°C. Also shown are lines indicating the solubility concentrations of Al^{3+} and individual hydroxyl complexes. [Used with permission of the publisher.*]

* Reprinted and electronically reproduced from *Aqueous Environmental Geochemistry*, Donald Langmuir, Copyright 1997, with permission from Pearson Education, Inc., Upper Saddle River, New Jersey.

7.2. Effect of Organic Complexing Agents on Aluminum Solubility

As previously noted in Section 7.1, the measured concentrations of aluminum were somewhat higher at room temperature than would be expected, even if the solubility-controlling aluminum hydroxide phase were amorphous. To explore this phenomenon, it has been noted that organics can increase the solubility.[60] Consequently, in this subsection we review numerous studies that have been conducted to investigate the effect of organics on the solubility of aluminum. However, before doing so it is first instructive to review some basic theory on the action of the complexing agents.

The stability of a complex is usually described by its stability constant, which is also known as its formation or association constant. The stability constant may refer to a stepwise or cumulative complex formation reaction. K_{assoc} applies to the simple reaction

$$M + L = ML \ , \tag{12}$$

where M, L, and ML are the cation and ligand ML complex, respectively. The free energy of the reaction may be written as

$$\Delta G = \Delta H - T\Delta S \ . \tag{13}$$

Thus, the stability of the complex depends on both the enthalpy of the reaction and the entropy. For most complexation reactions, the entropy stabilizes the reaction.[59] The net positive entropy change that reflects structural changes in the solution consequent to complexation may be broken into many terms, as expressed in

$$\Delta S^o = \Delta S^o_{netchg} + \Delta S^o_{tr} + \Delta S^o_{vibr} + \Delta S^o_{dehydr} \ , \tag{14}$$

In those cases in which there is an entropy reduction ΔS^o_{netchg} because of the decrease in the number of charged particles, some of the translational entropy, ΔS^o_{tr}, of the separate cation and ligand is converted to rotational and vibrational entropy of the complex**.** However, the chief contribution is usually the ΔS^o_{dehydr} term that reflects partial dehydration of the cation and/or ligand. Complexation leads to a breakdown of the structured water of hydration, especially around the cation, with a resultant decrease in the order of the solution. Therefore, ΔS^o_{dehydr} is proportional to the number of water molecules displaced by the ligand. Thus, ΔS^o_{dehydr} is greatest for multivalent ion complexation because these species are initially the most hydrated. Because chelating agents bond a cation via more than one electron-donating atom, they tend to free several cation-coordinating waters on complexation. The result is an unusually large $+\Delta S^o$, as opposed to that of monodentate complexes.[59,61]

Speciation calculations for typical hydroxyl organic ligands and their aluminum(III) complexes may be performed based on established protonation constants and reaction

quotients.[62] Citric acid has been investigated and found to establish three aluminum(III) complexes 1, 2, 3: the 1:1 complex and its protonated and deprotonated forms.

Another possible chelating agent that has been studied is catechol. Catechol has been observed to have the highest stability. However, because of its high pKa's, strong competition by hydrogen ions occurs, even in alkaline solutions. Ethylenediamine-tetraacetic (EDTA) is another polydentate complexing agent that forms complexes with many metals. The anion of EDTA has a quadruple negative charge. The four carboxylate ion groups and also the two nitrogen atoms can form bonds with aluminum; the anion is accordingly a hexadentate complexing agent. Another promising chelating agent is desferriferrioxamine (Desferal R DFB). This agent is a microbial siderophore that has been used for the treatment of Colley's anaemia and is now being used for the treatment of aluminum overload.[62]

Experimental evidence for the effectiveness of chelating agents has been found.[10] In these investigations, small quantities of FA (0–50 mg) were added to aluminum chloride solutions, 450 ml of a 10^{-3} M solution. (FA resembles citric acid in that it contains CO_2H and resembles aliphatic OH groups and quercetin in that it also contains phenolic hydroxyl and ketonic C=O groups. It is through these functional groups that FA can form stable complexes with aluminum.) The solutions were then titrated with 0.1 M NaOH to raise the pH to 6, 8, and 10. All experimental solutions were allowed to age at 30°C for 70 days, with occasional shaking while maintaining pHs at the initial values. It was found that FA inhibited the formation of gibbsite at a pH of 6, leading to the formation of pseudoboehmite. In systems with a pH of 10, the addition of as little as 0.0125 mg/L of FA was sufficient to prevent the formation of any precipitate. A simple explanation may be that at a pH of 10, the surface of the aluminum and FA are both negative such that electrostatic repulsion between the two components appears responsible for the lack of precipitation.

Polybasic acids have also been studied in conjunction with altering the solubility of aluminum hydroxide.[13] In this study, 20 ml of 0.1 M $AlCl_3$ was titrated with 0.1 M NaOH. Before titration, an appropriate quantity of potassium acetate, oxalate, or citrate was dissolved in $AlCl_3$ solution. It was found that increasing the amounts of the organic acid delayed the onset of precipitation and, in the case of citric acid, precluded precipitation if a molar ratio of citric acid to aluminum were above 0.475. An infrared analysis of the air-dried 1:1 citrate-to-aluminum complex indicated that the complex may be similar to commercial aluminum citrate. From these studies it appears that the strength of the aluminum-anion bond is ordered as citrate>oxalate>acetate. Figure 42, Figure 43, and Figure 44[13] present the results of this investigation. In the figures, the arrows denote the appearance of visible precipitate.

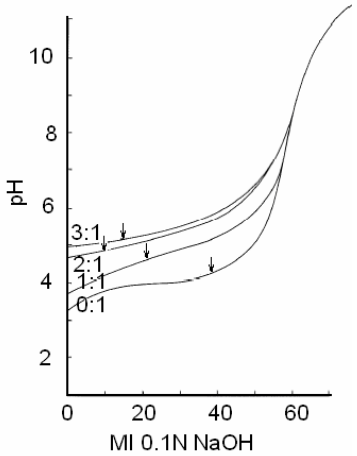

Figure 42. Effect of KOAc on the potentiometric titration of 0.1 $AlCl_3$ by 0.1 N NaOH. The molar ratio of acetate to aluminum was 0, 1.0, 2.0, and 3.0. [Used with permission of the publisher.*]

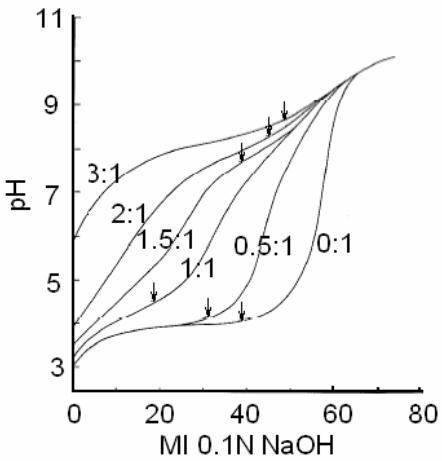

Figure 43. Effect of K oxalate on the potentiometric titration of 0.1 $AlCl_3$ by 0.1 N NaOH. The molar ratio of acetate to aluminum was 0, 0.5, 1.0, 1.5, 2.0, and 3.0. [Used with permission of the publisher.*]

*Reprinted from *Clays and Clay Minerals*, M. K. Wang et al., "Influence of Acetate, Oxalate, and Citrate Anions on Precipitation of Aluminum Hydroxide," **31**:1, pp. 65–68, Copyright 1983, with permission from Clays and Clay Minerals, The Macaulay Institute..

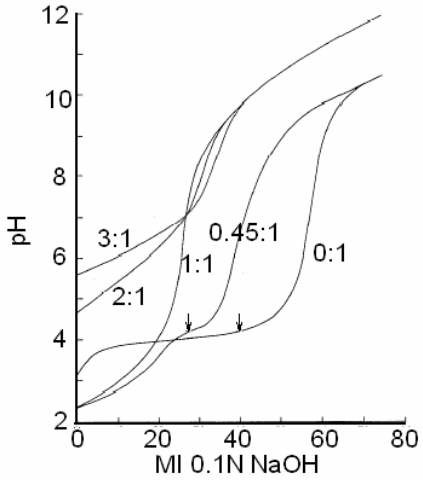

Figure 44. Effect of K citrate on the potentiometric titration of 0.1 $AlCl_3$ by 0.1 N NaOH. The molar ratio of acetate to aluminum was 0, 0.45, 1.0, 2.0, and 3.0. [Used with permission of the publisher.[*]]

In a study of aluminum silicate scale formation and inhibition, it was found that chelating agents with carboxylate functionality, such as citric acid, acetic acid, and EDTA, may inhibit aluminum silicate scale formation.[63] Nitrilotriacetic acid, diethylenetraminepentacetic acid, polycarboxylic acids, pyrocatechol, and humic acids may also be effective.[62]

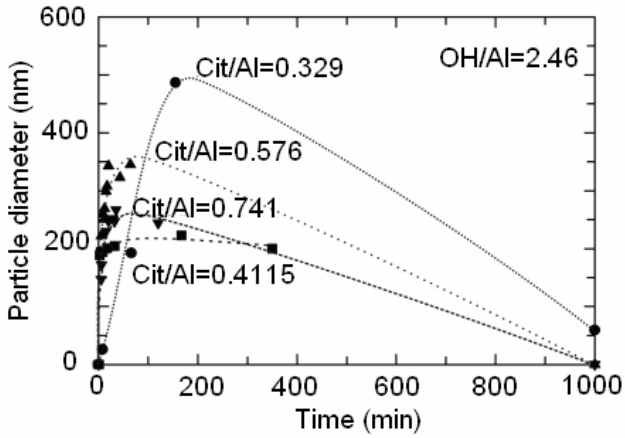

Figure 45. Particle growth in the presence of citric acid. [Used with permission of the publisher.[†]]

[*]Reprinted from *Clays and Clay Minerals*, M. K. Wang et al., "Influence of Acetate, Oxalate, and Citrate Anions on Precipitation of Aluminum Hydroxide," **31**:1, pp. 65–68, Copyright 1983, with permission from Clays and Clay Minerals, The Macaulay Institute.

[†] Reprinted from *Languir*, D. Dabbs and A. Aksay, "Precipitation and Deposition of Aluminum-Containing Phases in Tank Wastes," **21**, pp. 11690–11695, Copyright 2005, with permission from The American Chemical Society.

It is important to note that the dynamics of nucleation are also affected by the presence of complexing agents. In investigations using aluminum chloride with citric acid, using quasi elastic light scattering, it has been found that the addition of citric acid changed the dynamics of both solutions and suspensions.[57] In solutions of very high hydrolysis (OH/Al = 3.29), particles did not form when the mole/mole ratio of citrate to aluminum equaled 0.8. Under the same hydrolysis conditions but at citrate/Al ratios <0.8, particles formed but nucleation and growth were markedly slowed. Under conditions of high hydrolysis (OH/Al = 2.46), particles formed in the presence of citric acid when base was added, but the rate of formation was slowed. Figure 45 presents the results of this investigation.[57]

8. ALUMINUM CORROSION IN ALKALINE SOLUTION

8.1. Corrosion Mechanism

It is well known that aluminum metal is very inert in neutralized solution, whereas pure aluminum is too reactive to be used in concentrated alkaline solutions.[64] Experimental results show that two competing processes occur at the aluminum metal surface: direct dissolution of the aluminum metal and electrochemically formation/dissolution of the aluminum hydroxide films. The first process is very intense, which leads to a high corrosion rate. With time, a film forms on the metal surface, which acts as a barrier for species transport. Therefore, the corrosion rate is significantly reduced after the film forms.

When we consider that $Al(OH)_4^-$ is the only stable form of aluminum in alkaline solution, as shown in Figure 41, the direct dissolution of aluminum is due to

$$Al + 3H_2O + OH^- = \frac{3}{2}H_2 + Al(OH)_4^-. \quad (15)$$

It is evident that the direct aluminum dissolution is accompanied by hydrogen production. Gas bubbles were observed in experiments at the aluminum metal surface. Therefore, the corrosion of pure aluminum in an alkaline solution proceeds mainly by water reduction, according to Eq. (15). The reaction indicates that the dissolution rate depends on the concentrations of OH^- and aluminate ions $Al(OH)_4^-$ at the solid/liquid interface. Thus, the transportation of OH^- and $Al(OH)_4^-$ through the solution to and from the interface, respectively, is expected to play an important role in the aluminum dissolution rate.[64] If the reaction at the interface is much faster than the rate of mass transport provided by the flowing solution, then the dissolution rate is determined (or limited) by the mass transport efficiency. Thus, the aluminum corrosion rate will increase with increasing ability to remove the corrosion products, such as by increasing the solution velocity. However, if the transportation rate is greater than the reaction rate, the aluminum corrosion rate is determined by the reaction rate and depends little on the transportation of OH^- and $Al(OH)_4^-$ through the solution, which has been reported by several researchers.[65,66]

The electrochemical formation of hydroxide film on a pure aluminum surface in alkaline solution has been verified experimentally at an open circuit by the increases in the circuit potential obtained from the moment just after interrupting the abrading action on the specimen.[67] This increase in potential has been considered by several other authors.[64,67,68,69,70,71] The potential changes at the aluminum surface in alkaline solution as a function of time are shown in Figure 46.[71] The potential increases with increasing time until it reaches a constant value. The increase in potential with time is known to arise from the growth of a surface oxide film.[72]

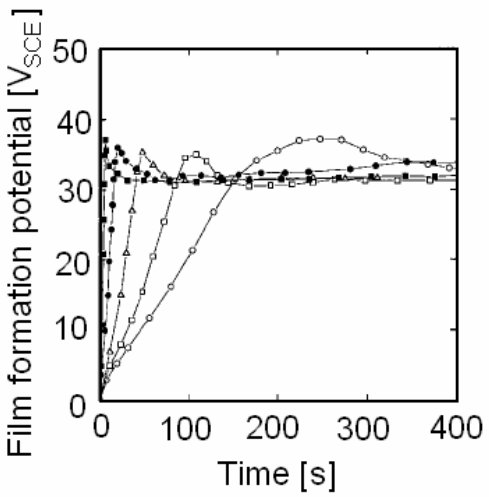

Figure 46. Changes in film formation potential obtained from the pure aluminum rod specimen with time in 10-3 M NaOH solution at various applied anodic current densities of ○, 5 mA cm^{-2}; □, 10mA cm^{-2}; △, 20mA cm^{-2}; ●, 50mA cm^{-2}; and ■, 100mA cm^{-2}. [Used with permission of the publisher.*]

As discussed in Ref. 64, the film formation is due to

$$Al + 3OH^- = Al(OH)_3 + 3e^- . \quad (16)$$

The film forms because of the inward diffusion of OH^- through the film. When a film with considerable thickness forms, the direct dissolution of aluminum metal ceases, as well as the hydrogen production. After that, the aluminum corrosion can be classified into a direct metal dissolution by the movement of aluminum ions through the film and an indirect metal dissolution by consecutive oxide film formation and dissolution.[64] Because Al^{3+} is not thermodynamically stable in an alkaline solution, the direct ejection of aluminum ions from the film into the solution can never occur, which was shown in Refs. 71 and 73. Thus, aluminum corrosion after the film formation occurs is due to

$$Al(OH)_3 + OH^- = Al(OH)_4^- , \quad (17)$$

which is indicative of an electrochemistry process. Thus, the corrosion of pure aluminum in an alkaline solution can be divided into two substeps of a partial anodic reaction comprising the electrochemical formation and chemical dissolution reactions of the film and a partial cathodic reaction of the water reduction reaction.[64]

In some applications, oxide layers are pre-formed on aluminum metal surfaces to protect the substrate. The oxide layer, composed of Al_2O_3, is compact and protective in neutral

*Reprinted from *J. Solid State Electrochem.,* S. M. Moon and S. I. Pyun, "Growth Mechanism of Anodic Oxide Films on Pure Aluminum in Aqueous Acidic and Alkaline Solutions," **2**, pp. 156–161, Copyright 1998, with kind permission of Springer Science and Business Media.

solution. However, the film can be attached by OH^- in an alkaline solution, resulting in film dissolution. If the oxide films were completely uniform, both physically and chemically, it would be expected that the thinning would be uniform over the entire surface. If not, it would be expected that the normal dissolution process would be a flow-assisted process or a flow-centered process. This latter process was found to be mainly responsible in a series of experiments.[74] The dissolution of the oxide film is due to

$$Al_2O_3 + 2OH^- + 3H_2O = 2Al(OH)_4^- . \quad (18)$$

It should be noted that the dissolution of the aluminum oxide is much slower than the direct dissolution of aluminum metal [Eq. (15)]. On the other hand, the aluminum oxide can be converted into aluminum hydroxide if OH^- ions take up the vacancies left by oxygen inward diffusion according to

$$Al_{Al}(ox) + \frac{3}{2}V_O^{2+} + 3OH^- = Al(OH)_3 . \quad (19)$$

Therefore, with time, the oxide layer may be converted to a hydroxide layer.

8.2. Corrosion Rate

The corrosion rate of aluminum in alkaline solution is a function of the operation conditions, such as the temperature, the pH, and the solution properties. Specifically, the corrosion rate depends on the time in a static solution. Because the aluminum concentration in the solution increases, the average corrosion rate decreases with time elapsing. Therefore, various authors obtained very different corrosion rates of aluminum in an alkaline solution because of the different exposure times. In this subsection, we will review experimental data on aluminum corrosion in an alkaline solution.

It has been experimentally verified that the corrosion rate depends logarithmically on the pH,[69] with different dependencies being noted on either side of the pH at which the corrosion rate is at its minimum (close to pH = 6). These results were reported by Pourbaix et al.[75] Vujicic and Loverecek[76] obtained a different logarithmic relation between the corrosion rate and pH value. The curves of corrosion rate as a function of pH[76] are shown in Figure 47. It is evident that for the systems considered in the reference, the point of minimum corrosion rate is greater than a pH of 7.0, which is greater than the pH value, as shown in Ref. 75. Long-term corrosion test results of aluminum in sodium hydroxide solution over the pH range of 8–13 were carried out by McKee and Brown[77] for up to 1 week and over the pH range of 7–12 were carried out by Tabrizi et al.[69] up to 80 days. A summary of corrosion rate data of aluminum in alkaline solutions is given in Table 9.

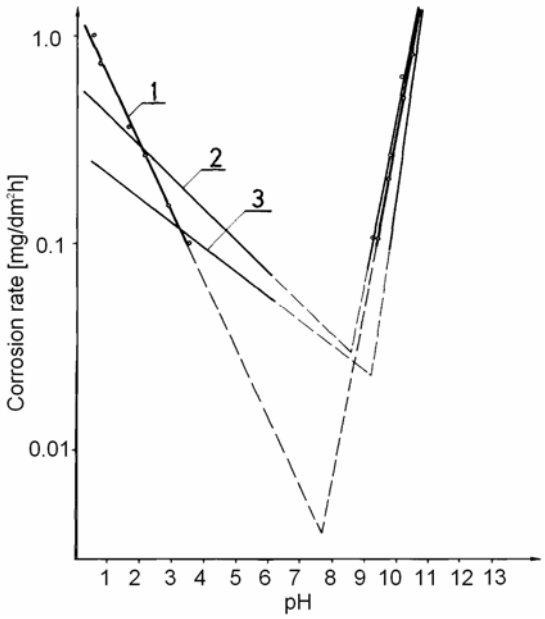

Figure 47. Corrosion rate as function of pH in systems (1) aluminum in 10^{-4} M KCl; (2) aluminum in 10^{-4} M KCl containing 10^{-4} M ethylenediamine; and (3) aluminum in 10^{-4} M KCl containing 10^{-3} M ethylenediamine. [Used with permission of the publisher.*]

Table 9 indicates that the corrosion rate depends on the exposure time, which is clearly shown in Figure 48.[69] Over 40 days of immersion, the weight loss increased with time elapsing. For immersion times beyond 40 days, in a solution having a pH of 10 and 11, the weight losses were similar to those measured at 40 days, indicating that no significant weight loss occurred during the last 20 days. Generally similar trends were evident for immersion at 60°C,[69] with initial high rates of weight loss that decreased with immersion time, particularly beyond 20 days. The weight losses were converted into corrosion rates, as shown in Figure 49. It is evident that the corrosion rate of aluminum in an alkaline solution depends strongly on the exposure time. It decreases with the exposure time increasing. The dependence on exposure time occurs because of the aluminate concentration increasing with time, where the rate is determined by the ratio of the sample surface to the solution volume. Therefore, when we discuss the corrosion rate of aluminum, we must consider the surface/volume ratio and the exposure time. This dependence can also explain why different authors obtained different corrosion rates at comparable conditions, e.g., temperature and pH, in the same solution at the same temperature.

*Reprinted from *Surface Technology*, V. Vujicic and B. Lovrecek, "A Study of the Influence of pH on the Corrosion Rate of Aluminum," **25**:1, pp. 49–57, Copyright 1985, with permission from Elsevier.

Table 9. Corrosion Rate of Aluminum in Static Alkaline Solution

pH	Temperature	Corrosion Rate	Exposure Time	Comments
9	25°C	45 $gm^{-2}y^{-1}$	1 hour	Ref. 76
	25°C	<30 $gm^{-2}y^{-1}$	7 days	Ref. 77
	60°C	242 $gm^{-2}y^{-1}$	7days	Ref. 78, alloy
10	25°C	355 $gm^{-2}y^{-1}$	1 hour	Ref. 76
	25°C	55 $gm^{-2}y^{-1}$	7 days	Ref. 77
	30°C	110 $gm^{-2}y^{-1}$	40 days	Ref. 69, solution replenished
	30°C	130 $gm^{-2}y^{-1}$	40 days	Ref. 69, 1000 ppm Cl^-
	60°C	165 $gm^{-2}y^{-1}$	40 days	Ref. 69, solution replenished
	60°C	65 $gm^{-2}y^{-1}$	40 days	Ref. 69, 1000 ppm Cl^-
	60°C	670 $gm^{-2}y^{-1}$	7 days	Ref. 78, alloy
11	30°C	270 $gm^{-2}y^{-1}$	40 days	Ref. 69, solution replenished
	30°C	285 $gm^{-2}y^{-1}$	40 days	Ref. 69, 1000 ppm Cl^-
	60°C	590 $gm^{-2}y^{-1}$	40 days	Ref. 69, solution replenished
	60°C	170 $gm^{-2}y^{-1}$	40 days	Ref. 69, 1000 ppm Cl^-

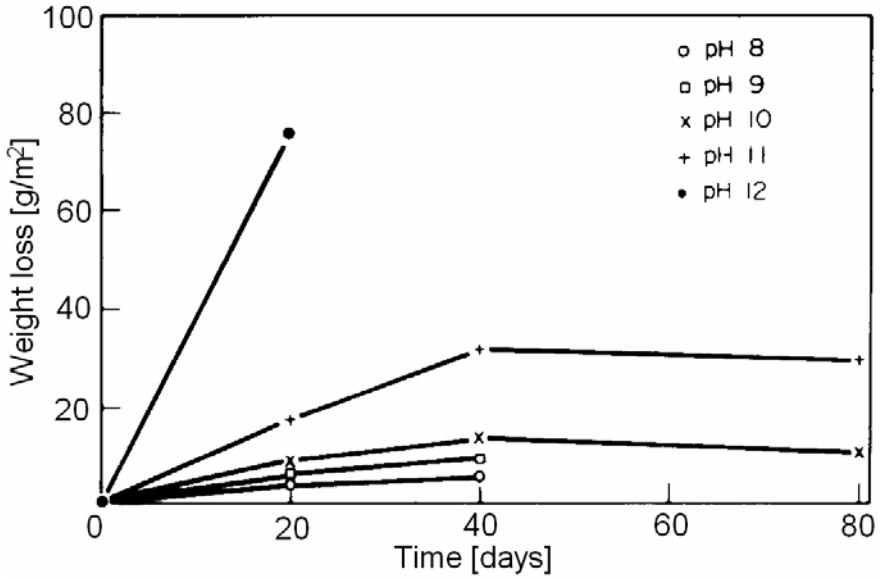

Figure 48. The variation of weight loss of aluminum with exposure time at 30°C. [Used with permission of the publisher.*]

*Reprinted from *Corrosion Sci.*, M. R. Tabrizi, S. B. Lyon, G. E. Thompson, and J. M. Ferguson, "The Long-Term Corrosion of Aluminum in Alkaline Media," **32**, pp. 733–742, Copyright 1991, with permission from Elsevier.

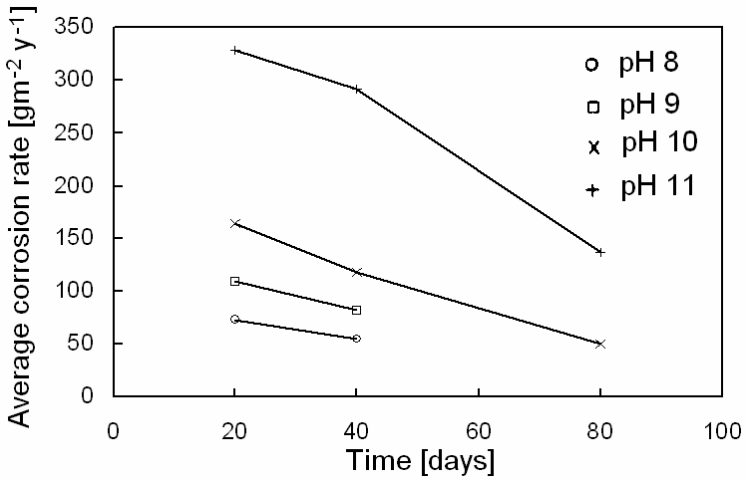

Figure 49. Corrosion rates based on weight loss shown in Figure 48.

From Table 9, the corrosion rate is observed to be dependent on the temperature. Because the reaction and diffusion rates increase with temperature increasing, the corrosion rate of aluminum in alkaline solution becomes larger as the temperature increases, as shown in Table 9. By plotting the aluminum concentration in a 5-M KOH solution as a function of temperature, Chu and Savinell[65] estimated the activation energy as $\Delta G \approx 13.7$kcal/mol for the corrosion of aluminum in alkaline solution, which agrees very well with the value of 12.3 kcal/mol reported for aluminum near the open circuit.[79] Chu and Savinell also reported that the film that formed on the metal surface became thin with increasing temperature, allowing easier OH^- diffusion through the film and resulting in an increase of the aluminum dissolution rate.

As discussed in Section 7.2, adding organic or inorganic ions into the solution has a significant effect on the aluminum concentration. As a result, these ions affect the corrosion rate. For example, the addition of 1000 ppm Cl^- reduces the corrosion rate by two-thirds of the chloride-free solution, as shown in Table 9 at 60°C and a pH of 10. The ions' effect depends on the temperature. As indicated in the table, the addition of 1000 ppm Cl^- has little effect on the corrosion rate at 30°C.

The corrosion rate can also be modified by changing the composition of the aluminum metal through adding small amounts of other elements, such as zinc, bismuth, tellurium, indium, gallium, lead, and titanium. The corrosion rate determination of various of aluminum alloys was conducted by Macdonald et al.;[80] the results are presented in

Table 10. The table indicates that the binary alloys containing <1% of the alloy elements exhibit corrosion rates in 4 M KOH at 50^{o}C that are higher than that for pure aluminum. Adding two or more alloying elements, such as aluminum alloys containing gallium, indium, tellurium, and phosphorus, can result in a sharp reduction in the corrosion rate to well below that for aluminum**.** The corrosion rate of Al-0.1%In alloy was also considered by Wilhelmsen et al.[81] It was reported in Ref. 81 that Al-0.1%In exhibits excellent corrosion-resistant properties, which is very different from those in Ref. 80.

In a static solution, the corrosion rate is a function of exposure time. With time, corrosion eventually can terminate when the corrosion product (aluminate ions) reaches its equilibrium concentration or solubility. The corrosion product does not reach an equilibrium concentration for a flowing system. Solution flow can carry corrosion products away from the metal and also can bring reactants to the metal surface, which accelerates the dissolution process. The dependence of corrosion rate on the flow velocity can be expressed simply, as shown in Figure 50.[82] The figure indicates that at low velocities, the corrosion is controlled or partially controlled by mass transfer; in other words, the dissolution rate is greater than the mass transfer rate and the corrosion product interface concentration is saturated. In such cases, the thickness of the laminar mass transfer layer becomes thinner with increasing velocity and, as a result, the corrosion rate increases; when the velocity exceeds a critical value, the mass transfer rate becomes high enough to transport all corrosion products away from the interface. In this case, the corrosion rate is determined by the dissolution/reaction rate and is independent of the flow velocity. The corrosion is activation controlled; for very high velocities, the high shear stress at the interface can strip off the protective film on the surface of the structure. Some cavities appear at the interface, and the corrosion rate increases sharply with the flow velocity. Therefore, the dependence of the corrosion rate of aluminum in a dynamic alkaline solution on mass transfer is a function of the flow velocity. In different flow velocity ranges, the dependence may be much different. This conclusion can explain why several authors[65,66] reported that the transport of OH^- and $Al(OH)_4^-$ has little effect on the corrosion rate, whereas others[64] found the corrosion rate increasing with the flow velocity increasing. Unlike the static solution, the corrosion rate is a constant in a flowing system when the flow is at a steady state.

Table 10. Corrosion Rate on Various Aluminum Alloys in 4 KOH at 50°C[80] [Used with permission of the publisher.[*]]

Element	Composition (wt %)	Corrosion Rate (mg/cm^2/min)
Pure Al	99.99	0.515
	99.999	0.876
	Alcoa1100-H14	2.735
Zn	0.1	1.030
	0.5	1.074
	1.0	1.097
	5.0	1.190
Bi	0.1	0.593
	0.5	0.461
	1.0	0.520
	5.0	0.507
Te	0.01	0.525
	0.05	0.584
	0.1	0.523
	0.5	0.529
In	0.01	1.910
	0.05	2.287
	0.1	1.965
	0.5	2.106
Ga	0.01	8.740
	0.05	5.707
	0.1	5.845
	0.5	7.627
Pb	0.5	0.736
P	0.2	0.918
	0.5	0.846
0.1% P, 0.1% Ga		153.351
0.1% P, 0.1% In, 0.2% Ga, 0.01% Ti		0.057
0.07% In,0.2% Ga, 0.01% Ti		0.051
0.05% In, 0.01% Ti		0.980
0.05% In, 0.05% Ti		0.733
0.2% In, 0.05% Ti		0.621
0.25% In, 0.01% Ga, 0.1% Ti		0.041
0.1% In, 0.2% Ga, 0.1% Ti		0.048

[*] Reprinted from *Corrosion*, D. D. Macdonald, K. H. Lee, A. Moccari, and D. Harrington, "Evaluation of Alloy Anodes for Aluminum-Air Batteries: Corrosion Studies," **44**, pp. 652–657, Copyright 1988, with permission from NACE International, 2006.

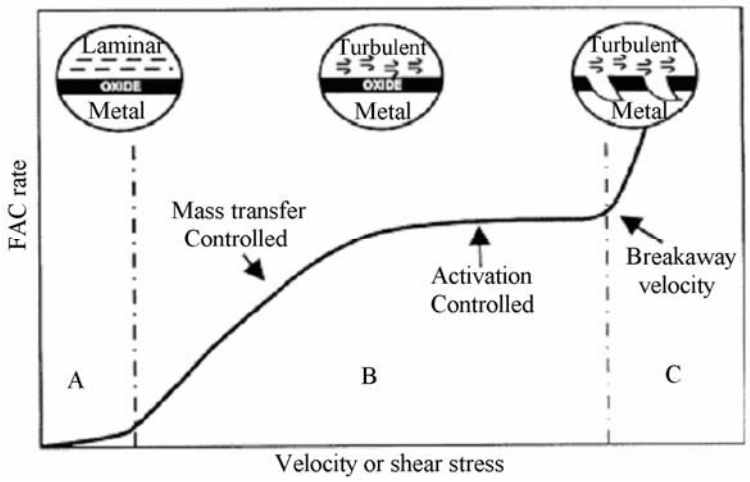

Figure 50. Dependence of corrosion rate on the flow velocity. [Used with permission of the publisher.[*]]

8.3. Corrosion Inhibitor

Inhibition of the corrosion of aluminum and its alloys in alkaline solutions is well known, and many inhibitors have already been described and investigated;[83] they may be organic,[84] or inorganic.[85] Using polarization methods as well as weight loss methods, Al-Suhybani et al.[86] studied in detail various organic and inorganic inhibitor effects on the corrosion rate of aluminum in alkaline solutions. It was reported that benzoin acids (BAs), as well as other organic acids, inhibit the corrosion but to different extents, depending on the structure, and the inhibition is due to the adsorption of these acids and not to the neutralizing effect. The effect of some organic and inorganic additives on the corrosion or aluminum in NaOH is presented in Table 11. It is evident that the citric acid shows the best inhibition at 5 M NaOH, as compared with other organic inhibitors. Some inorganic inhibitors in the table, such as chromate, metabisulphate, dihydrogen phosphate, disodium meta borate, and dihydrogenphosphate, are the best, with an inhibition efficiency of ~97.0%, whereas others, such as NaCl, $NaNO_3$, Na_2SO_4, and $NaIO_3$, are activators.

[*]Reprinted from *Journal of Nuclear Materials*, F. Balbaud-Celeier and F. Barbier, "Corrosion of Aluminum in Alkaline Solutions," **289**:1, pp. 227–242, Copyright 2001, with permission from Elsevier.

Table 11. Effect of Some Organic and Inorganic Additives on the Corrosion of Aluminum in NaOH Solutions[86] [Used with permission of the publisher.[*]]

(NaOH)	Additive	M	Efficiency (%)
5 M	Citric Acid	1.0	99.4
	2-Amino BA	1.0	15.6
	Tetraethylenediaminetetraactic Acid	1.0	37.3
	Chloramine-T	1.0	66.4
	Dithizone	Saturated	78.5
	Sodium Chromate	1.0	45.5
	Sodium Metabisulphate	1.0	55.9
	Sodium Dihydrogen Phosphate	0.01	8.3
	Sodium Dihydrogen Phosphate	0.05	31.0
	Sodium Dihydrogen Phosphate	1.0	96.9
3M	Disodium Metaborates	1.0	36.5
	NaCl, $NaNO_3$, Na_2SO_4, $NaIO_3$	1.0	Activators
	Dithizone	0.25	21.1
	Dithizone	Saturated	47.5
	Polyvinylalcohol	Saturated	12.6

Al-Suhybani et al.[86] reported that the inhibition efficiency depends on both the sodium hydroxide and the inhibitor concentrations. Increasing the sodium hydroxide concentration leads to a decrease in the inhibition efficiency, whereas the dependence on the inhibitor concentration is more complex. Figure 51 shows the dependence of inhibition efficiency on the concentration of several organic inhibitors. It is evident that the dependence is not linear. Specifically, the curve has a double-S shape for phthalic acid. The shape may indicate the formation of the second layer of adsorbed molecules. The figure also shows that phthalic acid and 3-hydroxy BA have stimulating effects at low concentrations, whereas citric acid inhibits the corrosion even at low concentrations. The effect of ethelencdiaminetetraacetic acid (EPTA) is also shown in the figure. The compound was found to be effective only at ~0.5 M. At low concentrations, it stimulates corrosion to the extent of ~90% at 0.01 M.

[*] Reprinted from *Materialwissenschaft und Werkstofftechnik*, A. A. Al-Suhybani, Y. H. Sultan, and W. A. Hamid, "Corrosion of Aluminum in Alkaline Solutions," **22**:8, pp. 301–307, Copyright 1991, with permission from Wiley-VCH Verlag GmbH & Co KG.

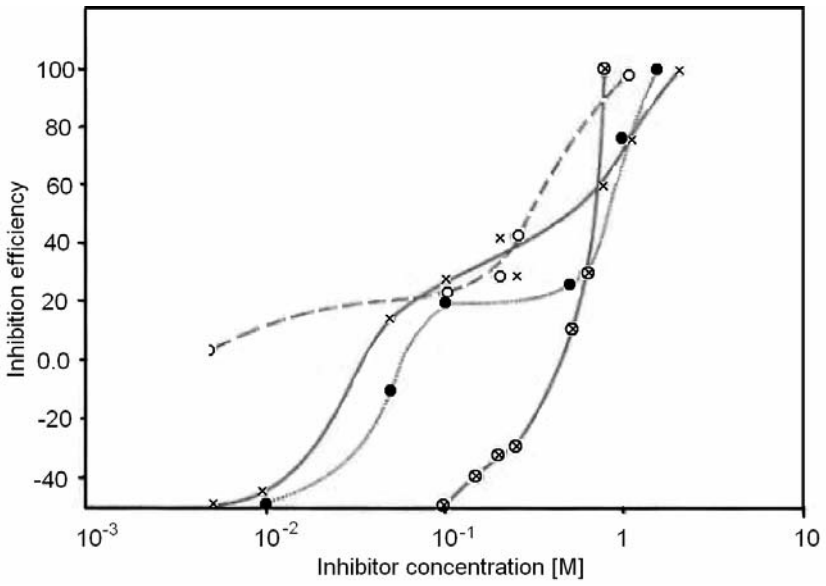

Figure 51. Variation of inhibition efficiency with the concentration of some organic acids in 3 M NaOH. [Used with permission of the publisher.[*]]

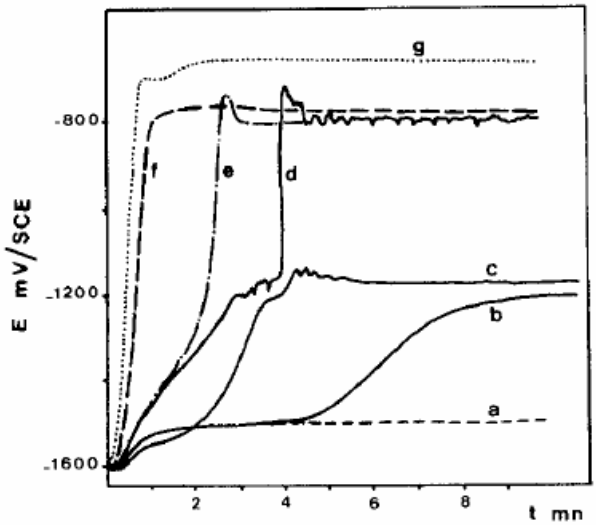

Figure 52. Potential-time curves for almasilium alloys immersed in 0.1 NaOH solution at 60°C, showing the effect of aluminate and "silicate" ions: curve a, 0.1 N NaOH alone; curve b, 0.03 M Si; curve c, 0.04 M Si; curve d, 0.04 M Si + 0.0003 M Al; curve e, 0.04 M Si + 0.0006 M Al; curve f, 0.04 M Si + 0.0012 M Al; and curve g, 0.04 M Si +0.0018 M Al. [Used with permission of the publisher.[†]]

[*] Reprinted from *Materialwissenschaft und Werkstofftechnik*, A. A. Al-Suhybani, Y. H. Sultan, and W. A. Hamid, "Corrosion of Aluminium in Alkaline Solutions," **22**:8, pp. 301–307, Copyright 1991, with permission from Wiley-VCH Verlag GmbH & Co KG.

[†] Reprinted from *Thin Solid Films*, J. P. Labbe and J. Pagetti, "Study of an Inhibiting Aluminosilicate Interface by Infrared Reflection Spectroscopy," **82**, pp. 113–119, Copyright 1981, with permission from Elsevier.

The sodium silicates have been found to be an effective inhibitor of corrosion in aluminum-alkaline systems.[83,87] The inhibition is due to the formation of amorphous aluminosilicate film on the metal surface. It has been reported that a total and almost instantaneous inhibition could be obtained if both Si^{IV} and Al^{III} are present in the solution. The same phase could be built up more slowly with silicate ions alone. The solution potential for different silicate concentrations was also measured as a function of time. The results are shown in Figure 52. After an initial drop in the solution potential because of the dissolution of aluminum, the potential increased with time, followed by a series of oscillations that revealed a tendency for the inhibition film to become alternately partially or totally inhibiting.[87] Finally, the potential reached a stabilization value. The larger the silicate concentration, the greater the stabilization, as shown in the figure. Another effective inorganic inhibitor of the corrosion of aluminum in an alkaline solution was calcium tartrate, which was studied by Shao et al.[88] The authors reported an inhibition efficiency >98% for the corrosion of pure aluminum in a 1-M KOH solution. When the inhibitor concentration was low, its inhibition effect for the anodic process was much higher than that for the cathodic process.

9. BENCHMARK EXPERIMENTS

To assist in developing a surrogate for the Tests 1 and 5 solutions, a series of benchtop tests was performed. The objectives of these tests were to (1) reduce the complexity of the Test 1 system to facilitate the production of a surrogate that could be used to perform head-loss testing and (2) gain additional understanding of the chemical speciation and the mechanisms for their formation. That is, by understanding the mechanisms for the formation of these species, we may be able to add chelating agents to keep the detrimental species in solution and avoid additional head loss due to chemical products. In the previous benchtop tests, we addressed the solubility of the aluminum and the properties of the precipitate. Several small experiments were carried out at LANL. In this section, we report our experimental results.

9.1. Test 1 Redissolution Test

To investigate further the solubility properties and the kinetic aspects of the approach to equilibrium for the Test 1 solution, an experiment was conducted in which the solution after 4 months of storage was heated and held at 60°C for 1 month. The pH during this test was lowered from 9.85 to 9.66, indicating that equilibrium had not been reached. (The initial pH before aging in ICET was 9.5.) Supernatant from the solution was then obtained, and aluminum nitrate at a concentration of ~0.02 M was titrated into the solution while the solution temperature was ~60°C. No noticeable precipitation occurred during this process. The lack of precipitation during the titration of the 0.02-M aluminum nitrate addition indicates that the solution may have been undersaturated with respect to aluminum at 60°C. The lack of precipitation can be explained by recognizing that the solution had previously precipitated while cooling to room temperature, where it was maintained for ~4 months. Following this precipitation process, the solution concentration was found to be ~48 mg/L. If the kinetics of the dissolution of the previously formed precipitate were slow, little precipitate would have redissolved, and the concentration of the solution at 60°C would not be much higher than the aluminum concentration at 25°C. Consequently, as may be seen from the solubility calculation in Section 5.1, the aluminum would have been undersaturated at 60°C. (The solubility at 60°C is ~1.3 gL, assuming that the phase-controlling solid is amorphous aluminum hydroxide.) Therefore, the addition of a 0.02-M solution would not induce precipitation at a pH of ~9.6.

After a small quantity of aluminum nitrate was added, the solution was allowed to cool at room temperature. No visible precipitation was observed after a few hours of aging. Subsequently, the solution was refrigerated to ~0°C and observable precipitation occurred. Finally, the solution was reheated and it was observed that the precipitate still remained 1 month after initial refrigeration. This result reinforces the point that either the reversibility is incomplete or the kinetics of redissolution is very slow, and equilibrium calculations may be of limited use in the 30-day period over which the ICET tests were operated.

9.2. Solubility of Aluminum-Based Surrogates

Benchtop tests have been performed to investigate the solubility limit of aluminum in a 2800-mg/L boron, pH = 9.6 NaOH system at 60°C. Two methods of introducing aluminum into solution have been examined. In the first method, aluminum metal (small pieces) initially was introduced at ambient temperature into the solution, followed by storage in an oven, where the temperature was maintained at 60°C. It should be noted that the metal dissolved very rapidly into the solution because the metal was produced in an inert atmosphere and apparently did not have an oxide layer to limit the dissolution process. Thus, the initial dissolution was very rapid, resulting in vigorous bubbling during the first few hours of dissolution. Furthermore, it cannot be ensured that the solubility limit of ~25 mg/L at room temperature was not exceeded initially. After a few weeks, all of the aluminum metal appeared to have dissolved into the solution. A considerable amount of precipitate settled to the bottom of the bottle. Concentration measurements on material that was filtered through a 0.7-mm filter were made via ICP and indicated an aluminum concentration of 126 mg/L in the filtered solution. During the course of the dissolution of the metal, the pH dropped to 9.25. Normalizing to the ICET conditions, pH = 9.6, we found an aluminum solubility of 282 mg/L. The second method of introducing aluminum into solution consisted of introducing aluminum nitrate crystals into the base solution at 60°C. In this system, the solubility at a measured pH = 8.69 was determined to be 80 mg/L. Converting to the Test 1 solution pH of 9.6 yielded a corresponding solubility of 650 mg/L.

ICP measurements for both systems did not indicate any discernable quantity of boron precipitated from solution. It should be noted that in this test, the solution was not allowed to cool and form precipitate before a sample of the solution was obtained for ICP analysis. This boron deficiency is in contrast to the relatively high percentage of boron found in the precipitate from the Test 1 solution.

9.3. Effects of the Boron in the Aluminum-Alkaline Solution

To examine the boron effects, an aluminum coupon was added to a solution comprised of 2800 mg/L boron and sodium hydroxide at a pH of 9.5. The solution was placed in a 60°C oven for 2 months and then hot filtered at the same temperature. The results of an XRD examination revealed that the precipitate was extremely disordered. A Rietveld refinement analysis revealed that the crystal cell dimensions were a = 2.83738, b = 12.26414, and c = 3.68170 (Å), with a crystallite size of 29 (±1) Å. Strain, if present, was very small. The coherent scattering domain was <10 unit cells, consequently resulting in very broad peaks. This phenomenon reveals similar cell dimensions for the amorphous precipitate.

A comparison of the crystal cell size with the XRD analysis of the Test 1 precipitate revealed an extremely close match. Furthermore, a thermogravimetric analysis (TGA) of the surrogate precipitate was performed. Figure 53 and Figure 54 present the results of the TGA analysis for the surrogate and ICET precipitate, respectively. A comparison of

Figure 53 and Figure 54 indicates that the surrogate precipitate and the Test 1 precipitate have comparable properties.

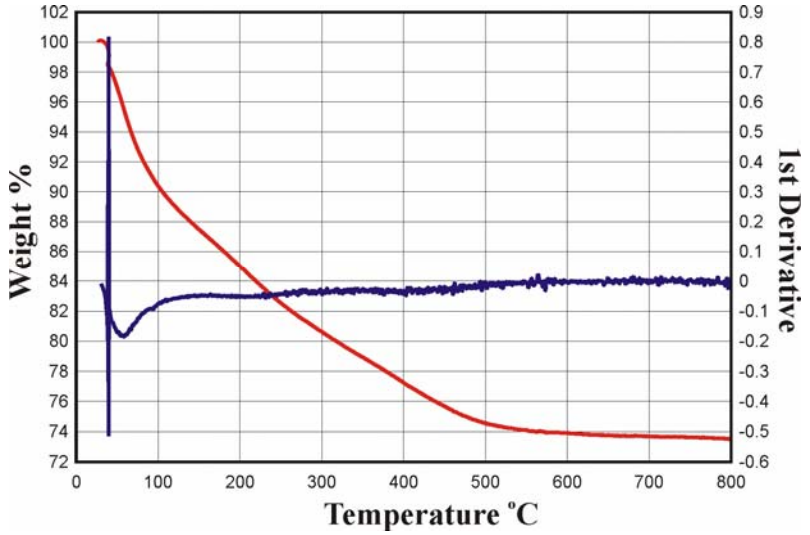

Figure 53. TGA for surrogate, where the red line is weight loss and the blue line is the derivative.

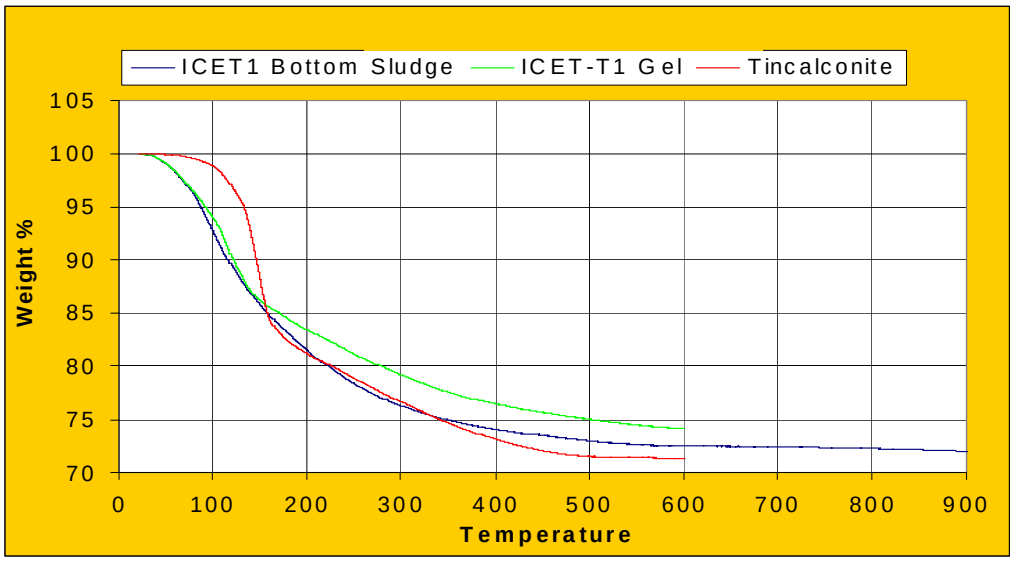

Figure 54. TGA for Test #1 precipitate.

As has been previously reported, it would appear that on cooling, the adsorption of boron onto the surface of the amorphous aluminum hydroxide precluded crystallization. To further investigate the nature of the solid phase formed when the solution was cooled, an ^{27}Al NMR analysis was performed. To perform these analyses, the solution was first centrifuged to isolate the solid. The sample was then dried at 100°C overnight. The ^{27}Al spectra are shown Figure 55a. The figure indicates that many chemical shifts exist; in addition to the broadening of the octahedrally coordinated aluminum, the shift at 60 ppm

is similar in nature to the shift reported for tetrahedral aluminum with four boron next-nearest neighbors.[89] In the reference, it was suggested that tetrahedrally and triagonally coordinated boron are both present. The relative amount depends on the B/Al ratio. To understand further the coordination between aluminum and boron solid-state ^{11}B, NMR was performed, and the curve is shown in Figure 55b. From peaks in Figure 55b, we see that both tetrahedral and triagonal boron is coordinated with the aluminate ion.

For further investigating the effects of boron on chemical speciation, sodium hydroxide, with a pH of 12.74, was titrated into a solution composed of ~2800 mg/L of boron and 0.05 M of aluminum nitrate. A white precipitate formed as soon as the first drop of sodium hydroxide was added. The precipitate dissolved in ~1 hour. Another experiment was performed by adding sodium hydroxide into the aluminum/boron solution to raise the pH of the solution to 9.7. The solution became opaque and remained so for 24 hours, whereupon significant settling of the gel-like material led to the appearance of two distinct phases. The bottom phase had a milky appearance with apparent gel-like characteristics, and the top liquid phase was relatively clear in appearance.

After ~2 weeks, ^{27}Al NMR analyses were performed, as shown in Figure 33. The figure shows that as the temperature was lowered from 60°C, the appearance of a chemical shift at ~74 ppm was noted. The observed chemical shift was similar to that observed in the systems with organics, thereby indicating that the presence of boron had a more dominant effect.

9.4. Particle Size Measurements of Surrogates at 60°C

To examine the behavior of solutions similar to Tests 1 and 5 at 60°C, surrogates were used because of the inability to obtain ICET samples at the test temperature. The surrogates were made by dissolving aluminum coupons into a sodium hydroxide solution with 2800 mg of boron. The pH of this solution was initially 9.6, and the temperature of the solution was maintained at 60°C. Distributions were obtained using a quasi-elastic light-scattering device with a range of particle detection of 2-nm–1-μm particle size. Figure 56 presents the particle distribution. From this figure it would appear that nanoparticles of ~30 and 500 nm were in solution. Furthermore, as was previously noted in the stored Test 1, 60°C precipitate, precipitate was noted after several weeks at 60°C. To understand the bimodal particle size distribution, additional investigations on the properties of the surface charge are needed.

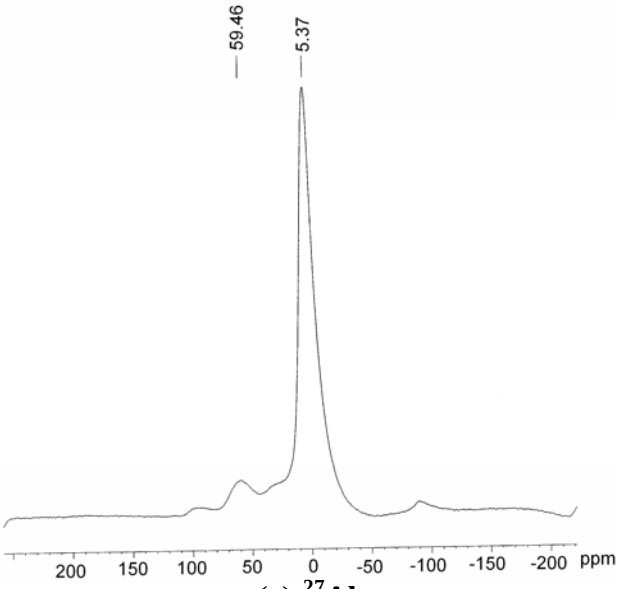

(a) ^{27}**Al**

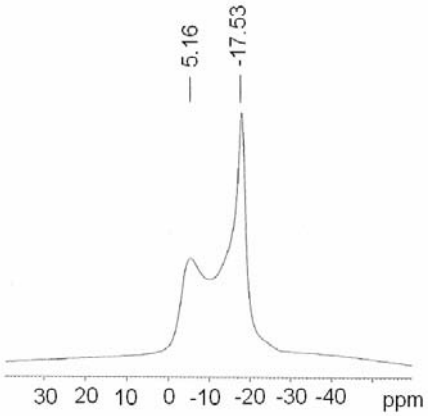

(b) ^{11}B

Figure 55. NMR solid-state spectrum of the precipitates.

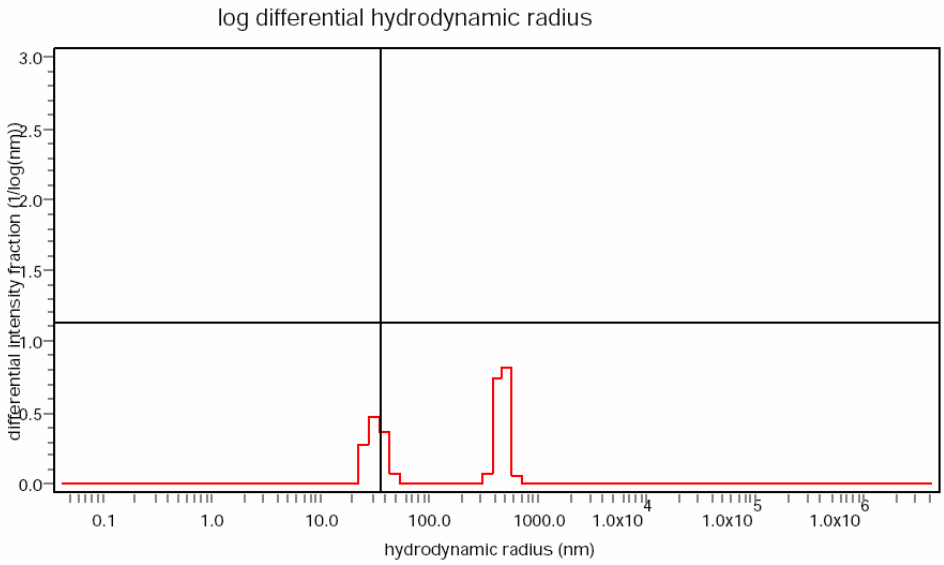

Figure 56. Particle size distributions for aluminum/boron metal dissolution surrogate solution at 60°C after 8 hours.

Furthermore, additional measurements at times comparable to the duration of the ICET tests would be helpful to elucidate the evolution of the particle distribution dynamics. From examination of the surrogate system, it is clear that colloids exist at test temperatures.

9.5. Inhibitor Passivation

To examine the possibility of inhibiting aluminum corrosion in alkaline solution, several experiments were performed. In these experiments, aluminum coupons and aluminum alloy 3003 [having dimensions of 24 (l) × 13 (w) × 1.8 mm (h) and a weight of ~1.59 g] were ultrasonically cleaned with 95% ethanol, followed by drying in air before the test was conducted. The test coupons were then inserted into three 1.0-L solutions (the water used for these tests came from a laboratory water purification system): boric acid, boric acid and silicon, and boric acid and calcium. The concentration of boric acid was 16,000 mg/L (i.e., 2800 mg/L of boron) in all of the three solutions. $Na_2SiO_3 \cdot 9H_2O$ and $CaCl_2$ were used to introduce silicon or calcium to the solution. For the solution containing silicon or calcium, its concentration was 88.7 mg/L or 50 mg/L, respectively. Each solution was put into a 1.0-L Nalgene® bottle. All of the solutions were preheated to 60°C, and the pH was adjusted to 9.5 using sodium hydroxide before putting aluminum coupons into the solutions. The temperature of the solution was maintained at 60°C by a constant-temperature oven (a Yamato DKN400) throughout the 30-day test. The corrosion of the aluminum coupons was monitored by an ICP-AES and pH measurements. The aluminum coupons were analyzed by EDS.

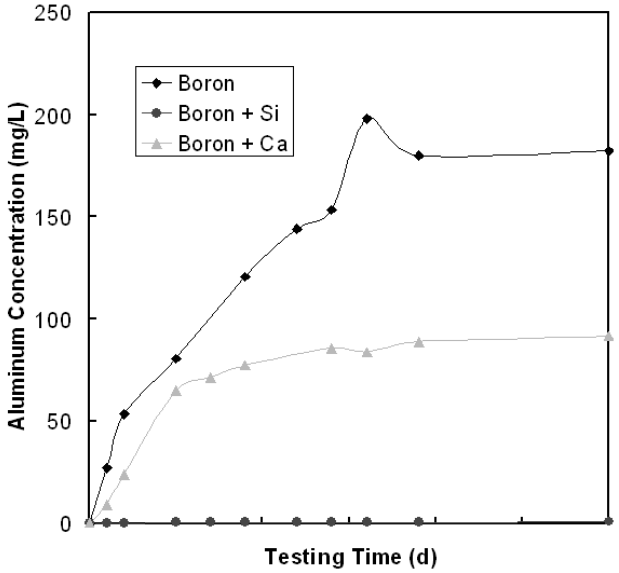

Figure 57. Aluminum concentration (mg/L) versus time.

The measured aluminum concentrations in the three solutions are shown in Figure 57. It is evident that the concentration in the boron+ silicon solution was almost zero and did not change with time, indicating that the inhibition film was instantaneously formed on the coupon surface and that the inhibition efficiency was almost 100%. For the other two solutions (boron and boron + calcium), the concentrations increased with time until they reached an asymptotic value. As may be seen from Figure 57, it is evident that the introduction of calcium reduced the aluminum corrosion rate and the final aluminum concentration also could be reduced, but the inhibition efficiency was much lower than the efficiency obtained by adding silicate. From the SEM images of the sample, it was hard to observe the film, indicating that the film was very thin. Elemental compositions of the surface and the substrate have been examined using EDS; the analyses indicate the presence of small quantities of silica at the surface, whereas no silicate was detected in the bulk of the aluminum coupons; this result verifies the experimental results obtained in Ref. 87. According to the reference, the film was an amorphous aluminum-silicate phase.

To provide direct evidence of the aluminum-silicate film formed on the aluminum alloy coupon surface, x-ray photoelectron spectroscopy (XPS) measurements were performed on a precleaned, virgin aluminum alloy coupon and on the silicate-passivated aluminum alloy coupon. The silicate passivated aluminum coupon was removed from the Na_2SiO_3 solution and gently rinsed with deionized water several times before storing it in a nitrogen-filled desiccator for drying. For the XPS measurements, a Kratos Axis Ultra spectrometer was used with an AlKa 1486-eV x-ray source with 300 W of power to generate x-rays. An electron flood gun for charge neutralization and a hemispherical analyzer with eight multichannel photomultiplier detectors were also used.

As elucidated in Figure 58, the XPS examination was carried out with Al 2p at 90 takeoff-angles (TOAs), which gives the chemical composition of the coupon subsurface up to a 10-nm depth. According to the result, the subsurface of the virgin aluminum

coupon up to 10-nm depth was composed of Al_2O_3 (64%), $Al(OH)_3$ (27%), and Al (9%). However, the subsurface of the silicon-passivated coupon was composed primarily of Al_2OSiO_4 (98%), with a small amount of Al_2O_3 (2%). This result indicates that silicon complexed significantly with aluminum at the coupon surface. The thickness of the complexation layer of silicon and aluminum is >10 nm. In addition, in contrast to the virgin aluminum coupon, no metal aluminum was detected up to 10 nm from the silicate-passivated coupon surface. This observation may be explained by the hypothesis that the complexation or passivation layer grew on top of the original coupon surface and consequently buried the aluminum metal in a deeper subsurface layer.

To examine the passivation layer stability, the passivated aluminum coupons were treated in the following ways: two of the coupons were heated in an oven at 250°C for 2 hours; these coupons are referred to as the "preheated" coupons in Figure 59. When the coupons were cooled down, one unheated coupon and one preheated coupon were transferred to a 12-ml HCl solution that was at a pH of 2.2, respectively. Similarly, one unheated and one preheated coupons were put into a 12-ml NaOH solution at a pH of 9.5, respectively. The concentration of aluminum in the solution with respect to the soaking time is shown in Figure 59. Based on the figure, the silicate passivation was stable below a pH of 9.5 because little aluminum concentration was detected. However, a significant aluminum concentration (>100 mg/L) was found in the solution having a pH of 2.2. Little difference was noted between the preheated and unheated aluminum coupons. This result indicates that the passivation layer of silicate was stable below a pH of 9.5 and likely was dissolved at a pH of 2.2.

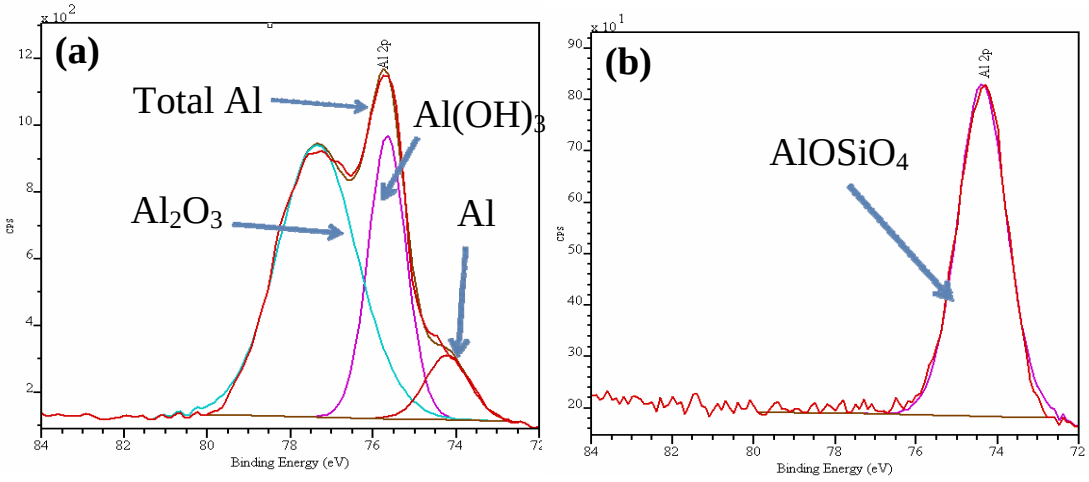

Figure 58. XPS spectra of Al 2p at 90 TOA on aluminum alloy coupons: (left) virgin aluminum, (right) aluminum soaked in Na_2SiO_3 solution.

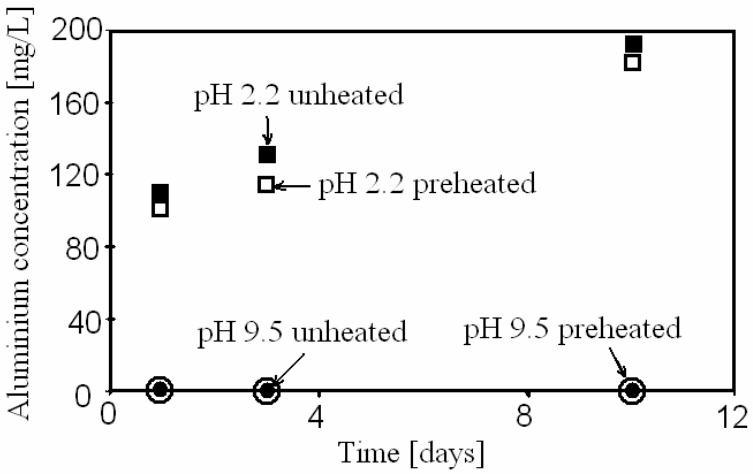

Figure 59. **The stability of a passivation layer of silicate with respect to high and low pH.**

This page intentionally left blank.

10. CONCLUSIONS

A comprehensive examination of both the test solution and precipitate from ICET Tests #1 and #5 has been performed. In addition, a comprehensive review of available literature and benchmark experiments of surrogates has been performed to assist in explaining the behavior of the aluminum in chemical solutions. The objective of this analysis was to elucidate the behavior of precipitate that formed when the Tests 1 and 5 solutions were allowed to cool. This examination included supplemental analytical measurements using XRD, ^{27}Al, ^{11}B NMR (both liquid and solid state), and quasi-elastic light-scattering measurements. The results of this investigation allow for the extrapolation of the behavior of ICET to prediction the behavior of aluminum under different pH and temperature conditions that might exist throughout the PWR following a LOCA. Finally, the characterization of the particle sizes and characterization of the corrosion properties of aluminum under LOCA conditions have been elucidated. These findings should allow for the development of a head-loss correlation using the existing cake filtration theory, which could be used in conjunction with a corrosion model to predict system performance following a LOCA.

Based on both ICP analysis and examination of the Tests 1 and 5 aluminum coupons, it was concluded that the aluminum weight loss from the metal coupons in these tests was consistent with the measured aluminum coupons. Furthermore, by examining the plateau of viscosity (at 23^{o}C), hydrogen production, and aluminum concentration, it was hypothesized that the plateau in the aluminum concentration was a result of passivation of the aluminum metal surface. The measured aluminum concentrations of aluminum in Tests 1 and 5 solutions did not approach predicted solubility limits, and calculations confirmed that the cooling of Tests 1 and 5 solutions to ambient temperature would indeed produce precipitation.

Examinations of the Tests 1 and 5 precipitates revealed that the precipitate after washing (performed to ensure that sodium borates were not allowed to develop during the drying process) was largely amorphous aluminum hydroxide, with a substantial quantity of boron adsorbed onto the surface. A survey of the literature suggests that the presence of the amorphous form of aluminum is indeed expected because of the solution's high concentration of anions, which have been shown to retard crystallization at temperatures <60^{o}C. Thus, if amorphous-phase aluminum does indeed form during cooling of the Test 1 solution, as both XRD and TEM analyses would indicate, then it is not surprising that significant boron would be found as a result of the adsorption of boron from the solution. As indicated from the ICP results, up to 35% of the boron from the initial solution may have been adsorbed onto the amorphous aluminum hydroxide precipitate. This degree of adsorption is certainly feasible. In fact, if we use the data from Su and Surez[47] at a pH of ~9.5, a boron adsorption of ~35% is predicted. A review of the literature and NMR measurements, which revealed complexation between aluminum and boron, was believed to be responsible for impeding the crystallization of aluminum. Furthermore, the measured weight percentage of boron on the aluminum precipitate was consistent with previous predictions based on adsorption models.

The solid hydroxide equilibrium phases play an important role in aluminum solubility. Generally, the crystalline form has a smaller aluminum solubility than does the amorphous form. The phase transition is a complex function of operating conditions and the nature of the materials used. In an alkaline solution, it is likely that the initial precipitates are always amorphous hydroxide, which can be transformed into other forms of aluminum hydroxide by the action of water. At a specific operating condition, more crystalline hydroxide is produced with aging. The crystallization process may be retarded, or the crystal habit of the precipitates may be changed by adding some organic or inorganic cation/anion, such as citrate or boron. The retardation behavior is due to the activity change at the solid/solution interface because of adsorption of the adding anion/cation, which leads to changes in the surface charge and interfacial tension and can influence the kinetics of the incorporation of the growth unit from the solution into the growing solid phase.

Aluminate ions ($Al(OH)_4^-$) are the only stable form of aluminum in an alkaline solution. The solubility is a function of solid hydroxide phases and increases with pH. It is noted that some organics and inorganics can increase the aluminum solubility. The solubility also can be affected by the particle size presented in the solution. Nanoparticles are found in the solution, and the particle size distribution is affected by the hydroxide phases and the adding organic elements. To determine if colloids exist in Tests 1 and 5 solutions, DLS was used. Results of these measurements revealed that colloids did indeed exist at ambient temperature with a mean radius of 65 nm.

Aluminum corrosion in an alkaline solution is an electrochemical process. In a static solution, the corrosion rate decreases with exposure time. In a dynamic solution, the corrosion rates increase with increasing flow velocity in mass transfer-controlled regimes and does not depend on flow velocity in actively controlled regimes. The corrosion rate is influenced by adding organic and inorganic inhibitors into the alkaline solution or some other metal elements into the aluminum metal. The sodium silicates have been found to be effective inhibitors, with an inhibition efficiency of almost 100%.

REFERENCES

1. Dallman, R. J., et al., "Integrated Chemical Effects Test Project: Consolidated Data Report," United States Nuclear Regulatory Commission report NUREG/CR-6914, Volume 1, Los Alamos National Laboratory report LA-UR-06-3673 (2006).

2. Johns, R. C., et. al., "Small-Scale Experiments: Effects of Chemical Reactions on Debris-Bed Head Loss," U. S. Nuclear Regulatory Commission, NUREG/CR-6868, Los Alamos National Laboratory, LA-UR-03-6415 (October 2003).

3. Parthasarathy, N. and Buffle, J., "Study of Polymeric Aluminum-III Hydroxide Solutions for Application in Waste Water Treatment Properties of the Polymer and Optimal Conditions of Preparation**,"** *Water Res* **19**:1, pp. 25–36 (1985).

4. Munson, B., *Fundamentals of Fluid Mechanics*, 4th Ed. (John Wiley and Sons, Inc., Indianapolis, Indiana, 2002).

5. McMurry, J., Jain, V., He, X., Pickett, D., Pabalan, R., and Pan, Y. M., "GSI-191 PWR Sump Screen Blockage Chemical Effects Tests-Thermodynamic Simulations," NUREG/CR-6912, U.S. Nuclear Regulatory Commission, Washington, DC (2006).

6. Bokhimi, X., "Crystallization of Sol-Gel Boehmite via Hydrothermal Annealing**,"** *Journal of Solid State Chemistry* **166,** 182–190 (2002).

7. Goldberg, S., et al., "Chapter 7: The Surface Chemistry of Aluminum Oxides and Hydroxides," in *The Environmental Chemistry of Aluminum*, 2nd Ed., G. Sposito, Ed. (CRC Press, Boca Raton, Florida, 1996).

8. Gerson, A., "Influence of Solution Constituents, Solution Conditioning and Seeding on the Crystalline Phase of Aluminum Hydroxide Using In Situ X Ray Diffraction," J*ournal of Crystal Growth,* **160** (1996), 346–354.

9. Van Straten, H., et al., "Precipitation from Supersaturated Aluminate Solutions," *Journal of Colloid and Interface Science* **98**:2, 342–362 (1984).

10. Kodama, H. and Schnitzer, M., "Effect of Fulvic-Acid on the Crystallization of Aluminum Hydroxides," *Geoderma* **24**:3, 195–205 (1980).

11. Nordstrom, D. and May, H. M., "Chapter 2: Aqueous Equilibrium Data for Mononuclear Aluminum Species," in *The Environmental Chemistry of Aluminum*, 2nd Ed., G. Sposito, Ed. (CRC Press, Boca Raton, Florida, 1996).

12. Vermeulen, A. C., et al., "Hydrolysis-Precipitation Studies of Aluminum (III) Solutions 1. Titration of Acidified Aluminum Nitrate Solutions," *Journal of Colloid and Interface Science* **51**:3, 449–458 (1975).

13. Wang, M. K., et al., **"**Influence of Acetate, Oxalate, and Citrate Anions on Precipitation of Aluminum Hydroxide," *Clays and Clay Minerals* **31**:1, 65–68 (1983).

14. Hayden, P. L. and Rubin, A. J., "Chapter 9: Systematic Investigation of the Hydrolysis and Precipitation of Aluminum(III)," in *Aqueous Environmental Chemistry of Metals*, A. Rubin, Ed. (Ann Arbor Science, Ann Arbor, Michigan, 1976), p. 338.

15. Gerson, A. R., "The Role of Fuzzy Interfaces in the Nucleation, Growth and Agglomeration of Aluminum Hydroxide in Concentrated Caustic Solutions," *Progress in Crystal Growth and Characterization of Materials* **43**:2–3, 187–220 (2001).

16. Hancock, K. E., et al., "The Effect of Humidity on the Physical and Chemical Stability of Spray-Dried Aluminum Hydroxycarbonate," *Journal of Colloid and Interface Science* **183**:2, 431–440 (1996).

17. Serna J., et al., "Factors Affecting Homogeneous Precipitation of Aluminum Hydroxide Gel," *Journal of Pharmaceutical Sciences* **67**:8, 1179–1181 (1978).

18. Prodromou, K. P., "Formation of Aluminum Hydroxides as Influenced by Aluminum Salts and Bases," *Clays and Clay Minerals* **43**:1, 111–115 (1995).

19. Bye, G. C., and Robinson, J. G., "Crystallization Processes in Aluminum Hydroxide Gels," *Kolloid-Zeitschrift and Zeitschrift Fur Polymere* **198**:1–2, 53 (1964)**.**

20. Aldcroft, D. J., et al., "Crystallisation Processes in Aluminum Hydroxide Gels A. Factors Influencing Formation of Crystalline Trihydroxides," *Journal of Applied Chemistry of the USSR* **19**:6, 167 (1969).

21. Hsu, P., *Mineral in Soil Environments*, Chapter 7, J. B. Dixon, Ed. (Soil Science Society of America, Madison, Wisconsin, 1989).

22. Nail, S. L., et al., “Comparison of IR Spectroscopic Analysis and X-Ray Diffraction of Aluminum Hydroxide Gel,” *Journal of Pharmaceutical Sciences* **64**:7, 1166 (1975).

23. Mullin J. W., *Crystallisation* (Butterwoth, CRC Press London, 1972), p. 207.

24. Hsu, P. H., *On Studies of Bauxite and Aluminum Oxides-Hydroxides*, J. Nicholas, Ed. (Proc. 3rd Int. Congr., Nice, France, 1973).

25. Luciuk, G. M., and Huang, P. M., “Effect on Mono Silicic-Acid on Hydrolytic Reactions of Aluminum,” *Soil Science Society of America Proceedings* **38**:2, 235–244 (1974).

26. Kwong, K. F., and Huang, P. M., “Influence of Citric Acid on Hydrolytic Reactions of Aluminum,” *Soil Science Society of America Journal* **41**:4, 692–697 (1977).

27. Ross, G. J., and Turner, R. C., “Effect of Different Anions on the Crystallization of Aluminum Hydroxide in Partially Neutralized Aqueous Aluminum Salt Systems,” Soil Science Society of America Proceedings, **3**:3, 389–392 (1971).

28. Beyrouty, C. A., et al., “Evidence Supporting Specific Adsorption of Boron on Synthetic Aluminum Hydroxides,” *Soil Sci Soc Am J* **48**:2, 284–287 (Mar–Apr 1984).

29. Hingston, F. J., et al., “Anion Adsorption by Goethite and Gibbsite 1. Role of Proton in Determining Adsorption Envelopes,” *Journal of Soil Science* **23**:2, 177 (1972).

30. Nakamoto, K., “Infrared Spectra of Inorganic and Coordination Compounds” (Wiley and Sons, Inc., New York, 1963).

31. Serna, C. J., et al., “Anion-Aluminum Hydroxide Gel Interactions,” *Soil Science Society of America Journal* **41**:5, 1009–1013 (1977).

32. Ferraro, J. R., “The Nitrate Symmetry in Metallic Nitrates,” *Journal of Molecular Spectroscopy* **4,** 99 (1960).

33. Feldkamp, J. R., et al., “Effect of Adsorbed Carbonate on Surface-Charge Characteristics and Physical Properties of Aluminum Hydroxide Gel,” *Journal of Pharmaceutical Sciences*, **70**:6, 638–640 (1981).

34. Little, L. H., “Infrared Spectra of Adsorbed Species” (Academic Press, London, 1966).

35. Burrel, L., “Aluminum Phosphate Adjuvants Prepared by Precipitation at Constant pH: Part 2, Physicochemical Properties,” *Vaccine* **19**:2-3, 282 (2001).

36. Van Straten, H. A., et al., “Precipitation from Supersatured Aluminate Solutions: IV Influence of Citrate Ions,” *J Colloid Interface Science* **106**:1, 175–185 (1985).

37. Baes, H., “The Hydrolysis of Cations” (Krieger Publishing Company, Melbourne, Florida, 1986).

38. Shcihigol, M. B., and Burchinskaya, N. B., “Properties of Aluminum Borates,” *Russian Journal of Inorganic Chemistry* **4**, 913 (1961).

39. Babko, A. K., “Some Properties of Aluminum Borates,” *Russian Journal of Inorganic Chemistry* **7**, 1373 (1962).

40. Ohman, L. O., and Sjoberg, S., “On the Insignificance of Aluminum Borate Complexes in Aqueous-Solution,” *Marine Chemistry* **17,** 91 (1985).

41. Tagirov, S., “Experimental Study of the Stability of Aluminum-Borate Complexes in Hydrothermal Conditions,” *Geochimica et Cosmochimica Acta* **68**:6, 1333 (2002).

42. Douy, A., “Aluminum Borates: Synthesis Via Precipitation Process and Study of Their Formation by DSC Analysis,” *Solid State Sciences* **7**:1, 117–122 (January 2005).

43. Simon, J., et al., “EPR and NMR Studies of Amorphous Aluminum Borates,” *Journal of the Chemical Society Faraday Transactions* **90**:18, 2663–7021 (September 1994).

44. Piel, K. P., et al., “Acid and Catalytic Properties of Nonstoichiometric Aluminum Borates,” *Journal of Catalysis* **115**:2, 441–451 (1989).

45. Sims, J. R., and Bingham, F. T., “Retention of Boron by Layer Silicates Sesquioxides and Soil Materials 2 Sequioxides,” *Soil Science. Society Am. Proc.* **32**, 364 (1968).

46. Toner, C. V., and Sparks, D. L.," Chemical Relaxation and Double Layer Model Analysis of Boron Adsorption on Alumina," *Soil Science Society of America Journal* **59**:2, 395–404 (1995).

47. Su, C., and Surez, D. L., "Coordination of Adsorbed Boron: A FTIR Spectroscopic Study," *Environmental Science Technology* **29**, 302 (1995).

48. Jordan, P. A., "Defining Speciation Profiles of Al^{3+} Complexed with Small Organic Ligands: The $A1^{3+}$-Heidi System," *Coordination Chemistry Reviews* **149,** 281 (1996).

49. Bingham, F. T., *In Methods of Soil Analysis, Part 2*, 2nd Ed. (American Society of Agronomy, Madison, Wisconsin, 1982).

50. Barrow, N. J., "A Brief Discussion on the Effect of Temperature on the Reaction of Inorganic Ions with Soil," *Journal of Soil Science* **43**:1, 37–45 (1992).

51. Stumm, W., et al., "A Ligand-Exchange Model for the Adsorption of Inorganic and Organic Ligands at Hydrous Oxide Interfaces," *Croatica Chemica Acta* **53**:2, 291–312 (1980).

52. Goldberg, S., "Reactions of Boron with Soils," *Plant and Soil* **193**:1–2, 35–48 (1997), Conference Proceedings: International Symposium on Boron in Soils and Plants (BORON97); September 7–11, 1997; Chiang Mai, Thailand.

53. Goldberg, S., et al.," Boron Adsorption Mechanisms on Oxides, Clay Minerals, and Soils Inferred from Ionic Strength Effects," *Soil Science Society of America Journal* **57**:3, 704–708 (May-Jun 1993); Conference: 57th Annual Meeting of the Soil Science Soc of America; November 7–12, 1993; Cincinnati, Ohio.

54. Hingston, F. J., "In Adsorption of Inorganics at Solid-Liquid Interfaces," M. A. Anderson, Ed. (Ann Arbor Science Publishers Inc., Ann Arbor, Michigan, 1981).

55. Oja, T., et al., "Acoustic Analysis of Concentrated Colloidal Systems," T. Provder, Ed., ACS Symposium Series, v. 881, pp. 231–248 (2004); Conference on Particle Sizing and Characterization; August 18–22, 2002; Boston, Massachusetts.

56. Bale H., and Rausch, W. V, "Small-Angle X-Ray Scattering from Hydrolyzed Aluminum Nitrate Solutions**,"** *Journal of Chemical Physics* 1, **40**:11, 3391–3394 (1964**).**

57. Dabbs, D. and Aksay, A., "Precipitation and Deposition of Aluminum-Containing Phases in Tank Wastes," *Langmuir* **21**, 11690–11695 (2005).

58. Bale H., and Schmidt, P. W., "Small Angle X-Ray Scattering from Aluminum Hydroxide Gel," *Journal of Chemical Physics* **62**:10, 1179–1183 (1958).

59. Languir D., *Aqueous Environmental Geochemistry* (Prentice Hall, Upper Saddle River, New Jersey, 1997).

60. Vance, G. F., et al., "Chapter 5: Environmental Chemistry of Aluminum-Organic Complexes," in *The Environmental Chemistry of Aluminum*, 2nd Ed., G. Sposito, Ed. (CRC Press, Boca Raton, Florida, 1996).

61. Cotton, "Advanced Inorganic Chemistry, A Comprehensive Text," 5th Ed. (New York, John Wiley & Sons, 1988).

62. Martell, A. E., et al., "Aluminum Complexes of Hydroxyaliphatic and Hydroxyaromic Ligands in Aqueous Systems Some Problems and Solution," *Polyhedron* **9**:2–3, 171–188 (1990).

63. Gallup, D. L., "Aluminum Silicate Scale Formation and Inhibition: Scale Characterization and Laboratory Experiments,**"** *Geothermics* **26**:4, 483-499 (August 1997).

64. Pyun, S., Moon, S-M., "Corrosion Mechanism of Pure Aluminum in Aqueous Alkaline Solution," *J. Solid State Electrochem.* **4**, 267–272 (2000).

65. Chu, D., and Savinell, R. F., "Experimental Data on Aluminum Dissolution in KOH Electrolytes," *Electrochim. Acta* **36**, 1631–1638 (1991).

66. Brown, O. R., and Whitley, J. S., "Electrochemical Behaviour of Aluminum Aqueous Caustic Solution," *Electrochim Acta* **321**, 545–556 (1987).

67. Moon, S. M., and Pyun, S. I., "The Corrosion of Pure Aluminum during Cathodic Polarization in Aqueous Solutions," *Corrosion Sci.* **39**, 399–408 (1997).

68. Wihelmsen, W., Arnesen, T., Hasvold, O., and Storkersen, N. J., "Electrochemical Behaviour of Al-In Alloys in Alkaline Electrolytes," *Electrochim Acta* **36**, 79–85 (1991).

69. Tabrizi, M. R., Lyon, S. B., Thompson, G. E., and Ferguson, J. M., "The Long-Term Corrosion of Aluminium in Alkaline Media," *Corrosion Sci*. **32**, 733–742 (1991).

70. Tuck, C. D. S., Hunter, J. A., and Scamans, C. M., "Electrochemical Behavior of Al-Ga Alloys in Alkaline and Neutral Electrolytes," *J. Electrochem. Soc.* **110** 2970–2981 (1987).

71. Moon, S. M., and Pyun, S. I., "Growth Mechanism of Anodic Oxide Films on Pure Aluminum in Aqueous Acidic and Alkaline Solutions," *J. Solid State Electrochem*. **2**, 156–161 (1998).

72. Burstein, G. T., and Cinderey, R. T., "Evolution of the Corrosion Potential of Repassivating Aluminium Surfaces," *Corrosion Science* **33**, 475–492 (1992).

73. Moon, S. M., and Pyun, S. I., "The Formation and Dissolution of Anodic Oxide Films on Pure Aluminium in Alkaline Solution," *Electrochim. Acta* **44**, 2445–2454 (1999).

74. Foley, T. T., "Localized Corrosion of Aluminum Alloys—A Review," *Corrosion* **42**, 277–287 (1986).

75. Pourbaix, M., *Atlas of Electochemical Equilibria in Aqueous Solutions* (N.A.C.E./Cebelcor, Houston) (1974).

76. Vujicic, V., and Lovrecek, B., "A Study of the Influence of pH on the Corrosion Rate of Aluminium," *Surface Technology* **25**:1, 49–57 (1985).

77. McKee, A. B., and Brown, R. H., "Resistance of Aluminum to Corrosion in Solutions Containing Various Anions and Cations," *Corrosion* **3**, 595–612 (1947).

78. Binger, W. W., and Marstiller, C. M., "Aluminum Alloys for Handling High-Purity Water," *Corrosion* 13, 591–596 (1957).

79. Continental Group Inc., "Aluminum-Air Battery Development. Final Technical Report," Lawrence Livermore National Laboratory report UCRL-15459 (1982).

80. Macdonald, D. D., Lee, K. H., Moccari, A., and Harrington, D., "Evaluation of Alloy Anodes for Aluminum-Air Batteries: Corrosion Studies," *Corrosion* **44**, 652–657 (1988).

81. Wilhelmsen, W., Arnesen, T., Hasvold, O., and Storkersen, N. J., "The Electrochemical Behaviour of Al-In Alloys in Alkaline Electrolytes," *Electrochim. Acta* **36**:1, 79–85 (1991).

82. Balbaud-Celeier, F., and Barbier, F. "Investigation of Metals to Predict the Corrosion of Steels in Flowing Liquid Lead Allows," *Journal of Nuclear Materials* **289**:3, 227–242 (2001).

83. Triki, E., Daufin, G., Labbe, J. P., and Pagetti, J., "Mechanisms of Corrosion Inhibition for an Aluminium-Silicon-Magnesium Alloy in 0.1 N NaOH Solutions at 60°C," *Werkstoffe und Korrosion* **30**, 259–265 (1979).

84. Putilova, I. N., Balezin, S. A., and Barannik, V. P., *Metallic Corrosion Inhibitors*, (Pergamon Press, Oxford, 1960), p. 121.

85. Ammar, I. A., and Nazmi, A. F., "Corrosion of Duraluminium in Acid and Alkaline Solution," *Corrosion Prevention and Control* **9**, 31–34 (1962).

86. Al-Suhybani, A. A., Sultan, Y. H., and Hamid, W. A., "Corrosion of Aluminium in Alkaline Solutions," *Materialwissenschaft und Werkstofftechnik* **22**:8, 301–307 (August 1991).

87. Labbe, J. P., and Pagetti, J., "Study of an Inhibiting Aluminosilicate Interface by Infrared Reflection Spectroscopy," *Thin Solid Films* **82**:1, 113–119 (1981).

88. Shao, H. B., Wang, J. M., Zhang, Z., Zhang, J. Q., and Cao, C. N., "Inhibition Effect of Calcium Tartrate on the Corrosion of Pure Aluminum in an Alkaline Solution," *Corrosion* **57**, 577–581 (2001).

89. Dupree, R., and Williams, D. S., "Examination by Magic Angle Spinning NMR of the Changes in the Environment of Al-27 during the Devitrification of an Aluminoborate Glass," *Physics and Chemistry of Glasses* **26**:2, 50–52 (1985).

NRC FORM 335
(9-2004)
NRCMD 3.7

U.S. NUCLEAR REGULATORY COMMISSION

BIBLIOGRAPHIC DATA SHEET

(See instructions on the reverse)

1. REPORT NUMBER
(Assigned by NRC, Add Vol., Supp., Rev., and Addendum Numbers, if any.)

NUREG/CR-6915

2. TITLE AND SUBTITLE

Aluminum Chemistry in a Prototypical Post-Loss-of-Coolant-Accident, Pressurized-Water-Reactor Containment Environment

3. DATE REPORT PUBLISHED

MONTH	YEAR
December	2006

4. FIN OR GRANT NUMBER

N6285

5. AUTHOR(S)

M. Klasky, J. Zhang, M. Ding, B. Letellier, Los Alamos National Laboratory
D. Chen, K. Howe, University of New Mexico

6. TYPE OF REPORT

Final

7. PERIOD COVERED *(Inclusive Dates)*

September 2005 - November 2006

8. PERFORMING ORGANIZATION - NAME AND ADDRESS *(If NRC, provide Division, Office or Region, U.S. Nuclear Regulatory Commission, and mailing address; if contractor, provide name and mailing address.)*

Los Alamos National Laboratory
Loa Alamos, NM 87545

University of New Mexico
Department of Civil Engineering
Albuquerque, NM 87110

9. SPONSORING ORGANIZATION - NAME AND ADDRESS *(If NRC, type "Same as above"; if contractor, provide NRC Division, Office or Region, U.S. Nuclear Regulatory Commission, and mailing address.)*

Division of Fuel, Engineering & Radiological Research
Office of Nuclear Regulatory Research
U.S. Nuclear Regulatory Commission
Washington, DC 20555-0001

10. SUPPLEMENTARY NOTES

T.Y. Chang, NRC Project Manager

11. ABSTRACT *(200 words or less)*

Generic Safety Issue 191 (GSI-191), "Assessment of Debris Accumulation on PWR Sump Performance" was established by the NRC to address the concern of the transport of debris to PWR sump screens following a LOCA and subsequent impact to ECCS and CSS during recirculation. NRC's Advisory Committee on Reactor Safeguards (ACRS) further raised a concern about "chemical effects" in 2003, namely, certain resultant products attributable to chemical interactions between ECCS and CSS water and exposed materials could form another source of debris that has the potential to impede the performance of ECCS recirculation following a LOCA at a PWR plant. To address this concern, the NRC and the nuclear energy industry jointly sponsored an integrated chemical effects test (ICET) program. ICET tests 1 and 5 raised the questions regarding the behavior of aluminum in sump pool solutions, and especially the behavior of aluminum-related chemical products that formed when ICET tests 1 and 5 solutions were allowed to cool. To answer these questions, the NRC sponsored a follow-on study, performed at Los Alamos National Laboratory, which included an analysis of both the test solutions and aluminum-related chemical products of ICET 1 and 5, as well as a comprehensive review of the literature to improve our understanding of the behavior of aluminum in sump pool solutions. That follow-on study is the subject of this report. This report provides information about the characterization of particle sizes and corrosion properties of aluminum under LOCA conditions. It also provides information that will allow extrapolation of ICET behavior to predict the behavior of aluminum under various pH and temperature conditions that might exist in PWR plants following a LOCA. This information will be useful to the nuclear utility industry and the NRC staff in assessing aluminum chemical effects on sump performance in a post-LOCA PWR containment environment.

12. KEY WORDS/DESCRIPTORS *(List words or phrases that will assist researchers in locating the report.)*

Generic Safety Issue 191 (GSI-191), pressurized-water-reactor (PWR), PWR containment, PWR sump screen, loss-of-coolant-accident (LOCA), insulation debris, fibrous insulation debris, particulate insulation debris, emergency-core-cooling systems (ECCS), recirculation, containment-spray systems (CSS), containment sump pool, chemical effects, integrated chemical effects test (ICET), aluminum chemistry, aluminum-ralated chemical products, behavior of aluminum in sump pool solutions

13. AVAILABILITY STATEMENT

unlimited

14. SECURITY CLASSIFICATION

(This Page)
unclassified

(This Report)
unclassified

15. NUMBER OF PAGES

16. PRICE

PRINTED ON RECYCLED PAPER